

# Errors in scalable quantum Computers

Dissertation  
zur Erlangung des Grades  
des Doktors der Naturwissenschaften  
der Naturwissenschaftlich-Technischen Fakultät  
der Universität des Saarlandes

von

**Tobias Chasseur**

Saarbrücken

2019

Tag des Kolloquiums: 21.05.2019  
Dekan: Prof. Dr. Guido Kickelbick  
Berichterstatter: Prof. Dr. David Gross  
Prof. Dr. Frank Wilhelm-Mauch  
Vorsitz: Prof. Dr. Jürgen Eschner  
Akad. Mitarbeiter: Dr. Adam Wysocki

*Für Claudia.*



# Abstract

A functional quantum computer potentially outperforms any classical machine exponentially in a number of important computational tasks. Therefore, its physical implementation has to scale efficiently in the number of qubits, specifically in tasks such as treatment of external error sources. Due to the intrinsic complexity and limited accessibility of quantum systems, the validation of quantum gates is fundamentally difficult. Randomized Benchmarking is a protocol to efficiently assess the average fidelity of only Clifford group gates. In this thesis we present a hybrid of Randomized Benchmarking and Monte Carlo sampling for the validation of arbitrary gates. It improves upon the efficiency of current methods while preserving error amplification and robustness against imperfect measurement, but is still exponentially hard. To achieve polynomial scaling, we introduce a symmetry benchmarking protocol that validates the conservation of inherent symmetries in quantum algorithms instead of gate fidelities. Adiabatic quantum computing is believed to be more robust against environmental effects, which we investigate in the typical regime of a scalable quantum computer using renormalization group theory. We show that a  $k$ -local Hamiltonian is in fact robust against environmental influence but multipartite entanglement is limited to combined system-bath state which we conclude to result in a more classical behavior more susceptible to thermal noise.



# Zusammenfassung

Ein Quantencomputer wäre in einer Reihe wichtiger Berechnungen exponentiell effizienter als klassische Computer, unter Voraussetzung einer fehlerarmen und skalierbaren Implementierung. Aufgrund der intrinsischen Komplexität und beschränkten Auslesbarkeit von Quantensystemen ist die Validierung von Quantengattern ungleich schwerer als die klassischer. Das Randomized Benchmarking Protokoll leistet dies effizient, ist jedoch beschränkt auf Cliffordgatter. In dieser Arbeit präsentieren wir ein Hybridprotokoll aus Interleaved Randomized Benchmarking und Monte Carlo Sampling zur Validierung von beliebigen Gattern. Trotz Verbesserung gegenüber vergleichbaren Protokollen skalieren die benötigten Ressourcen exponentiell. Um dies zu vermeiden entwickeln wir ein Protokoll, welches die Erhaltung von spezifischen Symmetrien von Quantenalgorithmen untersucht und dadurch Rückschlüsse auf die Fehlerrate der Quantenprozesse zulässt und demonstrieren seine Effizienz an relevanten Beispielen. Der Effekt von Umgebungseinflüssen auf adiabatische Quantencomputer wird als weit weniger gravierend angenommen als im Falle von konventionellen Systemen, ist jedoch im gleichen Maße weniger verstanden. Wir untersuchen diese Effekte mithilfe von Renormalisierungstheorie und zeigen, dass  $k$ -lokale Hamiltonoperatoren robust sind, vielfach verschränkte Zustände hingegen nur verschränkt mit der Umgebung existieren. Wir folgern daraus ein verstärkt thermisches Verhalten des Annealingprozesses.



# Contents

<b>Introduction</b>	<b>3</b>
<b>1 Basics of Quantum Information and Computation</b>	<b>5</b>
1.1 The Qubit . . . . .	5
1.2 Quantum Gates . . . . .	7
1.3 Imperfect Implementation – Error Channels . . . . .	10
1.4 Quantum Algorithms . . . . .	14
<b>2 Scaling and Fault Tolerance</b>	<b>19</b>
<b>3 Adiabatic Quantum Computation</b>	<b>23</b>
3.1 Universality of AQC . . . . .	24
3.2 The adiabatic Deutsch-Josza Algorithm . . . . .	26
<b>4 Methods and Formalisms</b>	<b>27</b>
4.1 Normal Ordering . . . . .	27
4.2 The Perron-Frobenius Theorem . . . . .	28
4.3 Statistical Inequalities . . . . .	28
<b>I Randomized Benchmarking</b>	<b>29</b>
<b>5 Introduction to Randomized Benchmarking</b>	<b>33</b>
5.1 Standard RB . . . . .	34
5.2 Interleaved Randomized Benchmarking . . . . .	36
5.3 Alternate Formalism . . . . .	38
<b>6 Hybrid Benchmarking</b>	<b>43</b>
<b>7 Symmetry Benchmarking</b>	<b>51</b>
7.1 Symmetry Benchmarking Protocol . . . . .	53
7.2 Benchmarking arbitrary Operations . . . . .	54
7.3 Number Conservation in Quantum Chemistry . . . . .	55

7.4	Parity Conservation and the Fermi-Hubbard Model . . . . .	57
7.5	Benchmarking logically encoded Processes . . . . .	58
7.6	Conclusion . . . . .	60
 <b>II Environmental Effects on adiabatic Quantum Computing</b>		<b>63</b>
<b>8</b>	<b>Renormalization Group Methods</b>	<b>67</b>
8.1	Adiabatic Renormalization . . . . .	67
8.2	Poor Man's Scaling . . . . .	69
8.3	The Flow Equation Approach . . . . .	70
<b>9</b>	<b>Multi-Spin-Boson Model</b>	<b>77</b>
9.1	Transformation under poor Man's Scaling . . . . .	78
9.2	Second Order Effects . . . . .	83
9.3	Flow Equations . . . . .	85
<b>10</b>	<b>Implications for Quantum Annealing</b>	<b>91</b>
10.1	LCGD Regime . . . . .	92
10.2	Discussion . . . . .	97
 <b>Conclusion</b>		<b>99</b>
 <b>List of Publications</b>		<b>103</b>
 <b>Bibliography</b>		<b>115</b>

# List of Figures

1.1	Visualization on the Bloch sphere . . . . .	6
1.2	Generating a Bell state . . . . .	8
1.3	Visualization of different error channels I . . . . .	12
1.4	Visualization of different error channels II . . . . .	13
1.5	Circuit of the Deutsch-Josza algorithm . . . . .	16
2.1	Circuit of the three qubit bit flip code . . . . .	20
2.2	Circuit of the three qubit phase flip code . . . . .	21
5.1	Circuit representation of an RB sequence . . . . .	35
5.2	Circuit representation of an IRB sequence . . . . .	37
5.3	Decay of the RB sequence fidelity . . . . .	40
7.1	Symmetry population decay . . . . .	56
7.2	Interleaved Symmetry Benchmarking . . . . .	59
8.1	Visualization of the flow equation approach . . . . .	71
9.1	Suppression of qubit operators . . . . .	83
10.1	The LCGD regime . . . . .	94
10.2	Analysis of an antiferromagnetic Hamiltonian I . . . . .	95
10.3	Analysis of an antiferromagnetic Hamiltonian II . . . . .	96
10.4	Analysis of an antiferromagnetic Hamiltonian III . . . . .	96



# Acknowledgments

I would like to thank the collaborators and colleagues that accompanied, guided and inspired me on my scientific journey. This includes first and foremost my supervisor Professor Dr. Frank Wilhelm-Mauch but also Lukas Theis, Dr. Daniel Egger, Dr. Per Lieberman, Dr. Daniel Reich, Professor Dr. Christiane Koch, Dr. Felix Motzoi, Michael Kaicher, Dr. Pierre-Luc Dallaire-Demers, Professor Dr. Stefan Kehrein, Dr. Luke Govia and Professor Dr. Bruno Taketani – in no particular order.



# Introduction



A computer is based on classical bits which can assume either of two states '0' and '1' and hence is fundamentally binary. As such, it is inherently powerful at logical and mathematical operations on bit strings and consequently on all integers and decimal numbers. This enables a great number of applications in computation and communication that are deemed an integral part of modern life. Computers have proven to be an invaluable asset in technology, science and communication but also for almost any challenge of a modern society. The scope of its application has not reached its limits with new fields such as the development of artificial intelligence still emerging .

Inconveniently nature is not binary. Fundamentally the world is described by quantum physics<sup>1</sup> which in turn is mathematically formulated via unitary operations on finite and infinite dimensional Hilbert spaces. Numerical simulation results in a computational overhead severely limiting the complexity of tractable quantum systems: Just storing the information of  $n$  interacting two-dimensional systems requires  $\mathcal{O}(2^n)$  in classical resources, while the computational power necessary to simulate the dynamics scales even worse. Following that reasoning physicist Richard Feynman among others proposed that, to simulate a quantum system efficiently, one has to use a machine that is build upon and relies on properties of a quantum system [1–3]. This approach established the field of quantum information processing. Evolving beyond just the simulation of quantum systems, a number of quantum algorithms have been developed. They are designed to act on quantum mechanical two-level-system – qubits – which form the foundation of a quantum computer. The most prominent algorithms are Shor’s algorithm which allows for factorization of the product of two prime numbers with non-exponential resources. This result implicates an exponential speed up in comparison with conventional computation which is relevant not only to break RSA cryptography [4]. Grover’s search of unsorted databases also potentially outperforms classical algorithms fundamentally [5], adding incentive to the development of quantum algorithms. The computational power of those is not yet fully understood, however it is conjectured to be based upon the simultaneous application to many input states as well as many party entanglement.

There are many possible candidates for the physical implementation of qubits such as superconducting devices or trapped ions. However, there is no free lunch in quantum computation. For the same reasons it is computationally powerful it is also difficult to implement. While the two states of classical bits are protected by an energy barrier that is almost impossible to overcome involuntarily, the state of a physical qubit is described by continuous parameters and thus much more fragile: It is easily disturbed by external influence requiring extensive cooling and shielding

---

<sup>1</sup>This statement is to be taken with the obvious limitations of the lack of a theory of everything and the incompatibility with relativity.

against the environment. It also requires a precise calibration and control as possible operations are continuous as well and as such prone to small errors while the control is limited by the properties of the physical system. The readout of quantum gates is additionally subject to the projective nature of measurement. David DiVincenzo formulated a list of five criteria necessary for constructing a quantum computer, coining the understanding of a promising candidate for implementation [6].

Despite these challenges the development of quantum computers is approaching the stage of what has been called noisy intermediate sized quantum computers describing systems composed of 50 to several hundred imperfect qubits [7]. This regime is significant as it cannot be simulated classically and allows for first, possibly useful applications in quantum simulation [8]. It faces a number of additional challenges in comparison to few qubit systems: It is increasingly hard to address qubits individually or to generate interaction between specific pairs of qubits. In this work we focus specifically on the validation of quantum gates and quantum algorithms as well as their efficiency, as we discuss in part I of this thesis.

The field of quantum computation evolves around mainly two, very distinct computational models: the conventional gate-based quantum computing and adiabatic quantum computation. We implicitly assumed the former so far. While also based on qubits, the adiabatic approach encodes the solution to a computational task in the ground state of a controllable system Hamiltonian. This ground state is reached by varying the Hamiltonian adiabatically starting from a well understood and easy to control configuration [9]. Both approaches are computationally equivalent with polynomial overhead, however their conceptual differences result in unique requirements for the construction of an adiabatic quantum computer. Of particular interest is its sensitivity to the environment, which is believed to be less harmful than in the case of gate-based machines. As they are also less understood, these environmental effects are the subject of part II.

In the following we introduce a choice of relevant topics tailored towards the research presented in this thesis. For a more complete introduction we refer to respective literature. We present the basic framework to describe a quantum computer in chapter 1 including the definition of a qubit, error channels, quantum gates and quantum algorithms. In chapter 2 we introduce error correction codes, discussing how to scale up to larger systems in the context of imperfect implementation. We discuss adiabatic quantum computation in chapter 3 and we then define methods and formalisms necessary throughout this work in chapter 4.

# Chapter 1

## Basics of Quantum Information and Computation

The mathematical framework to describe a quantum computer is based on the formulation of quantum mechanics and therefore differs from the description of conventional classical computation. The field of quantum information and computation also includes a number of distinct notations and conventions which we introduce in this chapter. We give a short review of the fundamentals, tailored towards the context of this work in the following; for a more exhaustive introduction see references [10, 11].

### 1.1 The Qubit

As conventional computers rely on bits to store information, a quantum computer is built around quantum bits – qubits. While the implementation of physical qubits varies, the mathematical description of a qubit is always given by a quantum mechanical two-level system. The state vector  $|\Psi\rangle \equiv \alpha|0\rangle + \beta|1\rangle$  on the two dimensional Hilbert space  $\mathcal{H}_{n=1}$  allows for arbitrary normalized superpositions of the computational basis states  $\{|0\rangle, |1\rangle\}$  compared to the binary representation of the classical bit which is assigned either 0 or 1. However this advantage is accompanied by the challenges and restriction of controlling a quantum system. A common representation of the qubit state is given by its vector on the Bloch sphere: Up to a global phase any qubit state can be written in the form  $|\Psi\rangle = \cos(\theta/2)|0\rangle + e^{i\phi}\sin(\theta/2)|1\rangle$  with angles  $\theta \in [0, \pi]$  and  $\phi \in [0, 2\pi)$ . The identification  $(x, y, z)_{|\Psi\rangle} = (\sin(\theta)\cos(\phi), \sin(\theta)\sin(\phi), \cos(\theta))$  assigns each state a unique vector on the three-dimensional Bloch sphere and vice versa as is demonstrated in figure 1.1. The Bloch sphere representation will prove to be helpful to convey an understanding of the single qubit dynamics. In particular it can

be shown in a straightforward fashion that the  $x, y, z$ -components of the vector represent the expectation value of the respective Pauli matrices  $\sigma_X, \sigma_Y, \sigma_Z$ . This interpretation also links mixed states with vectors which do not reach the surface of the Bloch sphere. The completely mixed state  $\rho = 1/2 |0\rangle\langle 0| + 1/2 |1\rangle\langle 1|$  for example marks the center of the sphere.

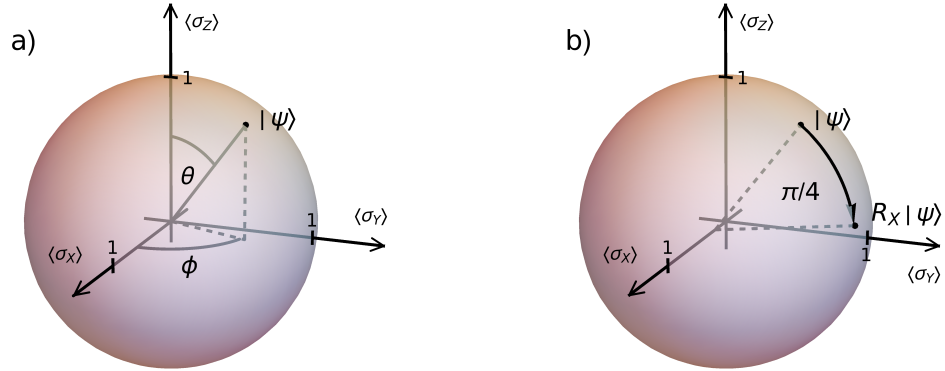


Figure 1.1: **Visualization on the Bloch sphere**

The pure state  $|\Psi\rangle = \cos(\theta/2)|0\rangle + e^{i\phi}\sin(\theta/2)|1\rangle$  is represented by a point on the surface of the sphere; its position is given by the angles  $\theta$  and  $\phi$  (a). In (b) the quantum gate  $R_X(\pi/4)$  is applied as a  $\pi/4$ -rotation around the  $\sigma_X$ -axis.

Like its classical counterpart a quantum computer is based on not one but many bits. The  $n$  qubit state vector is described on the  $2^n$  dimensional Hilbert space  $\mathcal{H}_n = \mathcal{H}_{n=1}^{\otimes n}$  and the computational basis states are given by the combinations of single qubit basis states, i.e., by  $|a_1\rangle \otimes |a_2\rangle \dots |a_n\rangle \equiv |a_1 a_2 \dots a_n\rangle$  with  $a_i \in \{0, 1\}$ . In contrast, there is no direct generalization of the Bloch sphere representation to multiple qubits.<sup>1</sup>

The readout of qubits is not fundamentally different to the projective measurement of any quantum system. Therefore it is fundamentally different from the readout of a classical bit as first only partial information can be obtained and second the state of a qubit is influenced by the measurement. Furthermore, the readout in current implementations is usually restricted to individual qubits or

<sup>1</sup>The Bloch sphere representation does rely on the correspondence of rotations in three-dimensional space and unitary operations on two-level-systems or that the Lie-algebras of  $SU(2)$  and  $\mathcal{SO}(3)$  are isomorphic. This does not transfer to higher dimensions.

even to the computational basis of those. This measurement of arbitrary operators can be realized with the help of quantum gates which will be discussed in the following section.

## 1.2 Quantum Gates

The dynamics of qubits is – as for any closed quantum system – described by a unitary operation. We define the controlled application of such a unitary operation  $U_g$  to one or several qubits as a quantum gate. While a classical single bit gate is restricted to the four possible mappings  $\{0, 1\} \rightarrow \{0, 1\}$ , it exists an infinite number of viable single qubit gates which are all unitary operations on a two-level-systems, i.e., all elements of the special unitary group  $SU(2)$ . In turn, quantum gates are restricted to being reversible due to their unitary nature. Prominent single qubit gates are the Pauli gates  $\sigma_X, \sigma_Y, \sigma_Z$ , the identity  $\mathbb{1} \equiv \sigma_0$  and the Hadamard gate

$$U_H = \begin{pmatrix} 1 & 1 \\ 1 & -1 \end{pmatrix}, \quad (1.1)$$

which maps the computational basis states onto the eigenstates of  $\sigma_X$  and vice versa. On the Bloch sphere any single qubit gate is represented by a rotation and the multiplications of unitaries maps to a concatenation of those. Specifically we find that  $R_i(\theta) = \exp(-i\theta/2\sigma_i)$  with  $i \in \{X, Y, Z\}$  implements a  $\theta$  - rotation around the corresponding axis as shown in figure 1.1.

Any combination of single qubit gates represents a multiple qubit gate via direct multiplication or rather simultaneous application to different qubits. However, these gates do not cover the full scope of gates on more than one qubit – specifically as they do not create entanglement between different qubits. The most prominent example of a two-qubit gate that is not in  $SU(2) \otimes SU(2)$  is the controlled-NOT gate

$$CNOT = \begin{pmatrix} 1 & 0 & 0 & 0 \\ 0 & 1 & 0 & 0 \\ 0 & 0 & 0 & 1 \\ 0 & 0 & 1 & 0 \end{pmatrix} \quad (1.2)$$

given in the Computational basis  $\{|00\rangle, |01\rangle, |10\rangle, |11\rangle\}$ . It inverts the second (target) qubit if the first (control) is in state  $|1\rangle$ . Other commonly used gates are *CPHASE*, *SWAP*, *iSWAP* or the Toffoli gate. Many of those are entangling gates, that is they map product onto entangled states. Specifically, as is depicted in figure 1.2, a combination of *CNOT* and the single qubit Hadamard gate maps the computational basis states onto the Bell states, the historicly most important

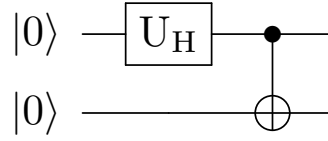


Figure 1.2: **Generating a Bell state**

The quantum circuit visualizing that the entangled Bell state  $|\Phi^+\rangle \equiv \frac{1}{\sqrt{2}}(|00\rangle + |11\rangle)$  can be obtained from the computational ground state via *CNOT* and a single qubit gate. Time runs from left to right.

examples of two-qubit entangled states [12, 13]. Entanglement is an essential prerequisite for quantum information.

A universal quantum computer is in theory able to apply any unitary operation on a set of qubits. As the implementation and even characterization of arbitrary gates has proven difficult, the current approach is to implement a universal gate set from which any unitary can be composed to arbitrary precision [14]. In order to introduce a universal gate set we first introduce a non universal set of gates: Be  $\mathcal{P}_n$  the  $n$ -qubit generalization of the Pauli group  $\mathcal{P} = \{\sigma_0, \sigma_X, \sigma_Y, \sigma_Z\}$  – which actually forms a group when disregarding global phases<sup>2</sup>. We define the Clifford group as the normalizer of the Pauli group, i.e., the set of gates mapping the Pauli group onto itself, i.e.,

$$\mathcal{C} = \{C \in \mathcal{SU}(d) | C\sigma_i C^\dagger \in \mathcal{P}_n \forall \sigma_i \in \mathcal{P}_n\}. \quad (1.3)$$

The Clifford group is of relevance for a number of applications within quantum computation. Its significance is based on a number of remarkable properties listed below.

- The *Gottesmann-Knill theorem* states that the application of Clifford group gates on computational basis states can be simulated efficiently on a classical computer, i.e., in time only polynomial in the number  $n$  of qubits [15, 16]. For the proof one relies on that  $n$  qubit states are uniquely identified by  $n$  stabilizer operators which leave the state invariant when applied to it. For the computational basis states those lie in the Pauli group. The effect of the Clifford operation can be encoded in updating those stabilizers, yielding a total computational time of order  $\mathcal{O}(n^2)$ . Although this theorem is one of the main reasons for the importance of the Clifford group, it also shows that the Clifford group does not hold the full power of quantum computation as it cannot achieve an exponential speedup compared to classical computation.

<sup>2</sup>More rigorously, one would define the Pauli group with global phases  $\pm 1$  and  $\pm i$ .

- The Clifford group is a *unitary two-design* [17]. Be  $f : (\mathcal{SU}(2^n), \mathcal{SU}(2^n)) \rightarrow \mathcal{V}$  a polynomial function of at most order two mapping two operators onto any vector space over  $\mathbb{C}$  - commonly  $\mathcal{SU}$  or  $\mathbb{C}$ . Then averaging  $f(U, U^\dagger)$  over  $U \in \mathcal{C}$  equals averaging over  $U \in \mathcal{SU}$  using the invariant Haar measure [18]:

$$\frac{1}{\#\mathcal{C}} \sum_{C \in \mathcal{C}} f(C, C^\dagger) = \int_{\mathcal{SU}} f(U, U^\dagger) dU, \quad (1.4)$$

where  $\#\mathcal{C}$  denotes the cardinality of  $\mathcal{C}$ . Corollarily, the Clifford group is also a *unitary one-design*: those equal the averaging of the Haar measure only for functions  $f$  of first order; another prominent example for one-designs is the Pauli group. The concept of unitary designs is particularly useful for the validation of quantum gates as we show in part I.

- Any gate of the Clifford group can be composed of just two single qubit gates and one two qubit gate. Specifically, *CNOT*, the Hadamard and the phase gate, which is the square root of  $\sigma_z$ , form a generating set.
- Together with any additional gate the Clifford group forms a universal gate set, i.e., a set generating  $\mathcal{SU}$ . While such a set can theoretically reach any unitary  $U \in \mathcal{SU}$  to arbitrary precision, the number of gates necessary is an important resource in the light of constraints to time as well as gate implementation. The *Solovay-Kitaev theorem* states that any generating set of  $\mathcal{SU}(d)$  containing the inverse of each element has the following property [19]. Be  $\alpha > 0$  given. Then the  $l$ -fold application of its elements forms an  $\alpha$ -net on the special unitary group with  $l = \mathcal{O}(\log^c(1/\alpha))$  and  $c \approx 4$ . An  $\alpha$ -net means that the worst error between any  $U$  and the closest element of the net is smaller than  $\alpha$ . Consequently any unitary operation can be achieved within a reasonably small number of generating gates.

From the Solovay-Kitaev theorem it is common to construct a universal gate via adding the T or  $\pi/8$  gate and its inverse, i.e.,  $\exp(\pm i\pi/8\sigma_z)$  to the Clifford group. This in fact allows for the construction of any gate to arbitrary precision. However, favorable scaling of the Solovay-Kitaev theorem in the precision defining  $\alpha$  coincides with an exponential scaling in the number of qubits. This scaling prohibits an actual implementation of quantum algorithms via the aforementioned universal gate set. For example, resource estimations show, that the implementation of a common algorithm on just a few thousand qubits would require at least in the order of  $10^{26}$  gates [20]. Finding an effective generating set for universal quantum computation however remains an open question: As any single or few qubit gate can be constructed efficiently with the Solovay-Kitaev algorithm it can not sponsor exponential speedup in comparison to the Clifford + T generating set.

Therefore, we believe that efficient generation of universal gates has to rely on multi qubit gates outside the Clifford group; the validation of those is inherently more complex which motivates chapter 6.

### 1.3 Imperfect Implementation – Error Channels

The endeavor to reliably implement quantum bits and quantum gates has sparked an entire field of research and developed a variety of approaches to quantum computation. Promising candidates for encoding qubits are found in superconducting circuits [21–25], trapped ions [26–28], Rydberg atoms [29] and semiconductors [30–33]. As this work is not tailored towards or based upon specific implementations we do not give a more detailed introduction; an overview of the different approaches and the current state of research is given in reference [34]. While the different approaches to implementation bring individual strengths and challenges, they all have in common that they are imperfect: Any implementation of a quantum gate on a physical system deviates from the ideal unitary evolution. Possible sources for errors are imperfect characterization of the two-level-system or application of changes to its Hamiltonian, as well as influence from the environment which can often be modeled as an external bath.

For the analysis of possible errors it is important to distinguish between qubit candidates that naturally consist of just two levels, such as spin 1/2 particles and those which are defined as a subspace of a larger Hilbert space, for example as the lowest levels of an altered harmonic potential. The later is prone to unwanted excitations to higher levels – an additional error source coined as leakage. As we discuss these leakage errors in detail in chapter 5, we focus on errors acting on just the two-level-system for this introduction.

We aim to treat errors on the two-level-system within the most general framework. However, we make the exception of assuming the Markov approximation as is common in the field. Typical time scales of the environment are much shorter than the time it takes to apply a quantum gate – we make this assumption throughout this work, specifically in part I where we exclusively treat Markovian errors. It is, therefore, justified to assume the bath to be independent of the qubit gate and qubit Hamiltonian at a past point in time. Hence, it is valid to trace out and discard the degrees of freedom of the bath after application of each quantum gate. Be  $U_{SB}$  the unitary evolution of combined system and bath when attempting to apply a gate  $U_{ideal}$  and  $\rho, \rho_B$  the density matrices; the dynamics of the system are given by the completely positive trace preserving map

$$\Omega_U(\rho) = \text{Tr}_B \left[ U_{SB} (\rho \otimes \rho_B) U_{SB}^\dagger \right] \quad (1.5)$$

$$\equiv \sum_k E_k \rho E_k^\dagger. \quad (1.6)$$

We introduced the operator sum representation and the Kraus operators  $E_k$  which satisfy  $\sum_k E_k^\dagger E_k = 1$  to be trace preserving. The operator sum representation combines motivation by external influence with the visualization of concrete effects to the qubits. To showcase that, we separate unitary and error channel  $\Lambda_U$  via

$$\Omega_U(\rho) = \Lambda_U(U\rho U^\dagger) \quad (1.7)$$

$$\Lambda_U(\rho) = \Omega_U(U^\dagger \rho U) \quad (1.8)$$

$$E_k \rightarrow U^\dagger E_k \quad (1.9)$$

where a single  $E_k = \mathbb{1}$  represents the ideal evolution. We will review a number of single qubit error channels with respect to the operator sum representation, error sources but also the representation on the Bloch sphere.

The bit flip error translates directly from its classical counterpart which is however virtually limited to data transfer as classical bits are protected by a sufficiently high energy barrier. With  $E_1 = \sqrt{1-p} \mathbb{1}$  and  $E_2 = \sqrt{p} \sigma_X$  it causes a switch of the computational ground states, i.e., the application of  $\sigma_X$  with probability  $p$ .

$$\Lambda_{\text{bit flip}}(\rho) = 1 - p \rho + p \sigma_X \rho \sigma_X \quad (1.10)$$

The Kraus operators do not only define the error channel but may provide hints towards possible error mechanisms. The bit flip error is characterized by the  $\sigma_X$  operator, it may be caused by a coupling to the environment of similar form. Similarly a coupling via  $\sigma_Z$  and miscalibration of or fluctuations in the qubit frequency are known to result in  $\sigma_Z$  Kraus operators. We define the corresponding phase flip or dephasing channel as  $E_1 = \sqrt{1-p} \mathbb{1}$ ,  $E_2 = \sqrt{p} \sigma_Z$  which weakens phase relation between the computational states. The bit-phase flip channel with  $E_2 = \sqrt{p} \sigma_Y Z$  combines the above effects. We see from the effects on the Bloch sphere depicted in figure 1.3 that this class of error channels leaves the eigenstates of its defining Pauli matrices invariant while affecting the eigenstates of the other Pauli matrices the most.

Accompanying the application of quantum gates a qubit is prone to all possible error channels, the effects of which are also highly dependent on the applied gates – e.g. a bit-flip in between Hadamards translates to a phase flip and vice versa. When left alone, the primary error source of a qubit is often the dissipation of energy over time into the environment which pushes the qubit towards the ground state  $|0\rangle$ . While this mechanism can be used to reset the qubit to the ground state, it is also erroneous to the effort of preserving a quantum state. Its occurrence is quantified by the relaxation time  $T_1$ , which originates from nuclear magnetic

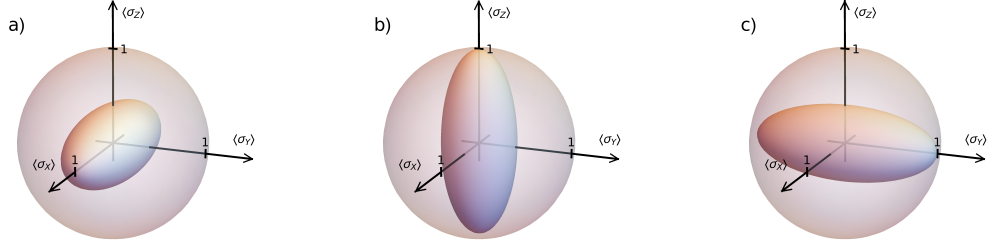


Figure 1.3: **Visualization of different error channels I**

We see the transformation of the Bloch sphere under bit flip (a), phase flip (b) and bit-phase flip (c). Each error occurs with probability  $p = 30\%$ . The space of density matrices is confined to ellipsoids; former pure states lie on the surface thereof.

resonance and is often used to describe the maximum coherence time of qubit candidates. We define amplitude damping via

$$\{E_k\} = \left\{ \begin{pmatrix} 1 & 0 \\ 0 & \sqrt{1-\gamma} \end{pmatrix}, \begin{pmatrix} 0 & \sqrt{\gamma} \\ 0 & 0 \end{pmatrix} \right\}; \quad (1.11)$$

it is visualized in figure 1.4. Note that for finite temperature the error channels also incorporate transitions to the excited state which causes a slightly more complex error channel and a stationary state which is not the ground state but a mixed state determined by Boltzmann factors.

The importance of another single qubit error channel is given not by its correspondence to classical errors or prominent occurrence in physical systems but rather by its convenient mathematical properties. We define the completely depolarizing channel such that a density matrix is mapped onto the totally mixed state (i.e. completely depolarized) with probability  $p$  and left untouched otherwise. It is described by

$$\Lambda_{\text{dep}}(\rho) = (1-p)\rho + p\frac{\mathbb{1}}{2}. \quad (1.12)$$

The completely depolarizing channel is unique in that it is invariant under unitary transformation and affects any state equally, which will prove useful in the following. It is also easily transferred to multiple qubits.

We have discussed a number of single qubit error channels. The quantification of their occurrence does not only convey how faithful a quantum gate is implemented but also hints towards underlying error mechanisms. Their experimental

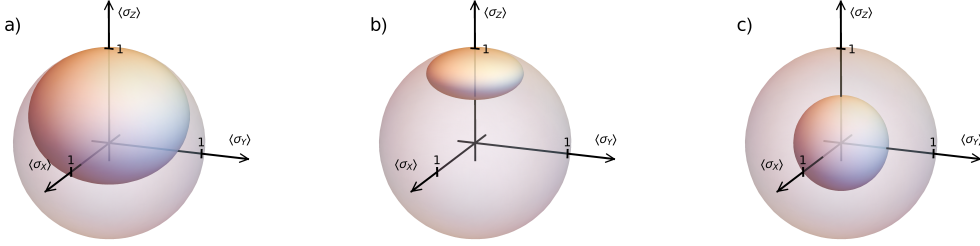


Figure 1.4: **Visualization of different error channels II**

The evolution of the Bloch sphere under amplitude damping for  $\gamma = 30\%$  and  $\gamma = 75\%$  is shown in a) and b) respectively. We see a push towards the ground state hence the deformed sphere is no longer centered around the origin. c) visualizes a depolarizing channel of  $p = 50\%$  simply shrinking the Bloch sphere. This channel is unique in that it is invariant under any unitary transformation.

identification is therefore useful not only for validation but also improvement of gates. The characterization of two or more qubit error channels, however, is much more complex due to the missing Bloch sphere representation and an exponentially growing Hilbert space with  $8^n$  parameters to describe linear maps on density matrices.

To treat such error channels we refrain from a detailed characterization but rather derive an accessible metric for how close  $\Lambda$  is to the identity, hence, how close the quantum channel  $\Omega$  is to the desired unitary  $U$ . We define the average fidelity as the average overlap of pure states with themselves after application of  $\Lambda$ .<sup>3</sup>

$$\Phi(\Lambda) = \int_{\rho} \text{Tr} [\Lambda(\rho)\rho] \quad (1.13)$$

$$= \int_{SU(d)} \text{Tr} [\Lambda(U\rho_0U^\dagger)U \rho_0U^\dagger] dU \quad (1.14)$$

$$= \text{Tr} \left[ \int_{SU(d)} U^\dagger \Lambda(U\rho_0U^\dagger)U dU \rho_0 \right] \quad (1.15)$$

where the Haar integration over the special unitary group implements an averaging

---

<sup>3</sup>The overlap between two density matrices  $\sigma$ ,  $\rho$  is defined as  $\Phi(\rho, \sigma) = \text{Tr} \left[ \sqrt{\sqrt{\sigma}\rho\sqrt{\sigma}} \right]^2$  which simplifies to the form in equation 1.13 if at least one of the density matrices is pure.

over all pure states in the  $d = 2^n$ -dimensional Hilbert space. The density matrix  $\rho_0$  can be chosen to represent any pure state. For consistency with the following, we set  $\rho_0$  to the ground state which is often the default preparation in implementations. It is sufficient to average pure states due to the facts that quantum computation is designed for those. While physical implementations deviate from the designated unitary evolution and inevitably incorporate mixed states, they do not deviate by much as to be considered eligible for quantum computations. We simply are less concerned with the fidelity of very bad gates. The fidelity  $\Phi$  assumes values in  $[0, 1]$ , it is invariant to change of the reference system via the Haar measure and it uniquely peaks for  $\Lambda$  being the identity channel.

We note that quantum channel  $\Lambda_{\text{twirl}}(\rho) = \int_{SU(d)} U^\dagger \Lambda(U\rho U^\dagger) U \, dU$  that is emerging in equation 1.15 also inherits the invariance to system transformations from the Haar measure. It is a completely depolarizing channel and defines the twirl of  $\Lambda$  over the special unitary group [17]. That it coincides with the twirl over the two-design  $\mathcal{C}$  will have impact in part I.

The quantity  $\Phi$  does not give the exact probability of successful application of a gate to any specific but rather to the average of all viable states. Therefore, its usefulness to assess the single application of a gate is limited. Typically, however, quantum gates are not applied in an isolated setting but part of a quantum algorithm comprised of many gates – as discussed in the following section. The complexity of these algorithms is characterized by the number of qubits  $n$  and the number of consecutive gates – the depth  $l$ .<sup>4</sup> For all but very small  $n$  and  $l$  this implies a large number of gates and therefore the average fidelity of the individual gates can be used to assess the success probability of the algorithm. That is because deviation from the average fidelity is averaged out for all but fringe cases of coherent interference between a major subset of the error channels. Hence,  $\Phi$  is a valid quantity to describe the implementation of a quantum gate.

## 1.4 Quantum Algorithms

The reason engineering a quantum computer is pursued, is its theoretical potential to outperform a classical computer and even to perform computations that cannot be done on a classical computer with all resources accessible to humankind. With qubits being vastly more fragile and costly to produce and maintain than the classical bit, this advantage can only be achieved via a favorable scaling in the problem size. Various algorithms have been proposed: Shor's algorithm can factorize an integer  $N$  in polynomial time in  $\log(N)$  which is polynomial in the number of qubits

---

<sup>4</sup>This is true only when considering a limited set of accessible gates: Defining the unitary representation of a quantum algorithm as a gate yields  $l = 1$  in any case.

necessary to represent the integer while the best known classical algorithm, the general number field sieve, takes sub-exponential but super-polynomial time in  $N$  [4, 35, 36]. The Grover algorithm can search unsorted databases in  $\mathcal{O}(\sqrt{N})$  time compared to  $\mathcal{O}(N)$  calls in any classical algorithm [5]. In this section we showcase the potential of quantum computation at the example of the Deutsch-Josza algorithm [3, 37, 38].

The Deutsch-Josza algorithm is a quantum algorithm to determine whether a function  $f$  is balanced or constant. We assume a function  $f : \{0, 1\}^n \rightarrow \{0, 1\}$  to be either constant 0/1 with  $f(x) = 0/1 \forall x \in \{0, 1\}^n$  or balanced with  $f(x) = 0$  for exactly half of the elements in  $\{0, 1\}^n$ . While this problem still lacks practical applications it is considered to having laid the foundation for the previously mentioned algorithms.

To access any information about the function  $f$  with a quantum algorithm it is inevitable that it can be called as a unitary operation. We therefore assume to be given the black-box  $(n + 1)$ -qubit gate  $U_f$ , defined to flip an additional target qubit if  $f(x) = 1$ , i.e.

$$U_f |x\rangle |y\rangle = |x\rangle |y +_2 f(x)\rangle, \quad (1.16)$$

with  $y \in \{0, 1\}$  and  $+_2$  denoting addition modulo 2. The concept of a black-box is prevalent in (quantum) information theory. However, its implementation is nontrivial. Nonetheless we assume to have access to both the classical and quantum version and compare the algorithms by the number of calls of  $f$ .

We review the quantum algorithm which is given by

1. Initialize the state  $|\Psi_0\rangle = |0\rangle^n |1\rangle$ .
2. Apply Hadamard gates to all qubits.
3. Call the black-box operator  $U_f$ .
4. Apply Hadamard gates to all qubits.
5. Measure the first  $n$  qubits in the computational basis.

The quantum circuit is depicted graphically in figure 1.5. We compute the state  $|\Psi\rangle$  throughout the circuit.

$$|\Psi_0\rangle = |0\rangle^n |1\rangle \quad (1.17)$$

$$\xrightarrow{2.} |+\rangle^n |-\rangle \quad (1.18)$$

$$= \frac{1}{\sqrt{2^n}} \sum_{x \in \{0,1\}^n} |x\rangle \frac{|0\rangle - |1\rangle}{\sqrt{2}} \quad (1.19)$$

$$\xrightarrow{3.} \frac{1}{\sqrt{2^n}} \sum_{x \in \{0,1\}^n} |x\rangle \frac{|0 + f(x)\rangle - |1 + f(x)\rangle}{\sqrt{2}} \quad (1.20)$$

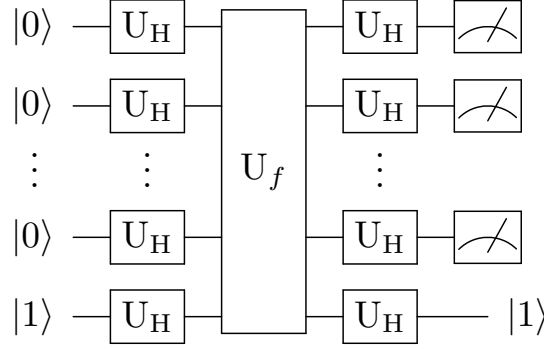


Figure 1.5: **Circuit of the Deutsch-Josza algorithm**

The quantum circuit to implement the Deutsch-Josza algorithm consists of Hadamard gates, a single call of the oracle  $U_f$  and measurement of the first  $n$ -qubits.

$$= \frac{1}{\sqrt{2^n}} \sum_{x \in \{0,1\}^n} (-1)^{f(x)} |x\rangle |-\rangle \quad (1.21)$$

$$\stackrel{4.}{\rightarrow} \frac{1}{\sqrt{2^n}} \sum_{x \in \{0,1\}^n} (-1)^{f(x)} U_H^{\otimes n} |x\rangle |-\rangle \quad (1.22)$$

$$= \frac{1}{2^n} \sum_{x \in \{0,1\}^n} (-1)^{f(x)} \sum_{z \in \{0,1\}^n} (-1)^{x_i z_i} |z\rangle |-\rangle \quad (1.23)$$

$$= \frac{1}{2^n} \sum_{x,z \in \{0,1\}^n} (-1)^{f(x) + x_i z_i} |z\rangle |-\rangle \quad (1.24)$$

We use the Einstein notation for the scalar product of  $x$  and  $z$  in the application of the second Hadamards which can be derived in a straightforward fashion. While not obvious at first sight, the final state in equation 1.24 does distinguish constant and balanced  $f$  with certainty. One way to demonstrate this is to investigate the probability to measure 0 in the first  $n$  qubits. The probability amplitude amounts to

$$\frac{1}{2^n} \sum_{x \in \{0,1\}^n} (-1)^{f(x)}. \quad (1.25)$$

This amplitude sums up to 0 for balanced functions as the summands are evenly split between 1 and -1 while for constant  $f$  equation 1.25 is either 1 or -1. Therefore measuring all qubits in 0 equals a constant and any other outcome a balanced function. As any classical algorithm can only test one  $f(x)$  per black-box call, it needs at least  $2^{n-1} + 1$  queries to verify a constant function and hence, as the

Deutsch-Josza algorithm requires a single call, it shows a fundamental advantage of quantum processing.

Note that the  $(n + 1)$ th qubit does a no point during the algorithm change its state non trivially or hold any information about  $f$  but is only used to apply the phase to certain states  $x$ . Such qubits are denoted ancilla qubits. Note also that the mentioned algorithms of Shor, Grover and Deutsch-Josza are just a small subset of quantum algorithms; for example quantum simulations using quantum systems to emulate other quantum systems form an open field of research with many promising candidates for useful applications on medium sized quantum computers. As it is however not the main focus of this work we leave an overview to references [39, 40].



# Chapter 2

## Scaling and Fault Tolerance

Despite the potential of quantum technologies, their usefulness only comes into play for a nontrivial number of qubits and gates. While algorithms as presented in the previous chapter typically require larger quantum computers than quantum simulations to surpass the capability of classical machines, this threshold is bound around 50 qubits by the maximum number to be simulated on a classical computer [41]. Implementing any computation on a quantum computers that a classical computer cannot solve has been coined quantum supremacy [42, 43]. Furthermore, noisy intermediate-scale quantum computers of 50 to 100 qubits are expected to be available in the next decade [7].

It is therefore necessary for any contemporary implementation to involve a strategy for scaling up in the number of qubits. This scalability of quantum systems poses nontrivial challenges to quantum architectures. Some of those challenges involve the arrangement of qubits in a way that allows for individual addressability when facing frequency crowding [44]; at the same time one aims to allow for as much connectivity as possible between different qubits and still avoid cross talk, i.e., involuntarily addressing one qubit while trying to implement a gate on one or several others. Those requirements are to be met with as little as possible resource investment per qubit – costs that are perfectly reasonable for a one or few qubit prototype may not be for a scaled up machine. The same reasoning applies to imperfect quantum gates: While the average error of a single gate is continuously improved upon and becomes more and more negligible [45, 46], for an increasing number of qubits and gates in a quantum circuits those errors amplify. In this chapter we introduce the control of error propagation via quantum error correction schemes.

Quantum error correction is unique to some extent. It poses a much broader range of challenges compared to classical error correction, which is mainly limited to data transfer as classical bits are protected by an energy barrier so large that it makes tunneling virtually impossible. While classical error correction can be

simplified as redundancy and majority vote as for the (3,1)-Hamming code [47], it cannot be transferred to qubits for several reasons. First it is impossible to create additional copies of a quantum state due to the unitary nature of evolution; this is known as the no-cloning theorem [48–50]. Second qubit measurement disturbs the quantum state and third quantum error channels are not restricted to simple bit flips but can be much more complex due to the continuity of quantum states. Subsequently quantum error correction gives rise to an interesting sub field of quantum information theory, generating various schemes to control quantum errors.

Initially we review a toy model of a single qubit in a state  $|\Psi\rangle = \alpha|0\rangle + \beta|1\rangle$  which is only subject to bit flip errors at given probability  $p$ . It is close to the classical case and can be solved by the three qubit bit flip code as is presented in figure 2.1 [10]. The idea is to encode the logical state  $|\Psi\rangle$  in the three qubit state  $|\Psi_{\text{enc}}\rangle = \alpha|000\rangle + \beta|111\rangle$  using *CNOT*s to differentiate the basis states – even after a single bit flip. It is straightforward to show that the error correction after the application maps  $\{|000\rangle, |001\rangle, |010\rangle, |011\rangle\}$  onto  $|\Psi'\rangle = |0\rangle$  and  $\{|111\rangle, |110\rangle, |101\rangle, |011\rangle\}$  onto  $|\Psi'\rangle = |1\rangle$  respectively. Consequently one shows  $|\Psi\rangle = |\Psi'\rangle$  for zero and one bit flips.

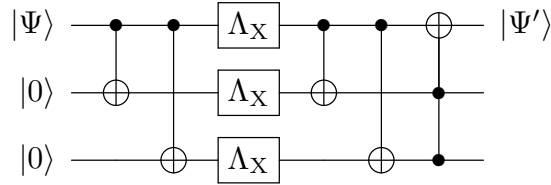


Figure 2.1: **Circuit of the three qubit bit flip code**

A single logical qubit is encoded in three physical qubits. Due to post  $\Lambda_X$  error correction we find  $|\Psi'\rangle = |\Psi\rangle$  for no or just one qubits flipped.

The three qubit bit flip code effectively changes the probability of flipping the logical qubit to that of flipping either two or three of the physical qubits, i.e.  $3p^2(1-p) + p^3$ . We define the error threshold at  $p = 1/2$  as it marks the minimum fidelity necessary to improve the fidelity of the logical state using this error correction scheme. It is important to note that the above scheme assumes the possible error to happen at a specific point during the circuit, it does not account for imperfect encoding and decoding gates or error channels on multiple qubits. Furthermore it does not correct phase errors; however, as those are just bit flips in the  $\sigma_X$  basis, they can be treated by the phase flip code as presented in figure 2.2. We note that, in turn, the phase flip code is susceptible to bit flips again. To account for both one can straightforwardly encode each of the three

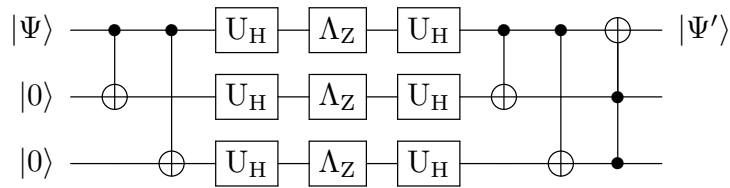


Figure 2.2: **Circuit of the three qubit phase flip code**

The additional Hadamard gates allow for the correction of phase flip instead of bit flip errors. The logical qubit is encoded as  $|\Psi_{\text{enc}}\rangle = \alpha |+++ \rangle + \beta |-- - \rangle$ .

qubits of the phase flip with the bit flip code or vice versa – this is known as the nine qubit Shor code [51]. As a  $\sigma_Y$  or bit phase flip error is just a combined bit and phase flip error the Shor code does account for those as well as all single qubit errors consequently. While it arises naturally it is not the most efficient method to encode against single qubit errors. For instance the Steane code does so only using seven physical qubits [52], the optimal number is five [53].

Although these error correction schemes can be concatenated to further improve the fidelity of a single logical qubit, they are known to suffer from several shortcomings that limit the viability in physical settings. As presented above they do not account for imperfect implementation of the encoding single and multi qubit gates or state preparation and measurement; they do not include gates on and between logical qubits. While these restrictions are addressable, they do severely impact the error threshold.

A different approach, aiming for a higher error threshold, is given by topological quantum error correction codes such as the surface code [54–56]. These protocols encode logical qubits using topological properties of their arrangement and interaction of an array of qubits. In contrast to the error correction schemes presented above topological error correction typically relies only on interaction between neighboring qubits. The surface code, as the name suggests, encodes its logical qubits on a two dimensional surface comprised of a two dimensional array of physical qubits.

In this introduction we do not focus on the detailed implementation of topological error correction to review papers such as reference [57] and focus on the mathematical formulation of an error corrected system, which is necessary in the context of chapter 7. As for any error correction code (ECC), a set of  $n + m$  physical qubits is used to encode just  $n$  logical qubits which then are accessible for quantum computation with higher fidelity. The full Hilbert space can be written as  $\mathcal{H} = \{0, 1\}^{\otimes n} \otimes \{0, 1\}^{\otimes m}$  – where the first  $n$  describe the logical qubits – via a unitary transformation given by the topological properties of the ECC. For the

surface code this, for example, translates to identifying the  $\sigma_X$  on a logical with a string of  $\sigma_X$  on several physical qubits. Generally, this transformation is constructed to map the most common single and few qubit errors onto more complex channels affecting both factors of the Hilbert space. Therefore, preparing the state in the last  $m$  qubits to a known quiescent state  $|\Psi_s\rangle$  allows to track and correct those errors via repeated syndrome measurement in the  $m$  ancilla qubits.

# Chapter 3

## Adiabatic Quantum Computation

In this chapter we discuss an approach to leveraging quantum systems for a computational purpose that is quite distinct from the standard gate-based model. Adiabatic quantum computation (AQC) aims to encode the solution to a computational problem in the ground state of a controllable quantum system. When changing the system prepared in the easy-to-reach ground state of a well understood initial Hamiltonian to the encoding target Hamiltonian sufficiently slowly, the evolution follows the instantaneous ground state as described by the adiabatic theorem [58]. AQC was first introduced as an optimization scheme [59] and coined as quantum annealing [60]. Remarkably, this inspired the optimization via simulated quantum annealing [61, 62] before the transition to a general computational context [63] and the proof that AQC can be as powerful as gate-based quantum computing [64]. We give a short introduction prioritizing topics by relevance for this work in the following; a more in depth overview is given in reference [9].

To formally define AQC we need to introduce the concept of  $k$ -locality: A Hamiltonian is considered  $k$ -local if all of its terms are acting nontrivially on at most  $k$  qubits. We then define  $H_0$  and  $H_1$  as the initial and target  $k$ -local,  $n$ -qubit Hamiltonians of a quantum system. We demand the initial ground state to be unique as well as to be a product state to allow for its efficient preparation. We define the annealing schedule a map  $s : [0, t_f] \rightarrow [0, 1]$  satisfying  $s(0) = 0$  and  $s(t_f) = 1$  so that the time dependent Hamiltonian is defined as  $H(s(t)) = (1 - s)H_0 + sH_1$  for all times  $t \in [0, t_f]$ .<sup>1</sup> The adiabatic theorem [58] states that for infinitely slow variation of  $s$ , i.e.,  $t_f \rightarrow \infty$ , the time evolution follows the ground state of  $H(s)$  and hence the final state is the ground state of  $H_1$ . Be  $1 - \varepsilon$  the overlap between target and output state for a given finite  $t_f$ .

Specification of efficiency is crucial for comparison with classical as well as

---

<sup>1</sup>Depending on the specific setting it can be beneficial to introduce an intermediate catalyst Hamiltonian for  $0 < s < 1$  [64].

gate-based algorithms. The cost of running an algorithm with maximum error  $\varepsilon$  is commonly defined as

$$K(\varepsilon, s) = t_f \max_s \|H(s)\|. \quad (3.1)$$

This definition is invariant under rescaling of the Hamiltonian as for multiplication of  $H(s)$  with any factor, dividing  $t_f$  by that factor results in the same  $\varepsilon$ ; it is therefore independent of the physical implementation. Assuming the order of magnitude of the Hamiltonian is limited the cost  $K$  directly corresponds to the run time  $t_f$ . The minimum eigenvalue gap  $\Delta$  between ground and first excited state is an indicator for the minimal run time which scales as  $1/\Delta^3$  or even  $1/\Delta^2$  for a more optimized schedule [65, 66]. Therefore, the efficiency of an adiabatic quantum algorithm in comparison with classical and gate-based counterparts is given by the scaling of the minimal gap.

Note that the above reasoning assumes a perfectly closed quantum system which is per se invalid for any physical device. As for gate-based quantum computation the qubit state is affected by imperfect implementation and external degrees of freedom. AQC is believed to be less sensitive against coupling to an environment or even benefit from that via thermal relaxation back into the ground state after an unwanted excitation. Those effects are studied comparatively little and still pose open questions. We will address environmental effects on AQC in part II.

### 3.1 Universality of AQC

Similar to the concept of universal gate sets the goal for an adiabatic quantum computer is to be able to access any target state as efficient as possible. We define a universal adiabatic quantum computer as follows [9]: Any quantum circuit of depth  $L$  represented by its unitary evolution  $U$  and its initial state  $|\Psi_0\rangle$ . The annealing Hamiltonian  $H(t)$  is universal if it reaches the target state  $U|\Psi_0\rangle$  to arbitrary precision with annealing qubits  $n_a$  scaling at most polynomial in the number  $n$  qubits of the algorithm and  $t_f$  is polynomial in  $n$  and  $L$ . Specifically it was shown that adiabatic evolution with two-local Hamiltonians is universal [67].

Note that adiabatic universality is based on that of gate sets. In fact it has been shown that the power and complexity of adiabatic and circuit-based quantum computation is equivalent up to polynomial overhead [64, 68, 69]. We present the key ideas to prove that one quantum computer can efficiently simulate the other. An adiabatic evolution  $U_a$  is unitary and can hence be implemented via a universal gate set. To do so we approximate the time evolution using a piecewise constant

Hamiltonian given by the annealing schedule, i.e.

$$U_a \approx \prod_{m=M}^1 \exp[-i\Delta t H(m\Delta t)] \equiv \prod_{m=M}^1 U_m \quad (3.2)$$

For small enough time slices  $\Delta t = t_f/M$  each unitary step is close to the identity and can be approximated as  $U_m \approx \mathbb{1} - i\Delta t H(m\Delta t)$  omitting quadratic terms in the time slices. A  $k$ -local Hamiltonian is always composed as a sum of terms coupling at most  $k$  qubits and can be written in the form  $H = \sum_l H_l$ . Still relying on the limit of small  $\Delta t$ , we can further approximate

$$U_m \approx \mathbb{1} - i\Delta t \sum_l H_l(m\Delta t) \quad (3.3)$$

$$\approx \prod_l (\mathbb{1} - i\Delta t H_l(m\Delta t)) \quad (3.4)$$

$$\approx \prod_l \exp(-i\Delta t H_l(m\Delta t)), \quad (3.5)$$

where the the individual terms of the Hamiltonian can be treated as separate gates acting on at most  $k$  qubits. Those gates can be implemented efficiently via the Solovay-Kitaev algorithm as discussed in chapter 1. Consequently the annealing schedule can be simulated via a gate-based quantum algorithm.

Showing the opposite direction is less straightforward and we are discussing the idea of proof of the original derivation [69]. While we can assume that any circuit consists of one- and two-qubit gates and acts on the  $n$ -qubit ground state, the ordering of their application – the emulation of time – proves difficult. To do that we introduce  $L$  ancilla qubits with  $L$  the total number of consecutive gates, i.e. the depth of the quantum algorithm. We define the history state  $|\Psi_a(l)\rangle = |1_1, \dots, 1_l, 0_{l+1}, \dots, 0_L\rangle$  to represent the point in time after the application of the  $l$ -th gate  $U_l$ . The ancillary space can be confined to this form by introducing a penalty. The application of  $U_l$  is implemented by coupling  $|\Psi_a(l-1)\rangle$  and  $|\Psi_a(l)\rangle$ , as is achieved by terms of the form

$$-U_l |\Psi_a(l)\rangle \langle \Psi_a(l-1)| + \text{h.c.} \quad (3.6)$$

Following this concept, it can be shown to enable efficient simulation of the evolution of a gate-based on an adiabatic quantum computer [64]. Consequently the computational power of both approaches to quantum computation is – in theory – equivalent.

## 3.2 The adiabatic Deutsch-Josza Algorithm

As we have done for the gate-based approach in chapter 1 we highlight the concept of AQC by presenting the adiabatic version of the Deutsch-Josza algorithm [70]. To do so, we revisit the function  $f : \{0, 1\}^n \rightarrow \{0, 1\}$  which is promised to be either balanced or constant. Again aiming to distinguish those possibilities with minimal number of calls of the function, we set our initial and target Hamiltonian to be

$$H_0 = 1 - |\Psi_+\rangle\langle\Psi_+| \quad (3.7a)$$

$$H_1 = 1 - |\Psi_f\rangle\langle\Psi_f| \quad (3.7b)$$

with

$$|\Psi_+\rangle = |+\rangle^n, \quad (3.8)$$

$$|\Psi_f\rangle = \frac{\mu}{\sqrt{N/2}} \sum_{i=0}^{2^{n-1}-1} |2i\rangle + \frac{1-\mu}{\sqrt{N/2}} \sum_{i=0}^{2^{n-1}-1} |2i+1\rangle, \quad (3.9)$$

$$\mu = \frac{1}{N} \left| \sum_{x \in \{0,1\}^n} (-1)^{f(x)} \right|. \quad (3.10)$$

We find that  $\mu$  vanishes for a balanced function, as we sum over an equal number of +1 and -1 summands, while it is 1 for constant  $f$ . Consequently  $|\Psi_f\rangle$  is a superposition of all even or all odd states if  $f$  is balanced or constant, respectively. This can be differentiated by a single measurement in the computational basis revealing an even or odd state. The implementation of the target Hamiltonian can be seen as the equivalent to the black-box unitary  $U_f$  of the gate-based algorithm. To control the annealing time  $t_f$ , we use that for an annealing Hamiltonian of the form of equations 3.7 the minimal energy gap has a lower bound in the overlap of the defining states [71]. As  $\langle\Psi_+|\Psi_f\rangle = 1/\sqrt{2}$ , energy gap and annealing time are constant in  $n$ , duplicating the performance of gate-based quantum computing.

Both complexity theory as well as the implementation of a specific task do not show a fundamental advantage of either gate-based or adiabatic quantum computing despite the vastly different approaches. Which of those approaches, if any, will prove to be suitable to build large universal quantum computer will depend on strategies for a faithful, scalable and universal physical implementation.

# Chapter 4

## Methods and Formalisms

In this chapter we give a non exhaustive review of methods and formalism that are important in the presentation of the results of this thesis. It is tailored specifically towards the scope of this thesis.

### 4.1 Normal Ordering

Normal ordering is a convention to efficiently describe operations comprised of creation and annihilation operators commonly used in quantum field theory [72]. The idea is to divide an operator  $O$  into its expectation value and fluctuation with respect to a reference state  $|\Psi_{\text{no}}\rangle$  describing the entire Hilbert space. To define normal ordering more rigorously we introduce the contraction

$$c_{kl} \equiv \langle \Psi_{\text{no}} | A_k A_l | \Psi_{\text{no}} \rangle \quad (4.1)$$

with  $A_k$  and  $A_l$  being either raising or lowering operators.<sup>1</sup> Denoted by  $: O :$ , normal ordering of the operator  $O$  is then defined by the following rules:

1. Scalars are invariant under normal ordering.

2. Normal ordering is linear.

3.  $A_k : O : = : A_k O : + \sum_l c_{kl} : \frac{\partial O}{\partial A_l} :$

When normal ordering with respect to the vacuum state, we witness remarkable properties. First, the expectation values of every normal ordered non constant operator vanishes as second normal ordering with respect to the vacuum can be

---

<sup>1</sup>The contraction could be defined in a more general way e.g. as expectation value of a mixed state as long as  $[A_k, A_l] = c_{kl} + c_{lk}$  is satisfied, which is, however, not necessary for the scope of this work.

simplified to writing creation operators to the left and annihilation operators to the right. Consequently the normal ordered operator with respect to the vacuum can be understood to only describe the vacuum fluctuations.

## 4.2 The Perron-Frobenius Theorem

Be  $M$  a positive square matrix, with positive referring to individual matrix entries. Then the *Perron-Frobenius theorem* [73–75] states that there is a unique positive eigenvalue  $\lambda_1$  which is called the Perron root and fulfills  $\lambda_1 > |\lambda_i|$ , for all other eigenvalues  $\lambda_i$ . Furthermore, all entries of the corresponding eigenvector are positive themselves. In the case of non-negative matrices, the theorem converts to  $\lambda_1 \geq |\lambda_i|$  and that eigenvector has non negative entries.

## 4.3 Statistical Inequalities

While standard deviation and variance are valid estimators of how precise the measurement of probabilistic quantities is, they do not directly provide a probability  $\delta$  of a distribution deviating more than an accuracy  $\alpha$  from the actual expectation value. Such estimations are given Hoeffding's and Chebyshev's inequalities which are introduced here [76, 77].

The Chebyshev or Markov's inequality limits probability of deviating from the expectation value based on the variance. Be  $Z$  a probabilistic variable with expectation value  $[Z] = \mu$  and variance  $\sigma$ . Then

$$\Pr\left(|Z - \mu| \geq \frac{\sigma}{\sqrt{\delta}}\right) \leq \delta. \quad (4.2)$$

In the case when a probability distribution is limited to an interval  $[a, b]$  it can be more feasible to rely on *Hoeffding's inequality* instead: Be  $S$  the sum of random variables  $Y_i$  which are situated in an interval  $[a_i, b_i]$ . Then, the inequality limits

$$\Pr(|S - \langle S \rangle| \geq \alpha) \leq 2\exp\left(-\frac{2\alpha^2}{\sum_i (b_i - a_i)^2}\right). \quad (4.3)$$

It is particular powerful in cases only two possible outcomes such as the measurement of a single qubit or the overlap of two states.

# Part I

## Randomized Benchmarking



As quantum gates are the fundamental parts of any quantum circuit, a quantum computer relies on their experimental implementation being a faithful representation – or at least a close approximation – to the ideal unitary. In fact, circuit-based machines are often compared primarily by their gate fidelities and the improvement of these is a major task in engineering a quantum computer, involving for instance optimal control theory. It is therefore essential to access the fidelity of any gate as efficiently and as reliably as possible. This task is non trivial. As the range of possible error channels is given by completely positive trace preserving maps the complete characterization via direct measurement, which is known as quantum process tomography, requires exponentially many resources ( $\mathcal{O}(2^{8n})$ )[78]. It is therefore impractical for more than one qubit and does not differentiate between gate errors and those associated with state preparation and measurement (SPAM). As in most contemporary physical implementations, the latter at least match gate errors, they potentially mask it completely.

Randomized Benchmarking (RB) is a scalable protocol to characterize the average gate fidelity of the Clifford group or any unitary two-design in time polynomial in  $n$  via validation of random gate sequences [79, 80]. Due to error amplification it does so irrespective of SPAM errors. The validation of individual Clifford gates is realized by interleaving the gate into the sequence [81]. In chapter 5 we give a short overview over Randomized Benchmarking, including an alternate formalism to describe RB which proves robustness of RB against gate dependent error channels and leakage. The Clifford group  $\mathcal{C}$  relies on additional gates to form a universal gate set – likely more than just single qubit gates are needed for efficient generation of universal evolution. It is therefore necessary to benchmark arbitrary gates as efficiently as possible. In chapter 6 we present a protocol for Interleaved RB of arbitrary quantum gates using Monte Carlo sampling of quantum states. It preserves key advantages of Randomized Benchmarking such as error amplification and independence from SPAM errors. The protocol still scales exponentially in the number of qubits, however, it is superior to direct Monte Carlo sampling, as well as process tomography. To avoid exponential scaling, we present a symmetry benchmarking protocol in chapter 7 that extracts the preservation of algorithm specific symmetries rather than gate fidelities. It does so via gate sequences of a unitary one-design engineered for the specific symmetry. We demonstrate its application in polynomial time for examples originated in quantum simulation.



# Chapter 5

## Introduction to Randomized Benchmarking

As discussed in chapter 1 any physical implementation of a quantum gate does not represent the intended unitary evolution perfectly and hence it introduces an error. To quantize this imperfection, we revisit the average fidelity  $\Phi$  of a quantum channel as described in equation 1.15, which provides a measure on how well a quantum channel is implemented, i.e. how close its associated error channel  $\Lambda$  is to the identity. This value, however, is not directly accessible; several challenges making its extraction far from trivial.

We have seen that any error channel  $\Lambda$  is represented by a completely positive trace preserving linear map on density matrices and as such is defined by  $\mathcal{O}(2^{4n})$  parameters. The original approach to extract the average fidelity is based on the complete characterization of the full quantum channel via quantum process tomography (QPT). To do that, one has to choose  $d^2$  pure states meeting two criteria: First, the density matrices of those form a basis for density matrices of the qubit Hilbert space  $\mathcal{H}$  and second, they can be prepared in the investigated quantum system. A full channel characterization in turn requires the characterization of each of those states after being subject to the quantum channel by exhaustive measurement of a complete basis set, known as quantum state tomography. Although the average fidelity can be extracted using this technique, it is highly inefficient since one has to extract much more information than is actually requested. Apart from the exponential scaling in the number of qubits, QPT is sensitive to SPAM errors which, as discussed, often equal or surpass those of individual gates.

There have been several approaches to improve upon the efficiency of fidelity

---

This chapter contains original work by T.C. which was part of his masters thesis "Robust Characterization of Quantum Gates via Randomized Benchmarking" (2015). In particular section 5.3 is a short version of the publication "T. Chasseur and F.K. Wilhelm, Phys. Rev. A **92**, 042333 (2015)". Copyright (2015) by the American Physical Society.

extraction. Compressed sensing for example provides full tomography with exponential speedup in comparison to standard QPT or state tomography in the respective tasks, while still scaling exponentially in the number of qubits [82]. It is, however, limited to specific states of low rank such as states only affected by local errors or transitions between these when regarding process characterization. While local errors can be assumed to dominate in certain scenarios we do not limit ourselves to those cases for the scope of this work. In contrast, Monte Carlo sampling aims to directly access the average fidelity [83–85]. With optimized sets of initial states and measurement operators, as well as sampling only over a subset of those, it achieves exponential speedup via reduction of necessary measurements; the benchmarking of Clifford gates can even be achieved with resources scaling polynomially. However, it does not differentiate between gate and SPAM errors, limiting the precision of the fidelity estimation to that of state preparation and measurement – a restricting that is inherent to direct measurement approaches. We will resolve that shortcoming and give a more in depth analysis in chapter 6.

In this chapter we focus on an introduction to Randomized Benchmarking (RB) [79, 80] which is a mean to scalably and SPAM independently assess the average error rate of unitary two-designs such as the Clifford group. It does so via random gate sequences utilizing that averaging over unitary two-designs emulates averaging over the entirety of unitary operation, as discussed in chapter 1. Furthermore we present interleaved Randomized Benchmarking, which allows to access the fidelity of individual gates [81] and introduce an alternate formalism to derive RB, allowing to prove the robustness against potential loopholes as well as laying the foundation for the following chapters [86].

## 5.1 Standard RB

The key idea of Randomized Benchmarking is to apply and validate random Clifford gate sequences of varying length  $y$  to determine the average error rate per gate. We will show, that applying random gates on average prevents interference between error channels and effectively concatenates a number of depolarizing channels with equal average error. As the Clifford gates form a mathematical group, for every possible gate sequence there is a unique Clifford gate  $C_{y+1}$  which inverts the sequence and which can be found efficiently via the Gottesmann-Knill theorem. Therefore, by applying the sequence and its inverse to any initial state and measuring the overlap with that state afterwards, the sequence fidelity is accessible experimentally. The initial derivation relies on the assumption that there is just one set error channel  $\Lambda$ , irrespective of the associated gate. This is not per se given but rather not true for most physical implementations. We further neglect SPAM errors as well as those of the inverting gate  $C_{y+1}$ , which, however, can be justified

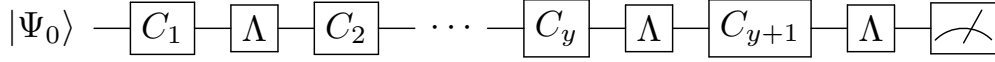


Figure 5.1: **Circuit representation of an RB sequence**

The state  $\Psi_0$  is subject to a sequence of random Clifford gates  $C_i$  inverted by  $C_{y+1}$  and the respective errors. This representation assumes a fixed error channel  $\Lambda$  and omits SPAM errors. The concluding measurement overlaps with the initial state at an average probability given by the sequence fidelity  $\Phi_y$ .

easily. The circuit of such a random sequence is given in figure 5.1.

By choosing the initial state to be the ground state represented by its density matrix  $\rho_0$  we find the average sequence fidelity to be

$$\Phi_y = \frac{1}{\#\mathcal{C}^y} \sum_{\{C_j\} \in \mathcal{C}^y} \text{Tr} \left[ \rho_0 \left( C_{y+1} \prod_{j=y}^1 (\Lambda C_j) \right) (\rho_0) \right], \quad (5.1)$$

where the right-to-left order of the product ensures that gates are applied in the correct order. We also introduce the notation for a gate  $U$  acting on a density matrix as  $U(\rho) \equiv U\rho U^\dagger$ . Writing out part of the product and inserting the identity  $\mathbb{1} = C_1 C_1^{-1}$  we find

$$\Phi_y = \frac{1}{\#\mathcal{C}^y} \sum_{\{C_j\} \in \mathcal{C}^y} \text{Tr} \left[ \rho_0 \left( C_1^{-1} C_2^{-1} \tilde{C}_{y+1} \prod_{j=y}^3 (\Lambda C_j) \Lambda C_2 C_1 C_1^{-1} \Lambda C_1 \right) (\rho_0) \right]. \quad (5.2)$$

$\tilde{C}_{y+1}$  inverts all sequence gates except the first two and is therefore independent of those. Consequently,  $C_2$  only contributes as terms in  $C_2 C_1$ . For any given  $C_1 \in \mathcal{C}$ , averaging over  $C_2$  assuming all elements of the Clifford group is equivalent to averaging over  $C_2 C_1 \in \mathcal{C}$  – this is given as  $\mathcal{C} C_1 = \mathcal{C}$ . We can therefore rename the term  $C_2 C_1$  as  $C_2$  and find

$$\Phi_y = \frac{1}{\#\mathcal{C}^y} \sum_{\{C_j\} \in \mathcal{C}^y} \text{Tr} \left[ \rho_0 \left( C_2^{-1} \tilde{C}_{y+1} \prod_{j=y}^3 (\Lambda C_j) \Lambda C_2 C_1^{-1} \Lambda C_1 \right) (\rho_0) \right]. \quad (5.3)$$

Repeating the above deliberation for all  $j$ , we conclude that

$$\Phi_y = \frac{1}{\#\mathcal{C}^y} \sum_{\{C_j\} \in \mathcal{C}^y} \text{Tr} \left[ \rho_0 \left( \prod_{j=y}^1 C_j^{-1} \Lambda C_j \right) (\rho_0) \right] \equiv \text{Tr} [\rho_0 \Lambda_{\text{twirl}}^y(\rho_0)], \quad (5.4)$$

separating the effect of individual random Clifford gates. We identify  $\lambda_{\text{twirl}}$  as the twirl of  $\Lambda$  over the Clifford group introduced in chapter 1. As the Clifford group is a unitary two-design, the twirl coincides with that over the special unitary group  $SU$ . That is a completely depolarizing channel, as can be shown rigorously using Schur's Lemma [87]. As such, it acts as

$$\Lambda_{\text{twirl}}(\rho) = p\rho + \frac{1-p}{d}\mathbb{1}, \quad (5.5)$$

with  $p$  denoting the probability of preserving a state  $\rho$ . The average associated with the channel  $\Lambda_{\text{twirl}}$  amounts to  $\Phi = p + 1 - p/d$ ; the average sequence fidelity becomes

$$\Phi_y = \text{Tr} \left[ \rho_0 \left( p^y \rho_0 + \frac{1-p^y}{d} \mathbb{1} \right) \right] = \frac{d-1}{d} p^y + \frac{1}{d}. \quad (5.6)$$

Note that the effects of neglecting SPAM errors and the error channel connected to  $C_{y+1}$  are typically small compared to the overall error due to error amplification over the sequence length. Furthermore, those errors only result in different prefactors but do not affect the decay rates and therefore result in a more general form of equation 5.6. This can be seen mathematically as the sequence fidelity is just a different linear functional of the exponentiation of the matrix  $\Lambda_{\text{twirl}}$  which has just the two eigenvalues 1 and  $p$  derived above.

$$\Phi_y = Ap^y + B \quad (5.7)$$

To access the decay parameter  $p$  one has to estimate  $\Phi_y$  for several sequence lengths  $y$  by sampling over a small subset of possible sequences for each length. The size of those subsets can theoretically already be limited to a rather small number [88], but experimental and numerical data provides reliable error estimations for even smaller subsets. The average fidelity of the unitary two-design is determined from a fit of the measurement results to equation 5.7. As the average fidelity only depends on  $p$  rather than the prefactors  $A, B$ , the RB protocol is robust against SPAM errors and since the measured quantities are not miniscule – even if the gate errors are – due to the error amplification of long sequences, it allows for a substantially lower measurement accuracy than more direct approaches. Furthermore, it is scalable with respect to the number of qubits in both experimental and classical computational resources thanks to the Gottesmann-Knill theorem – at least if the unitary two-design is the Clifford group. Because of those properties Randomized Benchmarking is widely used in experiment.

## 5.2 Interleaved Randomized Benchmarking

The RB protocol is designed to identify the average fidelity of a unitary two-design or rather the Clifford group and hence the average over a set of gates rather

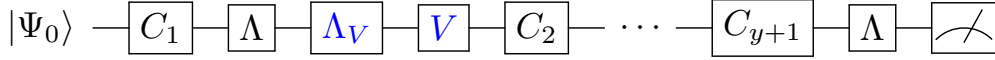


Figure 5.2: **Circuit representation of an interleaved Randomized Benchmarking sequence**

The state  $\Psi_0$  is again subject to random Clifford gates  $C_i$  but also interleaved specific gates  $V$  with the whole sequence inverted by  $C_{y+1}$  bar the respective errors. This representation still assumes the fixed error channel  $\Lambda$  but associates the interleaved gate  $V$  with an individual error channel  $\Lambda_V$ .

than the fidelity of a single individual gate. For the engineering and validation of specific gates this is often inconvenient, especially for gate calibration [89, 90]. In this section we briefly introduce Interleaved Randomized Benchmarking (IRB), extending the above RB protocol to estimate the fidelities of individual Clifford gates [81]. The core concept of IRB is to alternate a specific gate  $V$  with random Cliffords as shown in figure 5.2. Separately estimating the fidelity for both the combined error of group and single gate, as well as the average group error allows to estimate the error rate of  $\Lambda_V$  associated with the individual gate  $V$ . The corresponding sequence fidelity is given by

$$\Phi_y = \frac{1}{\#\mathcal{C}^y} \sum_{\{C_j\} \in \mathcal{C}^y} \text{Tr} \left[ \rho_0 \left( C_{y+1} \prod_{j=y}^1 (V \Lambda_V \Lambda C_j) \right) (\rho_0) \right] \quad (5.8)$$

$$\Phi_y = \frac{1}{\#\mathcal{C}^y} \sum_{\{C_j\} \in \mathcal{C}^y} \text{Tr} \left[ \rho_0 \left( \prod_{j=y}^1 (C_j^{-1} \Lambda_V \Lambda C_j) \right) (\rho_0) \right] \quad (5.9)$$

$$= A p_{\mathcal{C}^y}^y + B, \quad (5.10)$$

obtained similar to the above derivation of RB. Note that, as  $V$  is a Clifford gate, the inverting gate  $C_{y+1}$  is as well and can be found as efficiently as for the non interleaved case. Furthermore, the above sequences can be used to estimate the error  $\varepsilon_{\mathcal{C}^y}$  of the combined channel  $\Lambda_V \Lambda$ : Assuming small errors, an estimated error of  $V$  can be calculated as  $\varepsilon_V = \varepsilon_{\mathcal{C}^y} - \varepsilon_{\mathcal{C}}$  and lies within the bounds

$$\max(0, (\sqrt{\varepsilon_{\mathcal{C}^y}} - \sqrt{\varepsilon_{\mathcal{C}}})^2) \leq \varepsilon_V \leq (\sqrt{\varepsilon_{\mathcal{C}^y}} + \sqrt{\varepsilon_{\mathcal{C}}})^2. \quad (5.11)$$

Those limits can be derived in a straightforward way by assuming  $\Lambda$  as well as  $\Lambda_{\text{twirl}}$  to be unitary errors in either same or opposite direction, which leads to the worst possible over- and underestimation of the gate error rate  $\varepsilon_V$ .

### 5.3 Alternate Formalism

As discussed, RB allows to efficiently and scalably characterize the average error of a unitary two-design such as the Clifford group  $\mathcal{C}$  on any physical candidate for (gate-based) quantum computation. The above introduction, however, is vulnerable to possible loopholes in the derivation such as additional leakage levels of the physical qubits or error channels that specifically depend on the gate. As the RB protocol is used not only for benchmarking, but for closing the loop in experimental optimal control [89, 90], it becomes increasingly imperative to account for all possible weaknesses of this protocol. In this section we introduce a formalism that accounts for these loopholes and lays the foundation for subsequent work on RB.

Many promising candidates for implementing qubits on which RB is applied such as superconducting qubits [45, 87], NV-centers [91], trapped ions [79] or neutral atoms [92] are not natural two-level-systems making leakage into additional levels a viable error source. Since the physical qubit is protected from unwanted interactions with the environment so are in many cases the leakage levels. Therefore leakage is not accounted for by standard RB, not least because it is a non-Markovian process. A major consequence of the application of RB sequences is that there is no coherent interference between errors, including that the error channel does not maintain any well-defined phase relations between different states. This is not the case if one considers transitions into even just one non-computational level per physical qubit while still only applying *qubit* Clifford gates. For a single qubit this can be resolved with the rather simple procedure of randomly inserting phase factors  $\pm 1$  on the third level to achieve phase randomization and prevent coherence between computational and non-computational subspaces [93]. This is not easily generalizable to multiple qubits, as the non-computational subspace is  $(3^n - 2^n)$ -dimensional and allows for arbitrary uncontrolled unitary evolution. Consequently a generalization of the Clifford group to the full Hilbert space is not necessarily a group, hence it is neither guaranteed to be closed nor to contain an inverse or even a neutral element.

We specifically consider an implementation of the Clifford group  $\mathcal{C}$  on a physical system the qubits of which are no natural two-level systems but rather allow for a non negligible leakage error. Be each Clifford gate  $C$  acting close to ideal on the computational and as a non specified operation on the non computational subspace. The deviation satisfying this assumption exactly can be contained in an error channel  $\Lambda$  acting on both qubit and leakage subspace; again we initially consider the error channel to be independent of the gate. Revisiting equation 5.1,

the average sequence fidelity is

$$\Phi_y = \frac{1}{\#\mathcal{C}^y} \sum_{\{C_j\} \in \mathcal{C}^y} \text{Tr} \left[ \rho_0 \left( C_1^{-1} C_1 C_{y+1} \prod_{j=y}^2 (\Lambda C_j) \Lambda C_1 \right) (\rho_0) \right]. \quad (5.12)$$

Showcasing the initial derivation in the previous section, we relied on  $\mathcal{C}$  being a group. As this is no longer true, we cannot rewrite the sequence as a chain of twirled error channels, however we can take a different approach: With  $C_1 C_{y+1}$  being the inverse of all Cliffords but the first, one can see that multiplying  $C_1^{-1}$  from the left and  $\Lambda C_1$  from the right averaged over all  $C_1$  in  $\mathcal{C}$  defines a linear map  $T_\Lambda$  on the Hilbert space of maps on density matrices.<sup>1</sup> The resulting sequence fidelity

$$\Phi_y = \frac{1}{\#\mathcal{C}^{y-1}} \sum_{\{C_j\} \in \mathcal{C}^{y-1}} \text{Tr} \left[ \rho_0 T_\Lambda \left( \tilde{C}_{y+1} \prod_{j=y}^2 (\Lambda C_j) \right) (\rho_0) \right] \quad (5.13)$$

$$= \text{Tr} [\rho_0 T_\Lambda^y(\mathbb{1})(\rho_0)] \quad (5.14)$$

as a linear functional of a matrix exponential is given by

$$\Phi_y = \sum_i a_i \lambda_i^y. \quad (5.15)$$

As in the standard derivation of RB, one aims to describe the fidelity decay by a preferably simple formula fitted to experimental measurements of random sequences. This is complicated by the up to  $256^n$  different eigenvalues  $\lambda_i$ . However it can be shown that  $T_\Lambda$  has only non negative entries and therefore its eigenvalues are smaller than or equal to one as given by the Perron-Frobenius theorem. The above sequence fidelity can be fitted to a multi exponential decay with just few real-valued parameters [86], as we demonstrate in figure 5.3. Even just a single decay parameter can represent the sequence fidelity reasonably well – this explains the successful application of the RB protocol to physical systems.

In the above calculations we neglected all error channels induced by SPAM, the robustness to which is a key advantage of RB. To show the validity in leaky settings, we need to show that this robustness is preserved. Introducing a measurement error however jeopardizes the assumption that the last gate  $C_{y+1}$  can be considered the inverse of all previous ones which is only true in the computational subspace. To assess the accompanying impression we introduce an effective measurement operator:  $\rho_M = \sum_k E_k^\dagger \rho_0 E_k$  incorporates the effects of a measurement

<sup>1</sup>Note that the identity  $C_{y+1} = C_1^{-1} \dots C_y^{-1}$  technically no longer holds, or rather it is true only when projecting onto the computational subspace. As there is no further operation between application of  $C_{y+1}$  and measurement of the overlap with the initial state, it can be used here.

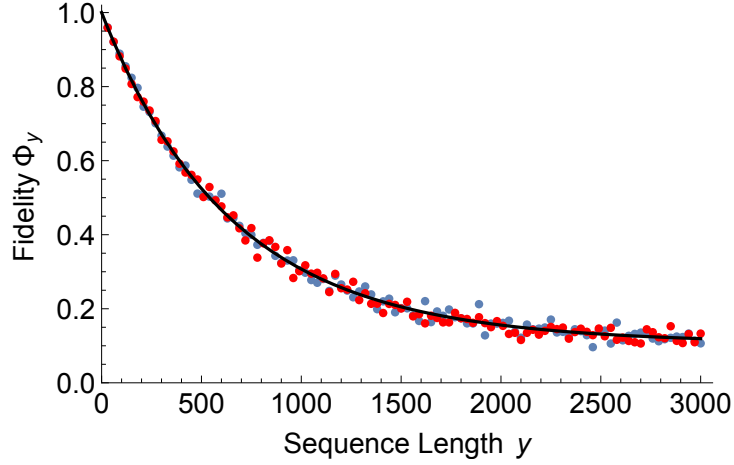


Figure 5.3: **Decay of the RB sequence fidelity**

Average fidelity  $\Phi_y$  for a unitary error of  $1.354 \times 10^{-3}$  for 40 different random sequences per sequence length  $y$ . We verify the alternate protocol by comparing an extended Clifford set that is a group (blue points) to a Clifford set that does not transfer the group properties onto the whole Hilbert space (red). The protocol estimates average errors of  $1.379 \times 10^{-3}$  and  $1.350 \times 10^{-3}$  respectively. Both two-qubit Clifford sets are generated from the single qubit Clifford sets and few two-qubit entangling gates [94]. The obtained average sequence fidelities  $\Phi_y$  are fitted to the multi exponential decay function and the average fidelity is calculated as  $\Phi_1/\Phi_0$ .

error channel  $\Lambda_M$  described by the Kraus operators  $E_k$ .<sup>2</sup> We project the effective measurement operator onto the two subspaces and  $C_{y+1} = C_1^{-1} \dots C_y^{-1}$  holds for the computational space. Also introducing the prepared state  $\rho_P = \Lambda_P(\rho_0)$  we find

$$\begin{aligned} \Phi_y &= \frac{1}{\#\mathcal{C}^y} \sum_{\{C_j\} \in \mathcal{C}^y} \text{Tr} \left[ (\rho_{M,\text{comp}} + \rho_{M,\text{leak}}) \left( C_{y+1} \prod_{j=y}^1 (\Lambda C_j) \right) (\rho_P) \right] \\ &= \text{Tr} [\rho_{M,\text{comp}} T_\Lambda^y(\mathbb{1})(\rho_P)] + \frac{1}{\#\mathcal{C}^y} \sum_{\{C_j\} \in \mathcal{C}^y} \text{Tr} \left[ \rho_{M,\text{leak}} \left( C_{y+1} \prod_{j=y}^1 (\Lambda C_j) \right) (\rho_P) \right] \end{aligned}$$

<sup>2</sup>When measuring the overlap of an arbitrary state  $\rho$  with the ground state using an imperfect measurement, we find  $\text{Tr}[\rho_0 \Lambda_M(\rho)] = \sum_k \text{Tr}[\rho_0 E_k \rho E_k^\dagger] = \sum_k \text{Tr}[E_k^\dagger \rho_0 E_k \rho]$ , motivating the definition of  $\rho_M$ .

$$\begin{aligned}
&= \text{Tr} [\rho_{M,\text{comp}} T_{\Lambda}^y(\mathbb{1})(\rho_P)] + \frac{1}{\#\mathcal{C}^y} \sum_{\{C_j\} \in \mathcal{C}^y} \text{Tr} \left[ \rho_{M,\text{leak}} \left( \prod_{j=y+1}^1 (C_j \Lambda) C_1 \right) (\rho_{P,\text{comp}}) \right] \\
&+ \frac{1}{\#\mathcal{C}^y} \sum_{\{C_j\} \in \mathcal{C}^y} \text{Tr} \left[ \rho_{M,\text{leak}} \left( C_{y+1} \prod_{j=y}^1 (\Lambda C_j) \right) (\rho_{P,\text{leak}}) \right] \tag{5.16}
\end{aligned}$$

Again,  $C_1$  is inverted by  $C_{y+1} \dots C_2$  only in the computational subspace and can hereon be written as  $C_1 = C_2^{-1} \dots C_{y+1}^{-1}$ . Consequently we find a second operator  $\tilde{T}_{\Lambda}$  on quantum channels and

$$\begin{aligned}
\Phi_y &= \text{Tr} [\rho_{M,\text{comp}} T_{\Lambda}^y(\mathbb{1})(\rho_P)] + \text{Tr} \left[ \rho_{M,\text{leak}} \tilde{T}_{\Lambda}^y(\mathbb{1})(\rho_{P,\text{comp}}) \right] + \mathcal{O}(\varepsilon_P(\varepsilon_M + \varepsilon)) \\
&\equiv \sum_i b_i \kappa_i^y + \mathcal{O}(\varepsilon_P(\varepsilon_M + \varepsilon)). \tag{5.17}
\end{aligned}$$

Here  $\varepsilon_P, \varepsilon_M, \varepsilon$  are state preparation, measurement and gate error rates respectively and hence the deviation from the model is negligibly small and not scaling with  $y$ . We find that accounting for SPAM does not impair the decay of the sequence fidelity – as for the standard derivation, we account for its effects by extracting the average fidelity as the ratio  $\Phi = \Phi_1/\Phi_0$ .

The derivations for the RB protocol analyzed so far assume  $\Lambda$  to be independent of the preceding gate or more specifically uses an effective gate error. This assumption is usually not true for any physical system. We reiterate the sequence fidelity for specifically gate dependent error channel while neglecting SPAM finding

$$\begin{aligned}
\Phi_y &= \frac{1}{\#\mathcal{C}^y} \sum_{\{C_j\} \in \mathcal{C}^y} \text{Tr} \left[ \rho_0 \left( \Lambda_{y+1} C_{y+1} \prod_{j=y}^1 (\Lambda_j C_j) \right) (\rho_0) \right] \\
&\approx \frac{1}{\#\mathcal{C}^y} \sum_{\{C_j\} \in \mathcal{C}^y} \text{Tr} \left[ \rho_0 \left( C_1^{-1} C_1 C_{y+1} \prod_{j=y}^2 (\Lambda_j C_j) \Lambda_1 C_1 \right) (\rho_0) \right] \\
&\equiv \text{Tr} [\rho_0 T_G^y(\mathbb{1})(\rho_0)] \equiv \sum_i c_i \tau_i^y. \tag{5.18}
\end{aligned}$$

The contained imprecision of the order of  $\|\Lambda\| \ll 1$  which does not scale with the length of the sequence. It ,therefore, does not interfere with the fidelity decay, which is given by the introduction of  $T_G$  as the average of applying  $\Lambda_C C$  before and  $C^{-1}$  after a quantum channel. Consequently RB accounts for gate dependent error without adjustment of the protocol beyond fitting for a multi-exponential decay.

All of the above findings translate directly to IRB with the additional benefit that the individual gate  $V$  is no longer restricted to be an element of the underlying unitary two-design. The challenges arising with the then non trivial inversion of the sequence will be discussed in the following chapter [6](#).

# Chapter 6

## Hybrid Benchmarking

In this chapter we present a protocol for Interleaved Randomized Benchmarking of arbitrary quantum gates using Monte Carlo sampling of quantum states. It is generally applicable to all gates, including those not in the Clifford group, while preserving key advantages of Randomized Benchmarking such as error amplification as well as independence from state preparation and measurement errors. This property is crucial for implementations in many contemporary systems. Although the protocol scales exponentially in the number of qubits, it is superior to direct Monte Carlo sampling of the average gate fidelity in both the total number of experiments by orders of magnitude and savings in classical preprocessing, that are exponential.

A central goal of quantum information science is to engineer a physical system capable of functioning as a scalable quantum computer that systematically outperforms classical computers in certain applications. To this end, it is imperative to drive arbitrary unitary evolution in a suitable quantum system consisting of  $n \gg 1$  qubits and to benchmark the implementation of that operation.

Efficient benchmarking protocols, i.e., protocols that scale at most polynomially in  $n$ , are available for quantum operations in the Clifford group  $\mathcal{C}$  [79, 80, 83, 84], an important subset of quantum operations [10, 17]. In particular, Randomized Benchmarking is a method to estimate the average error of the Clifford group based on the fidelity of random Clifford gate sequences [79, 80]. RB has proven itself as a popular and experimentally viable approach not only because of its scaling properties but also due to its independence from state preparation and measurement (SPAM) errors [79, 80]. For individual gates of the Clifford group,

---

This chapter contains original research by T.C. et al. with overlapping contributions from Masters and Ph.D. It was published in "T. Chasseur, D.M. Reich, C.P. Koch, and F.K. Wilhelm, Phys. Rev. A **95**, 062335 (2017)". Copyright (2017) by the American Physical Society. The majority of research was conducted and the majority of the text written by T.C. Parts of this paper have been shortened to avoid redundancy within this thesis.

the fidelity can be estimated with interleaved Randomized Benchmarking (IRB) [81]. The remarkable RB construction hinges on the Clifford group elements being distributed sufficiently uniformly on the special unitary group  $SU(d = 2^n)$ . A central prerequisite for the scalability of RB is that  $\mathcal{C}$  can be simulated efficiently on a classical computer [15]. However, for the same reason, quantum algorithms based on those Clifford gates alone cannot outperform a classical computer. To realize the full potential of quantum computation, one has to access the full unitary group which is generated by  $\mathcal{C}$  and one additional non-Clifford gate, e.g., a single qubit gate such as the  $\pi/8$  gate. While IRB for example can be generalized to an arbitrary gate, the fidelity estimation becomes highly challenging [86]: Simulation and inversion of the sequence becomes increasingly inefficient as alternating Clifford and e.g.  $\pi/8$  gates generate the full  $SU(2^n)$  [15]. In order to sample all gates, including those not in  $\mathcal{C}$  one needs to rely on strategies whose experimental and classical resources scale exponentially.

One such generally applicable protocol is given by Monte Carlo Sampling of the average gate fidelity which allows for the validation of arbitrary quantum gates [83–85]. It requires significantly less resources than the canonical approach, which is to extract this information from full quantum process tomography. However, Monte Carlo sampling is limited by SPAM errors, which for many physical systems can overshadow the gate error. Moreover its scaling in both experimental and classical resources, although favorable compared to process tomography, is still exponential in  $n$ . This poses the question whether it is possible to combine the generality of Monte Carlo Sampling, i.e. going beyond the Clifford group, with the experimental advantages of RB.

Here, we answer this question and demonstrate the benefit of combining both methods. We show how arbitrary gates can be benchmarked by replacing the inverting gate at the end of each IRB sequence with Monte Carlo sampling of the resulting quantum state. Our approach outperforms direct Monte Carlo sampling of the average gate fidelity regarding the number of measurements and yields an exponential saving in classical computational resources while retaining the independence on SPAM errors. Therefore it enables the benchmarking of arbitrary gates in experimental settings.

We briefly revisit the RB and IRB protocols as described in the previous chapter. RB provides an estimate for the average fidelity of a unitary two-design such as the Clifford group based on the idea that random sequences of Clifford gates also randomize the effect of error channels, turning them depolarizing. For every sequence of  $y$  Clifford gates  $C_j$ ,  $1 \leq j \leq y$ , there is a unique Clifford gate  $C_{y+1}$  inverting the sequence which can be efficiently found via the Gottesmann-Knill theorem. By applying the sequence and its inverse to an initial state  $\rho_0$  and measuring the survival probability of that state, the sequence fidelity is accessible

experimentally. Potential loopholes in Randomized Benchmarking, such as gate dependent errors and leakage can be accounted for by considering linear maps acting on quantum channels instead of just quantum channels [86].

In this chapter we go beyond the Clifford group. To do so, we rely on the alternate formalism introduced in chapter 5: as we do no longer rely on the group properties of  $\mathcal{C}$ , IRB does not depend on the specific gate  $V$  being an element of the Clifford group. If it is not, the unitary matrix representing an ideal implementation of the sequence can be quite general since  $\mathcal{C}$  and  $V$  generate a dense subset of the whole special unitary group. The construction of the inverse  $C_{y+1}$  would be highly challenging and defeat the concept of performing quantum computation using a restricted set of gates.

Alternatively, one could be content to approximate the inverting gate using the Solovay-Kitaev theorem. However, this turns out to be inadequate for the following reason: The theorem states that any gate can be composed out of a small number  $l$  of gates depending only logarithmically on the permitted inaccuracy, but exponentially on the number of qubits [95, 96]. For RB to be reliable, the error rate  $\varepsilon_{y+1}$  associated with  $C_{y+1}$  should be much smaller than the error of the sequence. Since both sequence and inverting gate are composed of the same gate set, this is roughly equivalent to  $l \ll y$ . Satisfying this is possible only for  $\varepsilon_V$  and  $\varepsilon_C$  sufficiently small, so that  $y$  is large while the Hilbert space dimension must be kept small as it enters the sequence length exponentially in the Solovay-Kitaev algorithm. In other words, satisfying  $l \ll y$  implies the ability to implement an arbitrary quantum gate to a relatively high precision, i.e., availability of a universal quantum computer as a starting point.

To overcome the limitations of these ideas, we present a pragmatic approach to the problem. Consider the fidelity of a specific sequence, represented by a vector  $\mathbf{y}$  of gates.

$$\begin{aligned} \Phi_{\mathbf{y}} &= \text{Tr} \left[ \rho_0 C_{y+1} \prod_{j=y}^1 (V \Lambda_V \Lambda_j C_j) (\rho_0) \right] \\ &\equiv \text{Tr} [\rho_{\text{id}}^{\mathbf{y}} \rho_{\text{act}}^{\mathbf{y}}], \end{aligned} \quad (6.1)$$

where  $\rho_{\text{id}}^{\mathbf{y}} = C_{y+1}^{-1}(\rho_0) = (\prod_{j=y}^1 C_j)(\rho_0)$  is the state ideally generated by the sequence and determined on a classical computer and  $\rho_{\text{act}}^{\mathbf{y}}$  the one actually realized by applying the gates  $V$  and  $C_j$  (including their errors  $\Lambda_V$  and  $\Lambda_j$ ) in the experiment. Equation 6.1 is of the form used in Refs. [83–85] to estimate the overlap of two states via *Monte Carlo sampling*. To do this, we follow the notation of Ref. [85] and rewrite the states in the basis of the generalized Pauli matrices on  $n$  qubits normalized for the canonical scalar product defined by the (unnormalized)

trace,  $\mathcal{W} = \{W\} = \frac{1}{\sqrt{d}}\mathcal{P}^{\otimes n}$ . We find the sequence fidelity

$$\begin{aligned}\Phi_{\mathbf{y}} &= \text{Tr} [\rho_{\text{id}}^{\mathbf{y}} \rho_{\text{act}}^{\mathbf{y}}] = \sum_{k=1}^{d^2} \text{Tr} [W_k \rho_{\text{id}}] \text{Tr} [W_k \rho_{\text{act}}] \\ &\equiv \sum_{k=1}^{d^2} \chi_{\text{id}}(k) \chi_{\text{act}}(k) = \sum_{k=1}^{d^2} \chi_{\text{id}}(k)^2 \frac{\chi_{\text{act}}(k)}{\chi_{\text{id}}(k)} \\ &\equiv \sum_{k=1}^{d^2} \text{Pr}(k) X_k,\end{aligned}\tag{6.2}$$

where  $\text{Pr}(k) = \chi_{\text{id}}(k)^2$  and  $X_k = \chi_{\text{act}}(k)/\chi_{\text{id}}(k)$ .  $\sum_k \text{Pr}(k) = 1$  since  $\sum_k \chi_{\text{id}}(k)^2 = \text{Tr} [\rho_{\text{id}}^2]$  and  $\rho_{\text{id}}$  being a pure state. Therefore,  $\text{Pr}(k)$  can be used as a sampling probability where the expectation value of the corresponding sampling is the desired fidelity  $\Phi_{\mathbf{y}}$ .

This is the core of our approach: Instead of actually implementing the gate that inverts the random sequence and measuring the error on identity, we treat  $\Phi_{\mathbf{y}}$  as a state fidelity which is estimated with Monte Carlo sampling. Following equation (6.2), this amounts to choosing a total of  $L$  Pauli measurement operators  $W_{k_l} \in \mathcal{W}$ ,  $1 \leq l \leq L$ , according to the sampling probability  $\text{Pr}(k)$  and measure  $W_{k_l}$  (and hence  $X_{k_l}$ )  $N_l$  times. We summarize the IRB protocol with Monte Carlo sampling of quantum states as follows:

1. Perform standard RB to estimate the average error of the Clifford group  $\epsilon_{\mathcal{C}}$  as a reference point.
2. Choose  $q$  different sequence lengths  $y$  such that the sequence fidelities  $\Phi_y$  can be assumed to provide a reliable fit. This means the  $\Phi_y$  shall neither be close to one nor to the fidelity limit for long sequences.
3. For each selected sequence length, choose  $m$  different sequences  $\mathbf{y}$  of random Clifford gates interleaved with the gate  $V$ . They are used to estimate the average fidelity  $\Phi_y$  by comparing the actual and ideal state, cf. equation (6.1), via Monte Carlo sampling.
4. Determine the ideal state on a classical computer, i.e., apply  $2y$  unitary matrices onto the pure initial state vector. This scales as  $\mathcal{O}(yd^2)$  as it cannot be done efficiently, since  $V$  is not necessarily a Clifford gate.
5. Choose  $L$  measurement operators  $W_k$  at random, following the distribution  $\text{Pr}(k)$  defined in equation 6.2.
6. For each chosen measurement operator apply the sequence  $\mathbf{y}$  and measure  $W_k$ . This is repeated  $N_l$  times.

7. Determine an estimate for the sequence fidelities  $\Phi_y$  by averaging over all  $N_l$  measurements, the  $X_k$  for all  $L$  measurement operators  $W_{k_l}$  and the  $m$  different sequences as given by equation 6.2.
8. Fit  $\Phi_y$  to the multi-exponential decay, as derived in the previous chapter, and derive the combined average error as  $\Phi_{y=1}/\Phi_{y=0}$ .
9. Calculate the average error of the arbitrary  $n$  qubit gate  $V$  as  $\varepsilon_V = \varepsilon_{CV} - \varepsilon_C$  and estimate the lower and upper bounds as  $\max(0, (\sqrt{\varepsilon_{CV}} - \sqrt{\varepsilon_C}))^2$  and  $(\sqrt{\varepsilon_{CV}} + \sqrt{\varepsilon_C})^2$  as in the original IRB.

The parameters of the protocol are chosen as follows: A valid fidelity estimate via RB requires sufficient experimental data for a fit to a (multi-)exponential decay; hence  $q$  different values for  $y$ , all provided with a substantiated estimate for  $\Phi_y$ . Because it is sufficient to fit to only a few decays, a rather small  $q$  suffices. The amount  $m$  of different sequences for each value of  $y$  can be upper bounded by a global constant using the leading order in gate errors, see [86, 88], yielding  $m$  not larger than 100. Higher order corrections to the uncertainty in the error per gate originating from finite  $m$  can be bounded using the fact that  $\Phi_y$  lies in the range  $[0, 1]$  and invoking Hoeffding's inequality [97]. We choose sequence lengths  $y$  in a way that the error is neither too small to be measured efficiently nor so big that the decaying terms are already close to zero. This condition is satisfied for

$$\varepsilon y = \mathcal{O}(1), \quad (6.3)$$

as can easily be seen using the simplified model of a single decay.

In Monte Carlo sampling, there are two sources for inaccurate fidelity assessment, namely the sampling inaccuracy due to *a)* the incomplete subset of the measurement operators and *b)* due to the finite number of measurements. The inaccuracies can be bounded by Chebyshev's and Hoeffding's inequality, respectively to be allowed to exceed  $\alpha/2$  with a probability of at most  $\delta/2$ . For a given error bound, this leads to an estimate of the total number of experiments [83–85].

The sampling inaccuracy *a)* is bounded by Chebyshev's inequality which provides an upper limit to the probability of deviating from the mean value of a distribution, depending on its standard deviation,

$$\Pr\left(|Z - [Z]| \geq \frac{\sigma_Z}{\sqrt{\delta}}\right) \leq \delta. \quad (6.4)$$

Here,  $Z \equiv 1/L \sum_{l=1}^L X_{k_l}$  is the fidelity estimate obtained by the random choice of measurement operators  $W_{k_l}$  and  $[Z]$  its classical expectation value, i.e.,  $\Phi_y$ . The variance can be estimated as

$$\sigma_Z^2 = [Z^2] - [Z]^2 = \sum_{l=1}^L \sum_{k_l} \Pr\left(\frac{X_{k_l}}{L}\right)^2 - \Phi_y^2 \quad (6.5)$$

$$\leq \frac{1}{L} \sum_k \chi_{\text{act}}(k)^2 = \frac{1}{L} \text{Tr} [\rho_{\text{act}}^2] \leq \frac{1}{L},$$

using the fact that  $\rho_{\text{act}}$  is a convex sum of projectors. Thus

$$\Pr \left[ |Z - \Phi_{\mathbf{y}}| \geq \sqrt{\frac{2}{L\delta}} \right] \leq \frac{\delta}{2} \quad (6.6)$$

and the choice  $L = \lceil 8/(\alpha^2\delta) \rceil$  ensures the intended inequality, where the outer brackets denote the ceiling function. To limit the deviation  $b)$  due to a finite number of measurements one relies on Hoeffding's inequality,

$$\Pr (|S - \langle S \rangle| \geq \alpha/2) \leq 2 \exp \left( -\frac{\alpha^2}{2 \sum_i (b_i - a_i)^2} \right). \quad (6.7)$$

$S$  is the sum over random variables with outcomes in the range  $[a_i, b_i]$ , given by the adequately normalized sum of all  $\sum_l N_l$  single shot measurements and  $\langle S \rangle = Z$ . Since the measurement outcomes of Pauli matrices are bimodal, they are situated at the boundaries of the respective range  $[a_i, b_i]$ . Therefore, the range over variance ratio is most suitable for Hoeffding's inequality. To ensure that the probability to exceed  $\alpha/2$  is at most  $\delta/2$ , it suffices to demand

$$\frac{\delta}{2} \stackrel{!}{\geq} 2 \exp \left( -\frac{\alpha^2}{2 \sum_l 4N_l d^{-1} (LN_l \chi_{\text{id}}(k))^{-2}} \right), \quad (6.8)$$

which, with the natural choice  $N_l \propto \chi_{\text{id}}(k)^{-2}$ , is satisfied for

$$N_l = \left\lceil \frac{8}{dL\alpha^2 \chi_{\text{id}}(k)^2} \log \left( \frac{4}{\delta} \right) \right\rceil. \quad (6.9)$$

Compared to Refs. [83–85], the total inaccuracy  $\alpha$  as well as the probability  $\delta$  of exceeding it were chosen smaller by a factor of two to simplify the further treatment.

The classical average over the total number of experiments can be estimated as follows using equation 6.9:

$$\begin{aligned} [N_{\text{exp}}] &= L \sum_{k=1}^{d^2} \Pr(k) N_k \\ &\leq L \left( 1 + \frac{8d}{L\alpha^2} \log \left( \frac{4}{\delta} \right) \right) \end{aligned}$$

$$\leq 1 + \frac{8}{\alpha^2 \delta} + \frac{8d}{\alpha^2} \log \left( \frac{4}{\delta} \right). \quad (6.10)$$

equation 6.10 is also valid for direct Monte Carlo sampling of the average gate fidelity and represents an exponential speedup in the number of qubits compared to full process tomography which scales as  $\mathcal{O}(d^4)$  [85]. An important aspect is the scaling with  $1/\alpha^2$ . It is key to the advantageous scaling of IRB with Monte Carlo sampling of quantum states in comparison with direct Monte Carlo sampling of the average fidelity as shown below.

For the resource estimate, we aim for an inaccuracy of fidelity measurements that is one order of magnitude smaller than the error rate  $\varepsilon$ . Average gate fidelities are not fundamental quantities of physics but estimators on how good a quantum algorithm composed of a set of gates performs. Therefore any attempt at an overly precise characterization of gate errors does not yield a valuable gain in information. In addition, the systematic uncertainty  $\alpha_{\text{IRB}}$  of IRB caused by Clifford gate errors limits the accuracy that can reasonably be achieved; even more so for other methods not robust against SPAM errors. Based on equation 6.3,  $\Phi_y \sim 1 - y\varepsilon$  such that uncertainties in its estimation affect the estimate of  $\varepsilon$  roughly with a factor of  $1/y$ . Therefore relative errors in  $\Phi_y$  approximately translate to relative errors in  $\varepsilon$ . Using the above statement and the fact that the inaccuracy of an IRB based estimation  $\alpha_{\text{IRB}}$  is aimed to be close to  $\varepsilon$ , one chooses an inaccuracy  $\alpha_{\text{MC}}(y)$  for the Monte Carlo sampling of sequence fidelities  $\Phi_y$  that result in an estimation without unnecessary additional precision compared to  $\alpha_{\text{IRB}}$ . It scales linearly with  $\varepsilon y$  which is on the order of 1. Therefore,  $\alpha_{\text{MC}}(y)$  varies distinctly but not excessively over the  $q$  different sequence lengths  $y$  but depends on neither the error rate  $\varepsilon$  nor the Hilbert space dimension  $d = 2^n$ . For the sake of simplicity, let  $\alpha_{\text{MC}}$  be defined as an effective average value for  $\alpha_{\text{MC}}(y)$  setting an average on to what precision each sequence fidelity has to be assessed.  $\alpha_{\text{MC}}$  as a system independent constant of the protocol, can safely be assumed to not exceed  $10^{-1.5}$ .

The above derivation of  $\alpha_{\text{MC}}(y)$  ensures the required accuracy for each of the  $q \times m$  single sequence fidelities rather than just for the resulting estimate for  $\varepsilon$ . This provides a reasonable fit to the decay function as each data point provides sufficient accuracy. Exploiting that in a more rigorous way may result in an improvement of prefactors but cannot improve the scaling since  $q$  and  $m$  are largely system independent [86, 88].

The total number of experiments then adds up to

$$[N_{\text{exp}}] \leq qm \left( 1 + \frac{8}{\alpha_{\text{MC}}^2 \delta} + \frac{8d}{\alpha_{\text{MC}}^2} \log \left( \frac{4}{\delta} \right) \right), \quad (6.11)$$

which differs by a factor of  $qm\alpha^2/\alpha_{\text{MC}}^2$  compared to direct Monte Carlo sampling of the average fidelity [85]. Translating this factor into numbers relating to recent

advances in the implementation of quantum gates as well as the error threshold for quantum computing highlights the advantage of our protocol. A specific set of values taking into account recent experimental results [45, 94, 98] corresponds to  $q = 20$ ,  $m = 50$  and  $\varepsilon = 10^{-3}$  based on relatively high error rates of two qubit gates. These values yield  $\alpha = 10^{-4}$  and two orders of magnitude of improvement in the total number of experiments via the above factor.

Another concern regarding scalability is the use of classical computational resources. Although more easily accessible, classical resources are not infinite and therefore become relevant eventually, especially for Monte Carlo sampling where classical resources scale exponentially with a higher exponent than the number of experiments. The sampling of measurement operators can be done using conditional probabilities, scaling with  $n^2 d^2$  for states and  $n^2 d^4$  for processes and hence outperforming the naive approach of calculating all  $\Pr(k)$  [84, 85]. Accounting also for the necessity to calculate  $\rho_{\text{id}}$  for each sequence, the classical resources needed for our protocol scale as

$$N_{\text{class}} = \mathcal{O} \left( \frac{qm}{\alpha_{\text{MC}}^2} \left( \frac{d^2}{\varepsilon} + n^2 d^2 \right) \right), \quad (6.12)$$

compared to  $\mathcal{O} \left( \frac{1}{\alpha^2} n^2 d^4 \right)$  for direct Monte Carlo sampling of the average gate fidelity. Hence, we obtain an exponential speedup of  $\mathcal{O}(d^2)$  in classical resources in addition to the reduction of the number of experiments.

Combining the currently best but individually restricted methods for estimating quantum fidelities (interleaved Randomized Benchmarking and Monte Carlo sampling), we have extended the former to arbitrary quantum operations, outside of the Clifford group, while reducing the enormous overheads and avoiding the SPAM dependence associated with the latter. The extension to non-Clifford gates is made possible by treating the RB sequence fidelity as a state fidelity that can be estimated with Monte Carlo sampling. This avoids the actual accurate physical implementation of the inverting gate in the RB sequence, which, for a non-Clifford gate, would require availability of a universal quantum computer. Our protocol inherits from IRB robustness with respect to SPAM errors; for current experimental settings this can completely mask the actual error channel. As a conclusion, the resulting hybrid algorithm is a viable tool for SPAM independent, robust benchmarking of arbitrary quantum gates. While non-exponential scaling is still out of reach and might well be impossible, the proposed protocol reduces the total number of experiments compared to direct Monte Carlo sampling of the gate fidelity due to error amplification and yields exponential savings in the classical preprocessing resources.

# Chapter 7

## Symmetry Benchmarking

As quantum devices scale up, many-body quantum gates and algorithms begin to surpass the abilities of classical simulation. Validation methods which rely on such classical simulation, such as process tomography and Randomized Benchmarking, cannot efficiently check correctness of most of the processes involved. In particular, non Clifford gates are required not only for universal quantum computation but for any algorithm or simulation that yields fundamental speedup in comparison with its classical counterpart. We show that it is in fact still possible to efficiently validate such non-simulable processes, by amplifying deviations from expected or engineered conservations laws in the system, combined with a unitary one-design strategy to randomize errors over the computational Hilbert subspace. We show that in the context of (fault-tolerant) quantum error correction, we can construct a one-design using the logically encoded Clifford/Pauli group over the engineered error-free stabilizer subspace to obtain average error for arbitrary logically-encoded gates and algorithms. In the case of benchmarking simulation of physical systems, these can potentially have various exotic symmetries over which one-design strategies can nonetheless be constructed. We give efficient examples for fermionic systems which conserve particle number, as well as for the Fermi-Hubbard model. The symmetry benchmarking method preserves the robustness to state preparation and measurement imperfections of Randomized Benchmarking protocols.

The successful development of quantum technologies requires not only the design and physical implementation of quantum protocols and algorithms, but the verification of their faithful operation. To what extent a black-box process can be characterized is limited by its complexity. For example, quantum cryptographic security can be validated via Bell tests [13, 99], while potential solutions to NP

---

This chapter can be found in similar form as the preprint "T. Chasseur, F. Motzoi, M. Kaicher, P.-L. Dallaire-Demers and F.K. Wilhelm, *Benchmarking non-simulable quantum processes via symmetry conservation*, arXiv:1710.04563 (2017)". The majority of research was conducted and the majority of the text written by T.C.

problems are classically verifiable in polynomial time [100]. Yet, full characterization (and error determination) of unknown processes through process tomography scales exponentially with system size, thus it is only tractable for small dimension or sparse Liouvillians [82, 101–103]. In the middle ground between validation and characterization, Randomized Benchmarking uses polynomial complexity processes to quantify average error due to exponentially complex noise, amplifying it relative to extraneous noise sources like SPAM.

Complex dynamical protocols such as digital quantum computation [10] and quantum simulation [8, 104–113] would typically be useful because classical emulation of the same tasks can require significantly more time. Yet most processes that can be validated to date involve only classically simulable ideal outcomes. As such, earlier proposals to expand the purview of RB, to include benchmarking individual operations [81], to remove assumptions about leakage and gate-dependent errors [86] (see chapter 5) and to test certain non-Clifford gates using a different basis [114, 115], are nonetheless restricted to processes that have efficient equivalent classical circuits. The benchmarking of arbitrary evolution, on the other hand, has shown to be exponentially hard [85, 116](chapter 6).

In this chapter, we present a novel efficient method that does not rely on classical simulation to benchmark general gates but instead verifies symmetry conservation laws given by specific gates or algorithms in sequences of arbitrary quantum operations. We achieve this by randomizing input states only within fulfillment of those symmetries instead of over the full Hilbert space while in turn omitting the sequence inversion. Such conservation laws vary between applications, but can typically be found anywhere from the algorithmic down to the hardware implementation level.

In the language of random matrix theory [17], we generalize the benchmarking requirements to eliminate the need for a unitary two-design, for which the randomization over the finite group must be classically simulated and subsequently inverted (hence any random gate appears twice). In contrast, by constructing a one-design strategy, we randomize not only the process itself, but also the desired final outcome within certain given boundaries. These boundaries are set by the specific symmetry which divides the gate set in block diagonal form. Maintaining a random phase relationship between blocks then ensures a monotonic exponential decay from which fidelity and error syndromes can be extracted in magnified manner. After describing the general methodology, we give examples of individual gates as well as symmetries that can be found in algorithms and provide specifically tailored protocols with polynomial scaling in the number of qubits. We close by applying the method to error correcting codes, where a single symmetry can be used to extract the (average) physical error associated with arbitrary logical operations.

## 7.1 Symmetry Benchmarking Protocol

Our objective is to reliably quantify the decay out of an ideally preserved subspace through the error channel(s) of one or several gates. The ideal dynamics of the system preserve the eigenstates of a conserved operator  $C$ , i.e. a stabilizer of the system. Let  $\lambda_\gamma$  be the degenerate eigenvalues of  $C$ . To conserve the symmetry, all operations in the algorithm (gates) must be block-diagonal in the  $C$ -eigenbasis, with the blocks corresponding to the eigenspaces, as any transition between  $\lambda_\gamma$ -eigenspaces would not preserve  $C$ . The approach of the proposed protocol is to find a set  $\mathcal{D}$  of gates on  $\mathcal{H} = \bigoplus_\gamma \mathcal{H}_\gamma$  that acts as a unitary one-design on any of the eigenspaces  $\mathcal{H}_\gamma$ . A unitary one-design is defined by having the same probability distribution as the Haar-measured special unitary group  $SU$  for first order polynomial functions in any gate and its adjoint. In particular this means

$$\frac{1}{\#\mathcal{D}} \sum_{D \in \mathcal{D}} D \rho D^\dagger = \int_{SU} dU U \rho U^\dagger, \quad (7.1)$$

with  $\#$  denoting the cardinality. We define the symmetry breaking  $\mu$  as the average population decay out of an initial  $C$ -eigenspace caused by an error channel  $\Lambda$ . We estimate the symmetry preservation  $\Gamma = 1 - \mu$  via an RB-like protocol, applying random one-design sequences of different lengths  $y$  and measuring the population of the initially populated subspace  $\mathcal{H}_{\gamma_0}$ . Using that  $\mathcal{D}$  is a unitary one-design one obtains the average symmetry preservation of a sequence as

$$\Gamma_y \equiv \frac{1}{\#\mathcal{D}^y} \sum_{\{D_j\} \in \mathcal{D}^y} \text{Tr}_{\gamma_0} \left[ \left( \prod_{j=y}^1 (\Lambda D_j) \right) (\rho_0) \right]. \quad (7.2)$$

Here  $\text{Tr}_{\gamma_0} [ \ ]$  denotes the trace over the preserved subspace  $\mathcal{H}_{\gamma_0}$ , the gates describe the effect on density matrices (superoperators) and the inverse order of the product ensures the correct succession of the quantum gates. We make use of the following definition: the *half twirl* of  $\Lambda$  over  $\mathcal{D}$  is  $\Lambda_{\text{ht}} \equiv 1/\#\mathcal{D} \sum_{D \in \mathcal{D}} \Lambda D$ , in contrast to the usual twirl  $\Lambda_{\text{twirl}} = 1/\#\mathcal{C} \sum_{C \in \mathcal{C}} C \Lambda C^{-1}$  over a group  $\mathcal{C}$  [17]. Similarly to the arguments in chapters 5 and 6,  $\Lambda_{\text{ht}}$  to the power of  $y$  is acted on by a linear functional, which is given by application to the initial state and a partial trace, hence the symmetry preservation can be simplified to

$$\Gamma_y = \text{Tr}_{\gamma_0} [\Lambda_{\text{ht}}^y(\rho_0)] = \sum_i \alpha_i \lambda_i^y. \quad (7.3)$$

As  $\Lambda_{\text{ht}}$  is a completely positive, trace preserving map, the entries on its matrix representation are real and positive and hence the absolute values of the  $\lambda_i$  are

smaller than or equal to one due to the Perron-Frobenius theorem [73–75]. This implies that the population decay can be fitted with just a few exponential decays, despite the maximum number of different eigenvalues scaling as  $d^2 \equiv 2^{2n}$ <sup>1</sup>. Finally, we can extract the averaged violation of symmetry by  $\Lambda$  per time step as

$$\mu = 1 - \int_{SU(d_0)} \text{Tr}_{\gamma_0} [\Lambda (U\rho_0 U^\dagger)] \, dU \quad (7.4)$$

$$= 1 - \frac{1}{\#\mathcal{D}} \sum_{D \in \mathcal{D}} \text{Tr}_{\gamma_0} [(\Lambda D)(\rho_0)] = 1 - \Gamma_1, \quad (7.5)$$

namely, the symmetry breaking of the gate  $C$ . The protocol inherits robustness against state preparation and measurement (SPAM) errors, similarly to Clifford benchmarking protocols [79, 80, 86]. This stabilizer leakage quantifies the error accumulation for any error channel that causes decays out of it. If error channels are predominantly manifested via decay out of the conserved subspace (i.e. the Hamming distance of the stabilized symmetry is large), this gives a metric for the cumulative average Haar-measure error.

## 7.2 Benchmarking arbitrary Operations

The error randomization over the one-design allows us to also benchmark operations outside of the set  $\mathcal{D}$ . Thus, we introduce a second set of operations that we want benchmark with respect to the error channel, which we call  $\mathcal{I}$ , containing one, several or all possible gates of the algorithm. Inspired by Interleaved Randomized

---

<sup>1</sup>The multi-exponential decay of equation 7.3 has exponentially many decay parameters  $\lambda_i$  while in practice one needs to have only a small number of parameters  $l_i$  for the fit function. We show that this is justified by Taylor expanding the symmetry preservation in the reasonably small parameter  $\varepsilon y$  and omitting terms that are of higher order in  $\varepsilon_i$  than in  $y$ :

$$\begin{aligned} \sum \alpha_i \lambda_i^y &= \sum \alpha_i (1 - \varepsilon_i)^y \\ &\approx \sum \alpha_i \left( 1 - \varepsilon_i y + \frac{1}{2} (\varepsilon_i y)^2 - \frac{1}{6} (\varepsilon_i y)^3 + \dots \right) \end{aligned}$$

while the fit function is given as

$$\begin{aligned} \sum a_i l_i^y &= \sum a_i (1 - e_i)^y \\ &\approx \sum a_i \left( 1 - e_i y + \frac{1}{2} (e_i y)^2 - \frac{1}{6} (e_i y)^3 + \dots \right) \end{aligned}$$

As we want these terms to match as close as possible, this provides a system of equations for the  $a_i$  and  $e_i$ ; just 3 different exponential decays for the fit function provides congruences up to 5th order (4th for pathological cases).

Benchmarking (IRB) [81] we interleave the random  $\mathcal{D}$ -sequence with random elements of  $\mathcal{I}$  to assess a combined stabilizer decay  $\mu_{\mathcal{ID}}$ . The symmetry preservation for that combined sequence of length  $2y$  gives

$$\Gamma_y = \frac{1}{\#\mathcal{D}^y\#\mathcal{I}^y} \sum_{\{I_j\},\{D_j\}} \text{Tr}_{\gamma_0} \left[ \left( \prod_{j=y}^1 (I_j \Lambda_{\mathcal{I}} \Lambda_{\mathcal{D}} D_j) \right) (\rho_0) \right] \quad (7.6)$$

$$= \frac{1}{\#\mathcal{D}^y\#\mathcal{I}^y} \sum_{\{I_j\},\{D_j\}} \text{Tr}_{\gamma_0} \left[ \left( \prod_{j=y}^1 (\Lambda_{\mathcal{ID}} D_j) \right) (\rho_0) \right], \quad (7.7)$$

where  $\Lambda_{\mathcal{ID}} \equiv \Lambda_{\mathcal{I}} \Lambda_{\mathcal{D}}$ . As before, we can derive  $\Gamma_1$ , or  $\Gamma_1/\Gamma_0$ , from experimental values to assess the combined error  $\mu_{\mathcal{ID}}$ . An estimate for the average decay rate of  $\mathcal{I}$  is given by  $\mu_{\mathcal{I}} \approx \mu_{\mathcal{ID}} - \mu_{\mathcal{D}}$ . This, as well as strict bounds are derived as for Interleaved Randomized Benchmarking. However, in this case, we can also efficiently benchmark errors for operations that cannot be simulated classically, such as quantum algorithms themselves or specific non-Clifford gates.

### 7.3 Number Conservation in Quantum Chemistry

An example of a prominent symmetry in quantum simulation, as well as in quantum computing architectures, is the conservation of excitation or particle number. In many-body systems, the symmetry arises when mapping from the parafermionic to the fermionic basis with the Jordan Wigner transformation [117–120]. The electron number operator  $C_n$  divides the Hilbert space into  $n + 1$  eigenspaces  $\mathcal{H}_\gamma$  with  $0 \leq \gamma \leq n$  excited qubits and dimension  $\binom{n}{\gamma}$ .

To properly define the conditions for  $\mathcal{D}$  being a one-design we define a basis for the Hilbert space  $\mathcal{R}_{\gamma_0}$  of density operators of states in  $\mathcal{H}_{\gamma_0}$ .  $\mathcal{R}_{\gamma_0}$  can be seen as the union of  $\{|i\rangle\langle i|\}_{|i\rangle \in \mathcal{H}_{\gamma_0}}$ ,  $\{|i\rangle\langle j| + |j\rangle\langle i|\}_{|i\rangle,|j\rangle \in \mathcal{H}_{\gamma_0}, i < j}$  and  $\{-i|i\rangle\langle j| + i|j\rangle\langle i|\}_{|i\rangle,|j\rangle \in \mathcal{H}_{\gamma_0}, i < j}$  which we denote  $\{|B_i\rangle\}$ ,  $\{|X_{ij}\rangle\}$  and  $\{|Y_{ij}\rangle\}$  respectively. Let  $\mathcal{D}$  be the one-design acting on  $\mathcal{R}_{\gamma_0}$ , then  $\sum_{D \in \mathcal{D}} D$  maps any density matrix onto the completely mixed state. The action of the one-design in this basis can then be simply rewritten as

$$\frac{1}{\#\mathcal{D}} \sum_{D \in \mathcal{D}} D |B_i\rangle = \frac{1}{d_0} \sum_k |B_k\rangle \quad (\S 1)$$

$$\sum_{D \in \mathcal{D}} D |X_{ij}\rangle = 0 \quad (\S 2)$$

$$\sum_{D \in \mathcal{D}} D |Y_{ij}\rangle = 0, \quad (\S 3)$$

with  $\dim(\mathcal{H}_{\gamma_0}) = d_0$ . Due to the linearity of equation 7.1, these are the only non-trivial conditions needed for constructing a unitary one-design. Focusing on (§1), we want to ensure that by sampling over  $\mathcal{D}$ , the transition between each two basis states is realized with equal probability. We implement this using arbitrary qubit permutations to randomly redistribute the excited qubits' sites and, therefore, populate each basis state with equal probability. On average, these permutations map any basis state to the completely mixed state on the conserved subspace  $\mathcal{H}_{\gamma_0}$  regardless of the initial state, thus satisfying (§1). Note that although qubit permutations implement all transitions between two states, they are not equivalent to state permutation. This is in fact crucial for the scalability of this solution and shows importance in the following section.

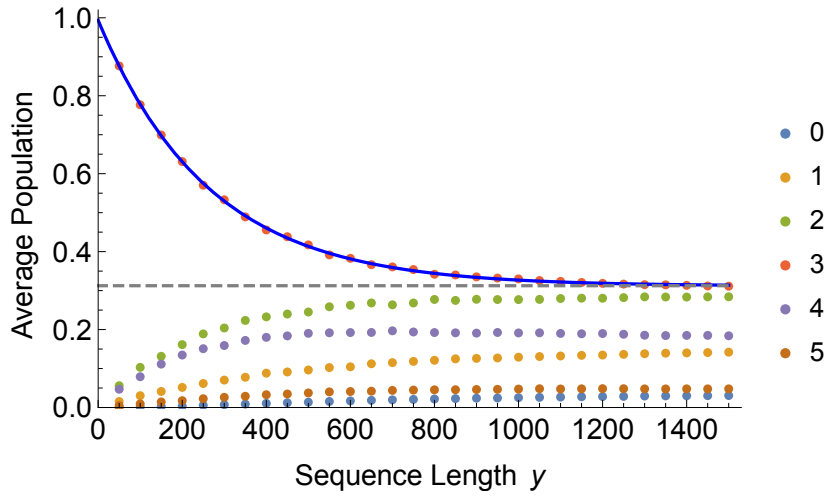


Figure 7.1: **Symmetry population decay**

Benchmarking the number preservation symmetry on five simulated qubits which are initialized in a state with three of them excited. Every permutation of qubits consists of iSWAPs which, in this example, contain predefined errors on the pair of qubits. Said error channel is derived as a unitary operator close to the identity acting on a four-qubit Hilbert space, then tracing out two qubits. The  $\gamma = 3$  subspace is benchmarked via a fit of the population decay to have an average population leakage of  $\mu = 0.88\%$  and  $\Gamma_1 = 99.12$ .

To satisfy the remaining conditions (§2) and (§3), we examine the effect of the qubit permutations via iSWAPs on the  $X_{ij}$  and  $Y_{ij}$  matrix elements, where each element again is mapped onto a density operator  $X_{i'j'}$ , or  $Y_{i'j'}$  on the space  $\mathcal{R}_{\gamma_0}$  corresponding to the preserved number of excited qubits. Introducing a uniformly random  $\pm 1$  phase between every two states ensures that these mappings occur with opposite signs equally likely, hence sum up to zero, satisfying (§2) and (§3). This random phase is not inherently given by the phases included in the iSWAPs but easily achieved by a probability  $1/2$   $\sigma_Z$ -gate on every qubit. This matches our intuition that  $X_{ij}$  and  $Y_{ij}$  represent coherent phases between states, so that randomizing all phases should eliminate them. The results of the above protocol using the derived unitary one-design are depicted in figure 7.1.

The dynamics of the random sequence can also be viewed in a more accessible fashion: Since applying the ideal  $\sum_{D \in \mathcal{D}} D$  twice is equivalent to a single application – depolarization does not change a completely depolarized state – reviewing the average symmetry preservation of equation 7.2 gives

$$\Gamma_y = \frac{1}{\#\mathcal{D}^{2y}} \sum_{\{C_j\} \in \mathcal{D}^y} \sum_{\{D_j\} \in \mathcal{D}^y} \text{Tr}_{\gamma_0} \left[ \left( \prod_{j=y}^1 (C_j \Lambda D_j) \right) (\rho_0) \right]. \quad (7.8)$$

The updated  $\Lambda'_{\text{ht}} = 1/\#\mathcal{D}^2 \sum_{C,D} CAD$  commutes with any unitary evolution within subspaces  $\mathcal{H}_\gamma$  and can therefore be reduced to simple transition rates between those subspaces. This not only provides a more intuitive concept but also gives the motivation for the ansätze in the following sections.

## 7.4 Parity Conservation and the Fermi-Hubbard Model

Parity conservation is ubiquitous in error correction circuitry and measurement-based entanglement generation. It also appears physically in models of strongly correlated electrons, including basic atomic structure and second quantization [121]. A medium-sized quantum computer can simulate the most costly parts of the Fermi-Hubbard Hamiltonian [122]. While some of the Hamiltonians employed in that scheme are number conserving and can be treated using the set  $\mathcal{D}$  derived previously, others are not, namely, the terms which induce superconductivity to the model. However, these terms always change the electron number by two (a Cooper pair), thereby preserving parity.

As the Fermi-Hubbard model involves an even number  $n$  of electron sites/qubits, the subspaces  $\mathcal{H}_{\text{even}}$  and  $\mathcal{H}_{\text{odd}}$  are of equal dimension  $2^{n-1}$ . It is in principle possible to map the  $(n - 1)$  qubit Clifford group onto those subspaces. However, such

a protocol would potentially increase gate complexity exponentially, hence we refrain from finding a new unitary one-design for  $\mathcal{H}_{\text{even}}$  and  $\mathcal{H}_{\text{odd}}$  but rely on the transition rates derived for the number conservation. The symmetry preservation on the even subspace for only one individual gate  $I$  and an assumed one-design on the even subspace is

$$\Gamma_1 = \frac{1}{\#\mathcal{D}} \sum_{D \in \mathcal{D}_{\text{even}}} \text{Tr}_{\text{even}} [(I\Lambda_{\mathcal{I}}\Lambda_{\mathcal{D}}D)(\rho_0)] \quad (7.9)$$

$$= \frac{1}{2^{n-1}} \text{Tr}_{\text{even}} [(I\Lambda_{\mathcal{I}}\Lambda_{\mathcal{D}})(\mathbb{1}_{\text{even}})], \quad (7.10)$$

as the average application of the unitary one-design  $\mathcal{D}_{\text{even}}$  to any even state would map to the identity matrix on the even subspace. Writing this matrix as sum of the identities on different subspaces gives

$$\Gamma_1 = \sum_{\gamma \text{ even}} \frac{d_{\gamma}}{2^{n-1}} \sum_{D \in \mathcal{D}} \text{Tr}_{\text{even}} [(I\Lambda_{\mathcal{I}}\Lambda_{\mathcal{D}}D)(\rho_{\gamma})] \quad (7.11)$$

$$\equiv \sum_{\gamma \text{ even}} \frac{d_{\gamma}}{2^{n-1}} \Gamma_1^{\gamma}, \quad (7.12)$$

where  $\rho_{\gamma}$  is an initial state in the respective subspace. Each  $\Gamma_1^{\gamma}$  can be derived by sequences of the usual form; an estimation for  $\mu_{\mathcal{I}}$  can be obtained for each subspace via interleaved symmetry benchmarking and consequently an overall estimation can be found. As there are only  $n/2$  or  $(n/2) + 1$  different subspaces, this scales linearly in  $n$  and is therefore efficiently scalable in the number of qubits. The protocol also translates easily to a set  $\mathcal{I}$  of gates allowing for an efficient symmetry benchmarking. Figure 7.2 shows an example of benchmarking parity conservation.

## 7.5 Benchmarking logically encoded Processes

Conserved symmetries play a fundamental role in error correction codes (ECC), where they are engineered to provide tolerance to error. The vast majority (asymptotically speaking) of error leaks through particular ‘syndrome’ states, that is, avoiding direct transitions between logical stabilizer eigenstates. There are many examples of engineered redundancy for the purposes of error suppression or monitoring, most notably in (fault-tolerant) ECC, but also in quantum cryptography, simulation, metrology and adiabatic quantum computation.

We consider here a Hilbert space encoded in the form  $\mathcal{H} = \{0, 1\}^{\otimes n} \otimes \{0, 1\}^{\otimes m}$  where the degrees of freedom of  $m$  qubits are used for syndrome measurements – typically  $\{0, 1\}^{\otimes n}$  and  $\{0, 1\}^{\otimes m}$  can not be understood as the Hilbert spaces of

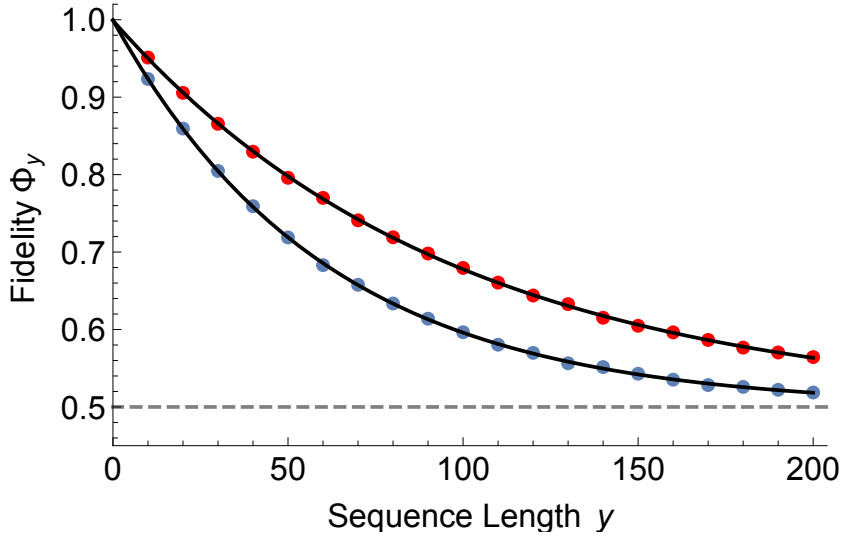


Figure 7.2: **Interleaved Symmetry Benchmarking** for the Fermi-Hubbard model on the 6 qubit even subspace for interleaved gate  $I = \sigma_2\sigma_3 + \sigma_2^\dagger\sigma_3^\dagger$  with an exact symmetry breaking of  $\mu_I = 0.30\%$ . Extracting  $\mu_{\text{ISB}} = 0.86\%$  and  $\mu_{\mathcal{D}} = 0.51\%$  provides an estimate of  $\mu_I = 0.35\%/\Gamma_1 = 0.9965$  which is remarkably close to the actual values as  $\Lambda_I$  is not the dominating error term. This better-than-expected performance is similar to observations from Interleaved Randomized Benchmarking of Clifford gates [81].

$n$  or  $m$  physical qubits. The Hilbert space can be written as  $\mathcal{H} \equiv \mathcal{H}_{\text{comp}} \oplus \mathcal{H}_{\text{err}}$  with  $\mathcal{H}_{\text{comp}} \equiv \{0,1\}^{\otimes n} \otimes \{|\Psi_s\rangle\}$ , such that the quiescent state  $|\Psi_s\rangle$  is used to check for possible errors. We look at logical operations  $L$  in the ECC which are comprised of a subsequence  $G$  of (faulty) local gates intended to apply the logical gate, followed by syndrome measurement  $M$  in  $\{0,1\}^{\otimes m}$  and correction feedback  $F_j$  towards  $\mathcal{H}_{\text{comp}}$ . Thus, at any time step  $j$ , we find  $L_j = F_j M_j G_j$ . As before, to benchmark the preservation of  $\mathcal{H}_{\text{comp}}$ , we require that no phase relations are built up with the  $\mathcal{H}_{\text{err}}$ , for which we use a generalized operation  $R_j$ . The one-design sequence can then be written as

$$\Gamma_y = \frac{1}{\#\mathcal{C}^y} \sum_{\{C_j\} \in \mathcal{C}^y} \text{Tr}_{\text{comp}} \left[ \left( \prod_{j=y}^1 (\Lambda_j R_j C_j) \right) \rho_0 \right] \quad (7.13)$$

where  $C_j$  are logically-encoded Clifford gates prior to error correction. As for the general protocol and the examples discussed above, we again ensure we take the correct group average that reduces our error channel to a depolarizing one; in the present case we do so achieving a half-twirl using the Clifford group amended

with phase randomization between the  $\mathcal{H}_{\text{err}}$  and  $\mathcal{H}_{\text{comp}}$  subspaces. In contrast to the number conservation case we achieve this not via implementing random phases but via syndrome measurements, i.e.  $R_j = M_j$ . These syndrome measurements – by construction – validate the integrity of  $|\Psi\rangle$  and therefore suppress all phase relation between  $\mathcal{H}_{\text{comp}}$  and  $\mathcal{H}_{\text{err}}$ . Another, more subtle, way is to apply both a syndrome measurement (throwing away the result) and a randomly chosen correction operation  $F'_j$  from amongst the possible correction operations  $\{F'_j\}$ , so that  $R_j = F'_j M_j$ . At the end, one obtains an average error per gate estimate of the compound operations  $\{R\} \times \mathcal{C}$ , i.e.  $\mu_{RC}$ . Note that since the native error rates of the logically-encoded Clifford gates  $C_j$  are obtainable via standard Randomized Benchmarking underlying Clifford operations, we can also derive estimates for syndrome measurement and error correction feedback as  $\mu_R \approx \mu_{RC} - \mu_C$ , as with standard IRB.

Using the above protocol, we now have a means to obtain the decay rate into the  $\mathcal{H}_{\text{err}}$  subspace. Note that this decay into  $\mathcal{H}_{\text{err}}$  does not correspond to a logical error, since the vast majority of errors is suppressed by the error correction feedback. However, these decay rates do give information about physical error statistics, which the one-design sequence averages over all input states and then amplifies above the noise level. Moreover, we can use the protocol with interleaved gates to benchmark arbitrary individual circuits  $G$ , e.g. non-Clifford, non-transversal logical gates needed for universal computation or entire algorithms, obtaining physical error  $\mu_G$ . Under the standard assumption in ECC that correlated errors longer than the distance  $d$  of the code are negligible, we can bound the logical fault rate as  $\mu_L \lesssim (\mu_F + \mu_M + \mu_G)^d$  with  $\mu_F, \mu_M$  and  $\mu_G$  the symmetry breaking associated with feedback, syndrome measurement and gate sequence. With the above protocol we do not only provide a means to verify the ECC – which can often be done in a more direct way with RB [123] – but also provide a more specific validation of the underlying components. This analysis could be particularly helpful for concatenated ECC, where logical errors at one layer correspond to the physical errors at the level above.

## 7.6 Conclusion

Both quantum simulation and universal quantum computation involve complex processes that cannot be efficiently predicted classically. We showed that this restriction does not prohibit their validation, provided the implementation being benchmarked can be found or engineered to conserve symmetries in the system. This is the case for many quantum simulation tasks, such as fermionic systems and the Fermi-Hubbard model, as well as for fault-tolerant quantum computation, where stabilizers of error correcting codes are preserved by logical operations. We

present a symmetry benchmarking protocol relying on randomization via unitary one-designs on conserved subspaces, that allows assessment of average channel error while maintaining robustness to state preparation and measurement imperfections.



## Part II

# Environmental Effects on adiabatic Quantum Computing



We have discussed two very different approaches to implementing quantum computation and taking advantage of its unique properties in comparison with classical machines. These approaches show very different strategies to scaling and the treatment of environmental influence: While gate-based quantum computing requires fidelities to meet hard thresholds and relies on error correction codes to increase fidelities, adiabatic quantum computing is conjectured to be more tolerant against coupling to the environment [124] or to even benefit from it [125, 126]. As a result current quantum annealing architectures operate with a larger number of qubits, but less shielding from the environment [127]. Therefore, its susceptibility to environmental effects is a different but equally important open question, essential to a scalable implementation.

In fact, the robustness against the environment is limited: It is a known result in strong coupling physics, that high frequency bath modes correspond to structural changes of the effective Hamiltonian, e.g., the suppression of coupling in a two-level-system as shown using renormalization group theory [128, 129] as well as experimentally [130]. With increasing bath coupling the two-level-system undergoes a dissipative phase transition towards a complete suppression of coupling between the qubit states – this would mark a breaking point for adiabatic quantum computation as it would limit its complexity to that of single qubits. In chapter 8 we give an introduction to renormalization group theory and related methods. We specifically use poor man’s scaling [131] to derive an effective Hamiltonian and reduced density matrix, to describe the qubits influenced by Ohmic baths in chapter 9. We go beyond weak coupling, which can be treated with perturbative master equations [124, 132] but is insufficient for describing a scaled quantum annealer and rather focus on a more suitable regime, which we coin locally coherent but globally dephased (LCGD). In chapter 10 we will show that this regime is limited by an effective dephasing of both system Hamiltonian and reduced density matrix. We discuss implications for annealing algorithms with regard to the desired ground state and extractable information as well as potential drawbacks or benefits from system-bath entangled states.

---

The content of chapters 9 and 10 has in similar form been submitted for publication in Nature Communications. It can also be found in the preprint ”T. Chasseur, S. Kehrein, and F.K. Wilhelm, *Environmental effects in quantum annealing*, arXiv:1809.08897 (2018)”. The majority of research was conducted and the majority of the text written by T.C.



# Chapter 8

## Renormalization Group Methods

The renormalization group describes a family of techniques to address the occurrence of vastly varying energy scales in physical systems. While formalized in particle physics and being substantial to the initial derivation of the Lamb shift [133], it is applied across fields, e.g., in quantum electrodynamics to solve the Kondo problem [134, 135]. Renormalization group theory relies on the assumption that high energy affects the dynamics near the ground state only weakly and/or in a well controlled fashion. Its approach is to discard the highest energy levels via reducing a cutoff frequency  $\omega_c$  and translate the effect of the dropped energy level into a change to the remaining Hamiltonian. Historically, but not necessarily, the energy range is rescaled by multiplying the Hamiltonian with a constant factor. The above can be repeated successively, which in the limit of small changes to  $\omega$  describes a continuous transformation [136].

In the scope of this thesis we rely on different renormalization techniques which will be introduced and demonstrated in the following. We employ the single-spin-Boson model as a sufficiently nontrivial example. It is extensively studied, suitable to model a dissipative qubit and relates naturally to the multi-spin-Boson model [128].

### 8.1 Adiabatic Renormalization

A prominent instance of renormalization group techniques is the adiabatic renormalization [128]. It is tailored specifically towards a single spin coupled to a Bosonic bath. As the two-level-system is frequently reoccurring in quantum physics, either as spin 1/2 or to approximate larger Hilbert spaces, it is of relevance for a variety of fields – and especially important throughout this thesis, as it describes the qubit. We introduce the protocol following the arguments of reference [128]. The

full spin-Boson model is given by the Hamiltonian

$$H = -\frac{\Delta}{2}\sigma_X + \varepsilon\sigma_Z + \sum_k \frac{\sigma_Z}{2}\lambda_k(a_k + a_k^\dagger) + \sum_k \omega_k a_k^\dagger a_k. \quad (8.1)$$

The bath frequencies are restricted by the cutoff frequency  $\omega_c$ ; the coupling strength of each mode is mediated by the  $\lambda_k$ . While the environment can often be modeled by an Ohmic bath [137], we do not impose a restriction to non pathological distribution of modes.

To realize the renormalization group approach we choose a new highest frequency  $\omega_0$  which is large compared to the frequencies  $\Delta$  and  $\varepsilon$  of the two-level system, but smaller than  $\omega_c$ . As the contribution of high energy bath modes  $\omega_0 < \omega_k < \omega_c$  is dominant we find the two lowest energy eigenstates of the last three terms, i.e., of

$$H_{\text{part}} = \varepsilon\sigma_Z + \frac{\sigma_Z}{2}\lambda_k(a_k + a_k^\dagger) + \omega_k a_k^\dagger a_k. \quad (8.2)$$

It is diagonalized by the displacement operator  $D(\sigma_Z\lambda_k/2\omega_k) = \exp\left(\sigma_Z\lambda_k/2\omega_k(a_k^\dagger - a_k)\right)$  in optical phase space. Using a variant of the Baker Campbell Hausdorff formula we find

$$\begin{aligned} DH_{\text{part}}D^\dagger &= \varepsilon\sigma_Z + \frac{\sigma_Z}{2}\lambda_k(a_k + a_k^\dagger) + \left[\sigma_Z\frac{\lambda_k}{2\omega_k}(a_k^\dagger - a_k), \frac{\sigma_Z}{2}\lambda_k(a_k + a_k^\dagger)\right] \\ &\quad + \omega_k a_k^\dagger a_k + \left[\sigma_Z\frac{\lambda_k}{2\omega_k}(a_k^\dagger - a_k), \omega_k a_k^\dagger a_k\right] \end{aligned} \quad (8.3)$$

$$= \varepsilon\sigma_Z + \frac{\sigma_Z}{2}\lambda_k(a_k + a_k^\dagger) + \text{const.} + \omega_k a_k^\dagger a_k - \frac{\sigma_Z}{2}\lambda_k(a_k^\dagger + a_k) \quad (8.4)$$

$$= \varepsilon\sigma_Z + \omega_k a_k^\dagger a_k \quad (8.5)$$

when omitting constant terms. When restricting the Hilbert space to the lowest eigenvectors  $D^\dagger(\sigma_Z\frac{\lambda_k}{2\omega_k})\{|0\rangle, |1\rangle\} \otimes |0\rangle_k = \{|0\rangle \otimes D^\dagger(\frac{\lambda_k}{2\omega_k})|0\rangle_k, |1\rangle \otimes D^\dagger(-\frac{\lambda_k}{2\omega_k})|0\rangle_k\}$ , we need to reevaluate the coupling introduced by  $\Delta$  between those states. We find

$$\begin{aligned} \langle 0|_k D\left(\frac{\lambda_k}{2\omega_k}\right) \otimes \langle 0| - \frac{\Delta}{2}\sigma_X |1\rangle \otimes D^\dagger\left(-\frac{\lambda_k}{2\omega_k}\right) |0\rangle_k \\ = -\frac{\Delta}{2} \langle 0|_k D\left(\frac{\lambda_k}{\omega_k}\right) |0\rangle_k \end{aligned} \quad (8.6)$$

$$= -\frac{\Delta}{2} \exp\left(-\frac{\lambda_k^2}{2\omega_k^2}\right). \quad (8.7)$$

As other bath-modes are unaffected by the displacement of  $\omega_k$  and all terms but  $-\Delta/2$  commute with  $\sigma_z$  we can apply the above transformation to each  $\omega_0 < \omega_k < \omega_c$ , yielding

$$\Delta' = \Delta \prod_{\omega_k \geq \omega_0} \exp\left(-\frac{\lambda_k^2}{2\omega_k^2}\right) \quad (8.8)$$

as iteration of adiabatic renormalization. With the effective reduction of the qubit Hamiltonian it allows for a reevaluation of  $\omega_0$  and successive application. We note first that adiabatic renormalization relies on the approximation to neglect the coupling to displaced excited bath modes. This approximation is justified as these corrections can be shown to be smaller by a factor of  $\lambda_k/\omega_k$  [128] and can therefore be neglected in leading order. Secondly, it is important to remember that the effective Hamiltonian no longer describes pure qubit states but rather dressed system and bath ones.

We remark that for an Ohmic distribution of bath modes, i.e.  $J(\omega) = 2\alpha\omega\Theta(\omega_c - \omega)$  and continuous reduction of  $\omega_0$  the dynamics of equation 8.8

- for  $\alpha > 1$  result in reduction of  $\Delta$  faster than  $\omega_c$ , thus the  $\sigma_x$  terms effectively vanish.
- for  $\alpha < 1$  suppress  $\Delta$  slower and therefore the adiabatic renormalization can only be carried out as long as  $\omega_0 \gg \Delta$  resulting in a nonzero effective coupling.
- yield a phase transition at  $\alpha = 1$ .

The exact derivation of this last step is independent of the renormalization protocol and can be found in the given references as well as in the next chapter when discussing poor man's scaling of the multi-spin-Boson model.

## 8.2 Poor Man's Scaling

Poor man's scaling is a simple, yet effective take on renormalization originating in the theory of superconductivity [138] and the Kondo problem [139]. Characteristically for renormalization techniques, it assumes different energy scales within a system so that the Hilbert space can be separated into a high energy and lower energy part, i.e.  $\mathcal{H} \equiv \mathcal{H}_l \oplus \mathcal{H}_h$ . There is no necessity for a distinct gap in the energy spectrum; just for the energy scales of  $\mathcal{H}_h$  to be large in comparison to energies near the ground state energy. The approach of poor man's scaling is to derive an eigenvalue equation on the lower energy subspace, resulting in an effective Hamiltonian: We introduce the protocol in the following.

Let  $P_{(l/h)}$  be projectors onto the respective low and high energy Hilbert spaces and  $H_{(l/h)(l/h)'} = P_{(l/h)} H P_{l/h}'$  the respective part of the Hamiltonian. We rewrite the stationary Schrödinger equation to

$$\begin{pmatrix} H_{ll} & H_{lh} \\ H_{hl} & H_{hh} \end{pmatrix} \begin{pmatrix} |\Psi_l\rangle \\ |\Psi_h\rangle \end{pmatrix} = E \begin{pmatrix} |\Psi_l\rangle \\ |\Psi_h\rangle \end{pmatrix} \quad (8.9)$$

hence

$$H_{hl} |\Psi_l\rangle + H_{hh} |\Psi_h\rangle = E |\Psi_h\rangle \quad (8.10)$$

$$|\Psi_h\rangle = (E - H_{hh})^{-1} H_{hl} |\Psi_l\rangle \quad (8.11)$$

and therefore

$$(H_{ll} + H_{lh} (E - H_{hh})^{-1} H_{hl}) |\Psi_l\rangle = E |\Psi_l\rangle. \quad (8.12)$$

equation 8.12 is exact but nonlinear and therefore not easily solvable for  $E$ . In the low energy regime  $H_{hh}$  is the dominant term in  $(E - H_{hh})$ . The standard ansatz is to approximate  $E$  by the ground state energy  $E_{gs}$ ; however we found that this gives an unwanted shift in the effective change of the Hamiltonian resulting in non negligible errors. We therefore refrain from making the approximation while still assuming that  $E$  is small compared to all energy levels of  $\mathcal{H}_h$ . This leads to a nonlinear equation for determining  $E$  which can be linearized by approximations better suitable for the problem at hand.

The application to the multi-spin-Boson model is part of original research presented in chapter 9; the single-spin-Boson model emerges as a special case and coincides with the findings of adiabatic renormalization in leading order.

### 8.3 The Flow Equation Approach

The flow equation approach to renormalization was invented independently in many-particle [140], as well as high-energy physics [141, 142] under the name similarity renormalization scheme. It is unique in its ansatz to reduce the maximum energy difference rather than total energy levels: While the renormalization techniques introduced above discards the highest energy levels, the flow equations approach aims to eliminate the coupling between levels with the largest difference in energy, which is depicted in figure 8.1. Its advantage compared to other methods is that it is not necessary restricted to the low energy regime. We give an introduction in the following; a more detailed analysis can be found in reference [131].

To derive the flow equations we set the system Hamiltonian to be of the form

$$H = H_0 + H_{\text{int}} \quad (8.13)$$

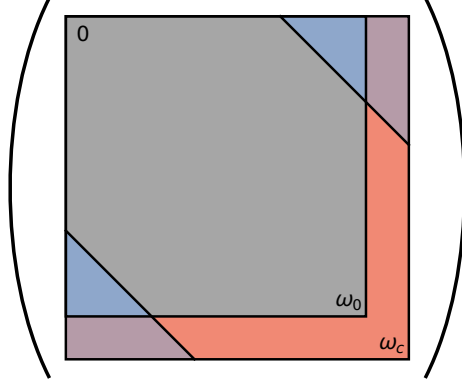


Figure 8.1: **Visualization of the flow equation approach**

We display a schematic representation of the matrix representing the initial Hamiltonian. Conventional renormalization approaches such as poor man's scaling eliminate frequencies above a threshold  $\omega_0$  (red) while flow equations aim to successively remove matrix entries with the highest energy difference (blue). A related visualization has been presented in reference [131].

where we assume  $H_0$  to be diagonal and  $H_{\text{int}}$  to introduce off diagonal terms that mediate a coupling between the eigenstates of  $H_0$ . We aim to introduce a unitary transformation  $U$  that reduces the couplings between pairs of states with maximal energy gap. Or, rather, we want to derive a continuous  $U(B)$  depending on a flow parameter  $B$  that successively removes couplings of decreasingly distant states. We aim to choose this transformation in a way that  $H(B) = U(B)HU^\dagger(B)$  equals the initial Hamiltonian at  $B = 0$  and approaches diagonality for  $B \rightarrow \infty$ . To do that we define  $U(B)$  via the antihermitian generator  $\eta(B)$  such that

$$\frac{dU(B)}{dB} = \eta(B)U(B) \quad (8.14)$$

$$\frac{dH(B)}{dB} = [\eta(B), H(B)]. \quad (8.15)$$

When comparing the flow parameter to time, the generator  $\eta$ , up to a factor, is equivalent to a Hamiltonian sponsoring the unitary evolution  $U(B)$  – one can borrow the intuitive understanding of that evolution. For example, we assume that the notion of 'flow' for the change in the off diagonal terms with varying the time-like parameter  $B$  likely sparked the idea for naming the protocol.

To realize a correctly directed flow a suitable choice of  $\eta$  is essential. The canonical choice  $\eta = [H_0, H_{\text{int}}]$  usually achieves the suppression of the most off diagonal terms. However, it is often not the most elegant choice as it is prone to

system specific downsides. We elaborate on both advantages and disadvantages of the canonical generator by calculating the derivative of the Hamiltonian.

$$\frac{dH}{dB} = [\eta, H] \quad (8.16)$$

$$= [[H_0, H_{\text{int}}], H_0 + H_{\text{int}}] \quad (8.17)$$

$$= [[H_0, H_{\text{int}}], H_0] + [[H_0, H_{\text{int}}], H_{\text{int}}] \quad (8.18)$$

Without loss of generality we write  $H_0 = \sum_n \varepsilon_n |n\rangle\langle n|$  and  $H_{\text{int}} = \sum_{i \neq j} c_{ij} |i\rangle\langle j|$ . Here the real-valued  $\varepsilon_n$  denote the energy levels of the  $H_0$ -eigenstates  $|n\rangle$  and the  $c_{ij} = c_{ji}^*$  a coupling between those. Evaluating the first term of equation 8.18 we find

$$[[H_0, H_{\text{int}}], H_0] = \left[ \sum_{i \neq j} (\varepsilon_i - \varepsilon_j) c_{ij} |i\rangle\langle j|, H_0 \right] \quad (8.19)$$

$$= \sum_{i \neq j} -(\varepsilon_i - \varepsilon_j)^2 c_{ij} |i\rangle\langle j|. \quad (8.20)$$

It introduces the suppression of couplings increasing with energy gap as intended. We evaluate the second term to

$$\begin{aligned} [[H_0, H_{\text{int}}], H_{\text{int}}] &= \left[ \sum_{i \neq j} (\varepsilon_i - \varepsilon_j) c_{ij} |i\rangle\langle j|, H_{\text{int}} \right] \\ &= \sum_{i \neq j} (\varepsilon_i - \varepsilon_j) c_{ij} |i\rangle\langle j| c_{ji} |j\rangle\langle i| \\ &\quad - \sum_{i \neq j} c_{ji} |j\rangle\langle i| (\varepsilon_i - \varepsilon_j) c_{ij} |i\rangle\langle j| \\ &\quad + \sum_{i \neq j \neq k} (\varepsilon_i - \varepsilon_j) c_{ij} |i\rangle\langle j| c_{jk} |j\rangle\langle k| \\ &\quad - \sum_{i \neq j \neq k} c_{ki} |k\rangle\langle i| (\varepsilon_i - \varepsilon_j) c_{ij} |i\rangle\langle j| \end{aligned} \quad (8.21)$$

$$\begin{aligned} &= 2 \sum_{i \neq j} (\varepsilon_i - \varepsilon_j) |c_{ij}|^2 |i\rangle\langle i| \\ &\quad + \sum_{i \neq j \neq k} (\varepsilon_i - \varepsilon_j) (c_{ij} c_{jk} |i\rangle\langle k| + h.c.). \end{aligned} \quad (8.22)$$

While the first term represents a shift in energy levels, we also introduce new couplings between pairs ( $|i\rangle, |k\rangle$ ) through a shared coupling to  $|j\rangle$ . This has two apparent downsides: First, as the intention of the flow equation approach is to

suppress off-diagonal terms it is important to ensure that the creation does not outweigh the suppression – at least beyond a set energy gap. This might be highly nontrivial depending on the system. Second, we are reviewing methods to treat high dimensional Hilbert spaces, the dynamics of which are often described, at least approximately, by sparse Hamiltonians. The introduction of exponentially many new coupling terms can render the Hamiltonian intractable by analytical and numerical means, or at least make its treatment significantly more complex. We conclude that, while the canonical generator provides a reasonable ansatz, it should be adjusted to the specific system to optimize the protocol. To substantiate this, we revisit the spin-Boson Hamiltonian of equation 8.1 in the special case of  $\varepsilon = 0$ .

$$H = -\frac{\Delta}{2}\sigma_X + \sum_k \frac{\sigma_Z}{2}\lambda_k(a_k + a_k^\dagger) + \sum_k \omega_k a_k^\dagger a_k \quad (8.23)$$

The identification

$$H_0 = -\frac{\Delta}{2}\sigma_X + \sum_k \omega_k a_k^\dagger a_k \quad (8.24)$$

$$H_{\text{int}} = \sum_k \frac{\sigma_Z}{2}\lambda_k(a_k + a_k^\dagger) \quad (8.25)$$

aims to eliminate the coupling between spin and bath. Note that  $H_0$  is not diagonal but easily diagonalizable. We compute the canonical generator to be

$$\eta = [H_0, H_{\text{int}}] \quad (8.26)$$

$$= i\sigma_Y \sum_k f_k^+ \frac{\Delta\lambda_k}{2}(a_k + a_k^\dagger) + \sigma_Z \sum_k f_k^- \frac{\lambda_k\omega_k}{2}(a_k^\dagger - a_k) \quad (8.27)$$

while introducing parameters  $f_k^+, f_k^-$ , which are equal to one for the canonical generator but allow to modify  $\eta$ . To understand the flow of the Hamiltonian we look at

$$\begin{aligned} [\eta, H_0] &= -\sigma_Z \sum_k f_k^+ \frac{\Delta^2\lambda_k}{2}(a_k + a_k^\dagger) + i\sigma_Y \sum_k f_k^+ \frac{\Delta\lambda_k\omega_k}{2}(a_k - a_k^\dagger) \\ &\quad + i\sigma_Y \sum_k f_k^- \frac{\Delta\omega_k\lambda_k}{2}(a_k - a_k^\dagger) - \sigma_Z \sum_k f_k^- \frac{\lambda_k\omega_k^2}{2}(a_k + a_k^\dagger). \end{aligned} \quad (8.28)$$

To prevent the generation of new coupling terms we set  $f_k^+ = f_k = -f_k^-$ . These terms arise for the canonical generator due to the energy difference  $\Delta$  between eigenstates of the qubit operator  $\sigma_X$ ; they do not contradict the findings of

equation 8.20. The commutator of generator and interaction term, completing the derivative of  $H(B)$ , is

$$[\eta, H_{\text{int}}] = -\sigma_X \sum_{k, \bar{k}} f_k \frac{\Delta \lambda_k \lambda_{\bar{k}}}{2} (a_{\bar{k}} + a_{\bar{k}}^\dagger)(a_k + a_k^\dagger) + \sum_k f_k \frac{\lambda_k^2 \omega_k}{2} \quad (8.29)$$

where the constant shift can be omitted. A striking difference in comparison to adiabatic renormalization and – as we will see – to poor man’s scaling are the terms coupling to multiple bath modes. They naturally do not arise in leading orders when eliminating bath modes one by one. To treat said terms, we apply normal ordering with respect to the vacuum or some finite temperature

$$(a_k + a_k^\dagger)(a_{k'} + a_{k'}^\dagger) =: (a_k + a_k^\dagger)(a_{\bar{k}} + a_{\bar{k}}^\dagger) : + \delta_{k, \bar{k}} \langle 2a_k^\dagger a_k + 1 \rangle, \quad (8.30)$$

an averaging out the fluctuations, thus omitting the normal ordered terms yields

$$\frac{dH}{dB} = \sigma_Z \sum_k f_k (\omega_k^2 - \Delta^2) \frac{\lambda_k}{2} (a_k + a_k^\dagger) - \sigma_X \sum_k f_k \frac{\Delta \lambda_k^2}{2} \langle 2a_k a_k^\dagger + 1 \rangle. \quad (8.31)$$

All of these terms appear in the initial Hamiltonian; the evolution in  $B$  can be expressed solely through the evolution of prefactors, i.e. their flow. The above differential equation can be cast in a different set of flow equation describing the evolution of the flow parameters. We find

$$\frac{d\lambda_k}{dB} = f_k \lambda_k (\omega_k^2 - \Delta^2) \quad (8.32)$$

$$\frac{d\Delta}{dB} = \sum_k f_k \Delta \lambda_k^2 \langle 2a_k^\dagger a_k + 1 \rangle. \quad (8.33)$$

Before analyzing these equation we revisit the assumption of Ohmically distributed bath modes. These can be approximated by a continuous spectral function. The transition  $\sum_k \lambda_k^2 \rightarrow \int J(\omega) d\omega$  is justified for any given spectral density and defined by  $J(\omega) \equiv \sum_k \lambda_k^2 \delta(\omega - \omega_k)$ ; the flow equations for the spectral function are given as

$$\frac{dJ(\omega, B)}{dB} = J(\omega, B) f(\omega) (\omega^2 - \Delta(B)^2) \quad (8.34)$$

$$\frac{d\Delta}{dB} = \int_{\omega=0}^{\omega_c} d\omega J(\omega, B) f(\omega) \Delta(B) \langle 2a_{k(\omega)}^\dagger a_{k(\omega)} + 1 \rangle. \quad (8.35)$$

As we aim to eliminate terms in  $H_{\text{int}}$ , i.e., the coupling between system and bath, we need to choose  $f(\omega)$  in a way that  $f(\omega^2 - \Delta^2)$  is negative. Looking at large  $\omega$  this means negative  $f$  and results in a suppression of the qubit term  $\Delta$ . This finding

coincides at least qualitatively with the results derived by adiabatic renormalization. For the scope of this thesis, where we examine qubits under the influence of an environment, the regime of  $\omega \gg \Delta$  is dominating and hence determines the effects. However the above flow equations are not limited to that assumption. We find that  $\omega < \Delta$  requires positive  $f$  and thus results in an increase in qubit coupling  $\Delta$ .

While in the above derivation flow equations are not limited to the regime of  $\omega \gg \Delta$ , they are not exact but rely on assumptions on the environment that allow to omit normal ordered terms. Both approaches are non equivalent and represent a different understanding of the environment; which is more suitable depends on the physical system in question. For this work the more decisive difference however was the applicability to multiple spins on which we focus in the following chapter.



# Chapter 9

## Multi-Spin-Boson Model

Any physical device geared towards quantum computation is built around a set of two-level-systems, i.e. qubits which can, within limitations, interact with each other as well as be controlled and measured by an outside observer. While a circuit model architecture relies on long qubit lifetimes and high fidelity implementation of universal gate sets [7, 143], the computational power of quantum annealing is encoded in the ground state of a widely adjustable Hamiltonian [9]. As such, it is believed to be more robust against imperfections. The consequently following faster scaling to larger system sizes comes at the cost of the aforementioned worse shielding against the environment [127]. To account for this, we describe the system bath dynamics employing the multi-spin-Boson model, i.e., a number  $n$  of qubits coupled to bath modes

$$H = H_q + \sum_k \frac{\sigma_z^{i_k}}{2} \lambda_k (a_k + a_k^\dagger) + \sum_k \omega_k a_k^\dagger a_k. \quad (9.1)$$

Here  $H_q$  is the Hamiltonian solely acting on the qubit system;  $k$  denotes the bath mode with frequency  $\omega_k$ ,  $i_k \in \{1, 2, \dots, n\}$  the respective qubit it is coupled to and  $\lambda_k$  mediates the coupling strength. While the above Hamiltonian implies separated bath modes for each qubit we will treat the effects of a shared bath as well. Regardless thereof, an Ohmic distribution of bath modes  $J_i(\omega) = 2\alpha_i\omega\Theta(\omega_c - \omega)$  has been found suitable to model environmental effects in the regarded frequency regime and will be used throughout this work [137].

Renormalization group techniques are tools to treat high dimensional quantum systems with varying energy scales. As discussed, its ansatz is to translate coupling to strongly off resonant terms into small changes to the Hamiltonian at a preferred frequency scale hence reducing the relevant Hilbert space. The generalization from the single spin case treated in the previous chapter 8 to many qubits, however, poses a nontrivial challenge: A challenge that we address in this chapter using mainly poor man's scaling but also investigating the use of flow equations.

## 9.1 Transformation under poor Man's Scaling

We revisit equation 8.12, describing the poor man's scaling approach as introduced in chapter 8. From that we will derive an effective Hamiltonian as well as a reduced density matrix in the settings of adiabatic quantum computation. To that end, we look at a quantum system of multiple qubits, coupling via Pauli  $\sigma_Z$  to a set of bath modes which we assume to be Ohmically distributed, i.e. a system that is described by equation 9.1 with  $H_q \equiv \sum_{\vec{s}} \Delta_{\vec{s}} \sigma_{s_1} \otimes \sigma_{s_2} \dots \sigma_{s_n}$  acting solely on the qubit system. We define the Hilbert space separation  $\mathcal{H}_1 = \mathcal{H}_q \otimes \mathcal{H}_{\omega_k < \omega_0} \otimes \{|0\rangle\langle 0|\}_{\omega_k \geq \omega_0}$  which excludes all state in which any bath mode above a threshold  $\omega_0$  is excited from the lower energy Hilbert space. This separation is not energy ordered, i.e.  $\mathcal{H}_1$  contains states with energies larger than the threshold. However, the separation ensures that any eigenenergy of  $H_{hh}$  is above  $\omega_0$ , which will be vital for the following. Firstly, we look at

$$H_{hh} = P_1 H_q P_h + P_1 \sum_k \frac{\sigma_Z^{i_k}}{2} \lambda_k (a_k + a_k^\dagger) P_h + P_1 \sum_k \omega_k a_k^\dagger a_k P_h \quad (9.2)$$

$$= P_1 \sum_k \frac{\sigma_Z^{i_k}}{2} \lambda_k (a_k + a_k^\dagger) P_h \quad (9.3)$$

$$= P_1 \sum_{k \geq k_0} \frac{\sigma_Z^{i_k}}{2} \lambda_k a_k P_h \quad (9.4)$$

and

$$H_{hl} = P_h \sum_{k' \geq k_0} \frac{\sigma_Z^{i_{k'}}}{2} \lambda_{k'} a_{k'}^\dagger P_1 \quad (9.5)$$

We make the assumption that only terms with  $k = k'$  contribute. This can be justified by neglecting second order terms of  $\{a_k, a_k^\dagger\}$  in the inversion  $(E - H_{hh})^{-1}$  in equation 8.12 or, more rigorously, by applying the poor man's scaling to every bath-mode individually. This restricts the inversion problem on the single excitation subspace of a specific mode, i.e.,  $\mathcal{H}_h(k') = \mathcal{H}_q \otimes \mathcal{H}_{\omega_k < \omega_0} \otimes \{|0\rangle\langle 0|\}_{\omega_0 \leq \omega_k \neq \omega_{k'}} \otimes \{|1\rangle\langle 1|\}_{\omega_{k'}}$ . In this subspace we find

$$\begin{aligned} H_{hh} &= H_q + \sum_{k < k_0} \frac{\sigma_Z^{i_k}}{2} \lambda_k (a_k + a_k^\dagger) + \sum_{k < k_0} \omega_k a_k^\dagger a_k \\ &\quad + \sum_{k \geq k_0} \frac{\sigma_Z^{i_k}}{2} \lambda_k (a_k + a_k^\dagger) + \sum_{k \geq k_0} \omega_k a_k^\dagger a_k \end{aligned} \quad (9.6)$$

$$\overset{\mathcal{H}'_h}{=} |1\rangle\langle 0|_{k'} H_{\parallel} |0\rangle\langle 1|_{k'} + 0 + \omega_{k'}. \quad (9.7)$$

As we focus on the lowest energy eigenstates,  $\omega_{k'}$  is the dominant term. Approximating the inversion in equation 8.12 to first order in  $H_{\parallel}$  and  $E$  one finds that

$$(E - H_{\parallel} - \omega_{k'})^{-1} \approx -\frac{1}{\omega_{k'}} \left( 1 + \frac{E}{\omega_{k'}} - \frac{1}{\omega_{k'}} H_{\parallel} \right) \quad (9.8)$$

and equation 8.12 accordingly transforms

$$E |\Psi_1\rangle = \left( H_{\parallel} + \sum_{k' \geq k_0} \frac{\lambda'_k}{2} \sigma_Z^{i'_k} \left[ -\frac{1}{\omega_{k'}} \left( 1 + \frac{E}{\omega_{k'}} - \frac{1}{\omega_{k'}} H_{\parallel} \right) \right] \frac{\lambda'_k}{2} \sigma_Z^{i'_k} \right) |\Psi_1\rangle \quad (9.9)$$

$$= \left( H_{\parallel} + \sum_{k' \geq k_0} \frac{\lambda_{k'}^2}{4\omega_{k'}^2} \sigma_Z^{i_{k'}} (H_{\parallel} - E) \sigma_Z^{i_{k'}} \right) |\Psi_1\rangle. \quad (9.10)$$

Since  $E$  is a number, thus commuting with any operator including  $\sigma_Z^{i_{k'}}$ , one finds the leading order effective Hamiltonian via recursive application to be

$$\begin{aligned} H_{\text{eff}} &= H_{\parallel} + \sum_{k' \geq k_0} \frac{\lambda_{k'}^2}{4\omega_{k'}^2} \left( \sigma_Z^{i_{k'}} H_{\parallel} \sigma_Z^{i_{k'}} - H_{\parallel} \right) \\ &= H_{\parallel} + \sum_{k' \geq k_0} \frac{\lambda_{k'}^2}{4\omega_{k'}^2} \left( \sigma_Z^{i_{k'}} H_q \sigma_Z^{i_{k'}} - H_q \right). \end{aligned} \quad (9.11)$$

Here, we omitted constant terms and used that all  $\sigma_Z$  operators commute with each other. One can see that whether  $H_q$  is affected by the above transformation depends on if it commutes with the  $\sigma_Z^i$ . Here, the definition  $H_q \equiv \sum_{\vec{s}} \Delta_{\vec{s}} \sigma_{s_1} \otimes \sigma_{s_2} \dots \sigma_{s_n}$  proves useful as  $\sigma_Z^i \sigma_{\vec{s}_i} \sigma_Z^i = \pm \sigma_{\vec{s}_i}$ . This implies the transformation of the  $\Delta_{\vec{s}}$  under poor man's scaling

$$\Delta_{\vec{s}} \rightarrow \Delta_{\vec{s}} \left( 1 - \sum_{\substack{i_{k'} \in \mathcal{M} \\ k' \geq k_0}} \frac{\lambda_{k'}^2}{2\omega_{k'}^2} \right) \quad (9.12)$$

with  $\mathcal{M} = \{i | [\sigma_{s_i}, \sigma_Z] \neq 0\}$ , i.e., each Pauli string is affected by only those bath modes where it does not commute with the  $\sigma_Z$  of the respective qubit the mode is coupling. The bath modes that do affect the Pauli string effectively reduce  $\Delta_{\vec{s}}$ .

It is important to note that poor man's scaling generates an equation to determine eigenenergies as well as the projection of the eigenvectors onto a Hilbert space of lower dimension. Therefore, the associated transformation neither preserves the orthogonality nor the normalization of the eigenvectors. Consequently, it is neither unitary nor does it necessarily preserve the Hermitian properties of

the qubit Hamiltonian. This effect becomes apparent in higher orders. Since the effective Hamiltonian is no longer a pure qubit Hamiltonian, it is important to understand the transformation of measurement accessible qubit operators  $Q$ . As those do not couple high and low energy Hilbert spaces, one can employ the ansatz in equation 8.9 for any eigenvector to find

$$\langle Q \rangle = \langle \Psi_l | Q | \Psi_l \rangle + \langle \Psi_h | Q | \Psi_h \rangle \quad (9.13)$$

$$= \langle \Psi_l | Q | \Psi_l \rangle + \langle \Psi_l | H_{lh} (E - H_{hh})^{-1 \dagger} Q (E - H_{hh})^{-1} H_{hl} | \Psi_l \rangle \quad (9.14)$$

$$= \langle \Psi_l | Q + \sum_{k \geq k_0} \frac{\lambda_k^2}{4\omega_k^2} \sigma_Z^{i_k} Q \sigma_Z^{i_k} | \Psi_l \rangle + \mathcal{O}\left(\frac{1}{\omega_k^3}\right). \quad (9.15)$$

Notably, the transformed operator derived in equation 9.15 acts on the projected eigenvectors which are no longer normalized. The easiest solution to finding  $Q$  for state vectors of full length is to exploit  $\langle \mathbb{1} \rangle = 1$ : Accordingly, we renormalize  $Q$  to

$$Q_{\text{eff}} = Q + \sum_{k' \geq k_0} \frac{\lambda_{k'}^2}{4\omega_{k'}^2} \left( \sigma_Z^{i_{k'}} Q \sigma_Z^{i_{k'}} - Q \right), \quad (9.16)$$

which equals the transformation of the effective Hamiltonian. While this is a remarkable coincidence, we find that it is not universally true by looking at higher orders or bath modes coupling to multiple qubits. To describe the transformation of operators in a compact form, we define the reduced density matrix  $\rho_r$  that describes the state accessible by qubit measurements such that  $\langle Q_{\text{eff}} \rangle = \text{Tr}[\rho_r Q]$ . As the density matrix undergoes the same transformation, we identify

$$\rho \rightarrow \left( 1 - \frac{\lambda_{k'}^2}{4\omega_{k'}^2} \right) \rho + \frac{\lambda_{k'}}{2\omega_{k'}} \sigma_Z^{i_{k'}} \rho \frac{\lambda_{k'}}{2\omega_{k'}} \sigma_Z^{i_{k'}} \quad (9.17)$$

as local dephasing of the qubit  $i_{k'}$  [10].

The restriction to just bath modes coupling to a single qubit is – although often motivated by the mechanics of the physical system – a simple approach to incorporate the incoherent nature of the environment. While the qubit-qubit interaction via bath modes is in fact limited by the coherence of the bath, the introduction of additional coupling is a known effect [22]. To account for both effects we incorporate bath modes that are less local, i.e. that couple to multiple qubits with varying strength. One finds

$$H_{lh} = P_l \sum_{k' \geq k_0} \left( \sum_i \frac{\sigma_Z^i}{2} \lambda_{k'}^i a_k \right) P_h \quad (9.18)$$

and therefore the effective Hamiltonian of equation 9.11 changes to

$$H_{\text{eff}} = H_{\text{ll}} + \sum_{k' \geq k_0} \sum_{i,j} \frac{\lambda_{k'}^i \lambda_{k'}^j}{4\omega_{k'}} \left[ \frac{1}{\omega_{k'}} (\sigma_Z^i H_q \sigma_Z^j - \sigma_Z^i \sigma_Z^j H_q) - \sigma_Z^i \sigma_Z^j \right]. \quad (9.19)$$

While the effects for  $i = j$  were discussed in equation 9.11 the remainder of terms ( $i \neq j$ ) is dominated by an introduced  $\sigma_Z \sigma_Z$  coupling between qubits  $i$  and  $j$ . These effects do not interfere as the generated terms commute with the bath coupling. The remaining terms are weaker by a factor  $\|H_q\|/\omega_{k'} \ll 1$  in the regime where poor man's scaling is applicable. We therefore find that for any system where  $\lambda_i \lambda_j \ll \lambda_i^2$  does not hold, the bath effects on the Hamiltonian are dominated by  $\sigma_Z \sigma_Z$  couplings. Thus, either all other bath effects are negligibly small or the entire effective Hamiltonian is dominated by  $\sigma_Z \sigma_Z$  couplings. Hence, we assume  $\lambda_i \lambda_j \ll \lambda_i^2$  to hold.

Nonetheless we characterize the terms  $1/\omega_{k'} (\sigma_Z^i H_q \sigma_Z^j - \sigma_Z^i \sigma_Z^j H_q)$  qualitatively. Firstly, we find that they vanish for  $\sigma_{s_j}$  commuting with  $\sigma_Z$ . Secondly, they do not change which of the bath couplings a term commutes with and thirdly for  $\sigma_{s_i} \in \{\mathbb{1}, \sigma_Z\}$  and  $\sigma_{s_j} \in \{\sigma_X, \sigma_Y\}$  they are antihermitian. Recall, that nonhermitian terms are just artefacts of truncating the state vector. They do not compromise the energy eigenvalues.

When including non-local bath modes, we find that the transformation of measured operators differs from the effective Hamiltonian. Most remarkably, the novel pure  $\sigma_Z^i \sigma_Z^j$  terms do not arise. However, the renormalization proves to be more difficult as  $\langle \mathbb{1} \rangle$  now depends on the qubit state. One finds to leading order that

$$\langle \Psi_1 | Q_{\text{eff}} | \Psi_1 \rangle = \langle \Psi_1 | Q + \sum_{k' \geq k_0} \sum_{i,j} \frac{\lambda_{k'}^i \lambda_{k'}^j}{4\omega_{k'}^2} (\sigma_Z^i Q \sigma_Z^j - Q \langle \Psi_1 | \sigma_Z^i \sigma_Z^j | \Psi_1 \rangle) | \Psi_1 \rangle, \quad (9.20)$$

which has to equal  $\text{Tr}[\rho_r Q]$  to ensure that the reduced density matrix accurately describes any expectation value. We find the transition

$$\rho \rightarrow \left( 1 - \frac{\lambda_{k'}^i \lambda_{k'}^j}{4\omega_{k'}^2} \text{Tr}[\rho \sigma_Z^i \sigma_Z^j] \right) \rho + \frac{\lambda_{k'}^i \lambda_{k'}^j}{4\omega_{k'}^2} \sigma_Z^i \rho \sigma_Z^j. \quad (9.21)$$

While this transition is nonlinear, it does preserve the trace of the density matrix and it describes the dephasing derived above for  $i = j$ . The smaller remaining terms of  $i \neq j$  only come into effect for either  $\sigma_{s_i}, \sigma_{s_j} \in \{\sigma_Z, \mathbb{1}\}$  or  $\sigma_{s_i}, \sigma_{s_j} \in \{\sigma_X, \sigma_Y\}$ , as otherwise the contributions are canceled out by switching  $i$  and  $j$ . Like for the transition of the Hamiltonian operator, we find that any Pauli strings in  $H_q$  is only changed to terms that commute with the same  $\sigma_Z$ . Consequently the newly derived terms do not interfere with the predominant dephasing.

To quantify the effects described above on a physical system, the relevant bath modes can typically be described by an Ohmic distribution  $J(\omega) = 2\alpha\omega\Theta(\omega_c - \omega)$  with cutoff frequency  $\omega_c$  and  $\alpha$  describing the coupling strength [137]. We focus on separated baths  $J_i$  for the individual qubits and make a transition from discrete to continuous modes, i.e.  $\sum_k \lambda_k^2 \rightarrow \sum_i \int J_i(\omega)d\omega$ . For an infinitesimal scaling  $\omega_0 = \omega_c - \delta\omega$  of the effective Hamiltonian of equation 9.11, one finds the transition

$$\Delta_{\vec{s}}(\omega_c - \delta\omega) = \Delta_{\vec{s}}(\omega_c) \left( 1 - \delta\omega \sum_i^{\substack{[\sigma_{\vec{s}}, \sigma_Z^{i_{k'}}] \neq 0 \\ i}} \frac{\alpha_i}{\omega_c} \right) \quad (9.22)$$

and

$$\frac{d\Delta_{\vec{s}}}{d\omega_0} = \frac{\Delta_{\vec{s}}}{\omega_0} \sum_i^{\substack{[\sigma_{\vec{s}}, \sigma_Z^{i_{k'}}] \neq 0 \\ i}} \alpha_i \quad (9.23)$$

$$\equiv \frac{c(\vec{s})\Delta_{\vec{s}}}{\omega_0} \quad (9.24)$$

$$\Delta_{\vec{s}}(\omega_0) = \Delta_{\vec{s}}(\omega_c) \left( \frac{\omega_0}{\omega_c} \right)^{c(\vec{s})} \quad (9.25)$$

with  $0 < c(\vec{s}) < \sum_i \alpha_i$  being a constant specific to the bath couplings the Pauli string  $\vec{s}$  does not commute with. We find  $\Delta_{\vec{s}}$  to be either constant or monotonically increasing with  $\omega_0$ , i.e., decreasing the effective cutoff frequency  $\omega_0$  reduces the contribution of the Pauli strings not commuting with all bath couplings. The above derivations are valid as long as the high energy frequencies are much larger than the effects of the qubit Hamiltonian and hence poor man's scaling can be applied until this condition is no longer met. As this implies  $\Delta_{\vec{s}} \ll \omega_0$  we examine the dependencies of  $\Delta_{\vec{s}}/\omega_0$  as shown in figure 9.1. We find the following regimes:

- $c(\vec{s}) = 0$ : Pauli strings that align with the bath coupling or act as the identity are not affected by the bath and are therefore independent of  $\omega_0$ . Notably the bath induced  $\sigma_Z\sigma_Z$  terms are unaffected, thus separating both effects.
- $0 < c(\vec{s}) = 0 < 1$ :  $\Delta_{\vec{s}}$  decreases slower than  $\omega_0$ , hence, at some point the condition  $\Delta_{\vec{s}} \ll \omega_0$  is no longer met, yielding a nonzero effective  $\Delta$ .
- $c(\vec{s}) = 1$ : the ratio  $\Delta_{\vec{s}}/\omega_0$  is constant. This case marks the transition between complete and incomplete suppression of the qubit Hamiltonian.
- $1 < c(\vec{s})$ :  $\Delta_{\vec{s}}$  decreases faster than  $\omega_0$  and therefore can vanish completely.

It is, however, important to note that for a nontrivial Hamiltonian the condition  $\Delta_{\vec{s}} \ll \omega_0$  has to be treated for the entirety of all Pauli strings.

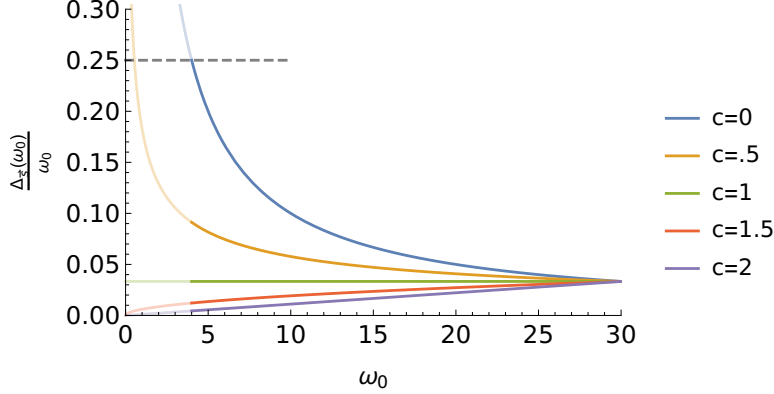


Figure 9.1: **Suppression of qubit operators**

The ratio  $\Delta_{\vec{s}}/\omega_0$  for different values of  $c(\vec{s})$  starting at  $\omega_0 = 30$  and  $\Delta = 1$ . The indicated validity limit at 0.25 marks the abortion of poor man's scaling as  $\Delta_{c=0} \ll \omega_0$  no longer holds.

## 9.2 Second Order Effects

The limitations of the above description stems from the approximate inversion in equation 9.8. Hence, we include higher (i.e. second) order terms to account for larger ratios  $\Delta/\omega_0$ , thereby covering smaller bath modes. We expect to possibly introduce more complex dynamics via interaction between the  $\Delta_{\vec{s}}$ . Reiterating the inversion with second order terms yields

$$\begin{aligned}
& (E - |1\rangle\langle 0|_{k'} H_{\parallel} |0\rangle\langle 1|_{k'} - \omega_{k'})^{-1} \\
& \approx -\frac{1}{\omega_{k'}} \left( 1 + \frac{E}{\omega_{k'}} - \frac{1}{\omega_{k'}} |1\rangle\langle 0|_{k'} H_{\parallel} |0\rangle\langle 1|_{k'} \right. \\
& \quad \left. + \frac{1}{\omega_{k'}^2} (E^2 - 2E |1\rangle\langle 0|_{k'} H_{\parallel} |0\rangle\langle 1|_{k'} + |1\rangle\langle 0|_{k'} H_{\parallel}^2 |0\rangle\langle 1|_{k'}) \right) \quad (9.26)
\end{aligned}$$

and, via recursive application, an effective Hamiltonian

$$\begin{aligned}
H_{\text{eff}} = H_{\parallel} & + \sum_{k' \geq k_0} \frac{\lambda_{k'}^2}{4\omega_{k'}^2} \left( \sigma_Z^{i_{k'}} H_{\parallel} \sigma_Z^{i_{k'}} - H_{\parallel} + \text{const.} \right) \\
& - \sum_{k' \geq k_0} \frac{\lambda_{k'}^2}{4\omega_{k'}^3} \left( \sigma_Z^{i_{k'}} H_{\parallel}^2 \sigma_Z^{i_{k'}} - 2\sigma_Z^{i_{k'}} H_{\parallel} \sigma_Z^{i_{k'}} H_{\parallel} + H_{\parallel}^2 \right). \quad (9.27)
\end{aligned}$$

Note that while reiterating the effective Hamiltonian, one cannot omit constant summands as before as they multiply with nontrivial terms. However, they do not play an important role in this case, as they result in terms of order  $\omega_{k'}^{-4}$ .

Furthermore the arising second line of above equation vanishes for all terms of  $H_{\parallel}^2$  commuting with  $\sigma_Z^{i_{k'}}$ . We find

$$\begin{aligned} & \sigma_Z^{i_{k'}} H_{\parallel}^2 \sigma_Z^{i_{k'}} - 2\sigma_Z^{i_{k'}} H_{\parallel} \sigma_Z^{i_{k'}} H_{\parallel} + H_{\parallel}^2 \\ &= \sigma_Z^{i_{k'}} H_q^2 \sigma_Z^{i_{k'}} - 2\sigma_Z^{i_{k'}} H_q \sigma_Z^{i_{k'}} H_q + H_q^2 \\ &+ \sum_{k < k_0} \frac{\lambda_k}{2} (a_k + a_k^\dagger) \left( [H_q, \sigma_Z^{i_k}] + [\sigma_Z^{i_k}, \sigma_Z^{i_{k'}} H_q \sigma_Z^{i_{k'}}] \right) \end{aligned} \quad (9.28)$$

and

$$\sigma_Z^{i_{k'}} H_{\parallel} \sigma_Z^{i_{k'}} - H_{\parallel} = \sigma_Z^{i_{k'}} H_q \sigma_Z^{i_{k'}} - H_q \quad (9.29)$$

The resulting effective Hamiltonian can no longer be described by the  $\Delta_{\bar{s}}$  as the second order terms do not only induce interactions between these but also additional coupling terms as in equation 9.28. The transition to the ohmic distribution, as well as infinitesimal scaling  $\omega_0 = \omega_c - \delta\omega$  yields the effective Hamiltonian

$$\begin{aligned} H_{\text{eff}} &= H_{\parallel} + \sum_{i=1}^n \delta\omega \frac{\alpha_i}{2\omega_0} (\sigma_Z^i H_q \sigma_Z^i - H_q) \\ &- \sum_i \delta\omega \frac{\alpha_i}{2\omega_0^2} \left( \sigma_Z^i H_q^2 \sigma_Z^i - 2\sigma_Z^i H_q \sigma_Z^i H_q + H_q^2 \right. \\ &\left. + 2 \sum_{k < k_0} \frac{\lambda_k}{2} (a_k + a_k^\dagger) ([H_q, \sigma_Z^{i_k}] + [\sigma_Z^{i_k}, \sigma_Z^i H_q \sigma_Z^i]) \right) \end{aligned} \quad (9.30)$$

and hence

$$\begin{aligned} \frac{dH_{\text{eff}}}{d\omega_0}(\omega_c) &= \sum_i \frac{\alpha_i}{2\omega_0} (H_q - \sigma_Z^i H_q \sigma_Z^i) \\ &+ \sum_i \frac{\alpha_i}{2\omega_0^2} \left( \sigma_Z^i H_q^2 \sigma_Z^i - 2\sigma_Z^i H_q \sigma_Z^i H_q + H_q^2 \right. \\ &\left. + 2 \sum_{k < k_0} \frac{\lambda_k}{2} (a_k + a_k^\dagger) ([H_q, \sigma_Z^{i_k}] + [\sigma_Z^{i_k}, \sigma_Z^i H_q \sigma_Z^i]) \right). \end{aligned} \quad (9.31)$$

Note that the inclusion of second order terms does not only affect the qubit Hamiltonian and introduces coupling terms, but also that these terms are no longer limited to only single qubits couplings. Furthermore, these terms again are not necessarily Hermitian as an artifact of the projection. An ansatz to treat the arising dynamics would be to determine fixpoints for the flow of  $\omega_0$  or at least find

fixpoints within a subspace of equal  $c(\vec{s})$ . Nontrivial fixpoints however can easily be precluded by looking at cases of  $\sigma_Z^i = \sigma_Z^{i_k}$  needing  $[\mathbf{H}_q, \sigma_Z^i] = 0$ .

Calculation or numerical solution of the full differential equation requires to keep track of the  $4^n \Delta_{\vec{s}}$  and additionally an equal number of bath coupling prefactors. As the matrices describing the dynamics are not sufficiently sparse, we cannot hope for an efficient simulation. However, we believe that arising terms might be suppressed by the initial  $\sigma_Z$  coupling, which we leave for further research to confirm or repudiate.

### 9.3 Flow Equations

In the following we employ flow equations, as presented in the previous chapter and its derivation of the single qubit case based on [131]. We compare the strengths and drawbacks of either protocol and show why poor man's scaling is more suitable for the problem at hand. While restricting ourselves to just two qubits, we separate the Hamiltonians

$$\mathbf{H}_0 = \sum_{m,n=1}^4 \Delta_{mn} \sigma_{mn} + \sum_k \omega_k a_k^\dagger a_k \quad (9.32)$$

$$\mathbf{H}_{\text{int}} = \sum_k \frac{\sigma_Z^{i_k}}{2} \lambda_k (a_k + a_k^\dagger) \quad (9.33)$$

where  $\sigma_{mn} \equiv \sigma_m \otimes \sigma_n$ . As in the previous chapter 8, we first calculate the canonical ansatz for the generator  $\eta$ , which is given by

$$\eta = [\mathbf{H}_0, \mathbf{H}_{\text{int}}] \quad (9.34)$$

$$\begin{aligned} &= \sum_k f_k^+ \sum_{mn} \frac{\Delta_{mn} \lambda_k}{2} [\sigma_{mn}, \sigma_Z^{i_k}] (a_k + a_k^\dagger) \\ &+ \sum_k f_k^- \frac{\sigma_Z^{i_k}}{2} \lambda_k \omega_k (a_k^\dagger - a_k). \end{aligned} \quad (9.35)$$

Again, as in the single spin case, introducing  $f_k^+, f_k^- = 1$  preemptively to allow for calibration of  $\eta$ . The flow of the Hamiltonian is given by its commutation relation with the generator. Hence, we first look at

$$\begin{aligned} [\eta, \mathbf{H}_0] &= \sum_k f_k^+ \sum_{mnm'n'} \frac{\Delta_{mn} \Delta_{m'n'} \lambda_k}{2} [[\sigma_{mn}, \sigma_Z^{i_k}], \sigma_{m'n'}] (a_k + a_k^\dagger) \\ &+ \sum_k f_k^- \sum_{mn} \frac{\Delta_{mn} \omega_k \lambda_k}{2} [\sigma_{mn}, \sigma_Z^{i_k}] (a_k - a_k^\dagger) \end{aligned}$$

$$\begin{aligned}
& + \sum_k f_k^- \sum_{mn} \frac{\Delta_{mn} \omega_k \lambda_k}{2} [\sigma_Z^{i_k}, \sigma_{mn}] (a_k^\dagger - a_k) \\
& - \sum_k f_k^- \frac{\lambda_k \omega_k^2}{2} \sigma_Z^{i_k} (a_k + a_k^\dagger).
\end{aligned} \tag{9.36}$$

To prevent the newly arising coupling terms in  $(a_k - a_k^\dagger)$ , we need to specify  $f_k^+ = f_k = -f_k^-$  eliminating the second and third line of the expression 9.36. The first line introduces an additional spin bath coupling term; its coupling to the qubit is not necessarily given by  $\sigma_Z$  but possibly introduces novel couplings. Note that first similar terms arise for second order poor man's scaling however there is no apparent lower order flow equation. We will address these new couplings later on in our analysis. Furthermore, terms with  $\sigma_{mn} = \sigma_{m'n'} = \sigma_X^{1(2)}$  (while acting trivially on the other qubit) are analogous to the single qubit case and result in native  $\sigma_Z$  coupling to the first (second) qubit – as does the last line. The commutator of generator and interaction term is given by

$$\begin{aligned}
[\eta, H_{\text{int}}] & = \sum_{k,k'} f_k \sum_{mn} \frac{\Delta_{mn} \lambda_k \lambda_{k'}}{4} [[\sigma_{mn}, \sigma_Z^{i_k}], \sigma_Z^{i_{k'}}] (a_k + a_k^\dagger) (a_{k'} + a_{k'}^\dagger) \\
& + \sum_k f_k \frac{\lambda_k^2 \omega_k}{2},
\end{aligned} \tag{9.37}$$

where the second term is just a constant shift. Both commutators sum up to the flow of the Hamiltonian, which we find to be

$$\begin{aligned}
\frac{dH}{dB} & = [\eta, H_0] + [\eta, H_{\text{int}}] \\
& = \sum_k f_k \sum_{mnm'n'} \frac{\Delta_{mn} \Delta_{m'n'} \lambda_k}{2} [[\sigma_{mn}, \sigma_Z^{i_k}], \sigma_{m'n'}] (a_k + a_k^\dagger) \\
& + \sum_k f_k \frac{\lambda_k \omega_k^2}{2} \sigma_Z^{i_k} (a_k + a_k^\dagger) \\
& + \sum_{k,k'} f_k \sum_{mn} \frac{\Delta_{mn} \lambda_k \lambda_{k'}}{4} [[\sigma_{mn}, \sigma_Z^{i_k}], \sigma_Z^{i_{k'}}] (a_k + a_k^\dagger) (a_{k'} + a_{k'}^\dagger).
\end{aligned} \tag{9.38}$$

A striking difference in comparison to the second order poor man's scaling of equation 9.31 are the terms coupling to multiple bath modes. These are inherently forbidden for poor man's scaling because modes are treated and eliminated one by one. To treat said terms we apply normal ordering as presented in chapter 4 with respect to the vacuum or some finite temperature depending on the physical system

$$(a_k + a_k^\dagger)(a_{k'} + a_{k'}^\dagger) = : (a_k + a_k^\dagger)(a_{k'} + a_{k'}^\dagger) : + \delta_{k,k'} \langle 2a_k^\dagger a_k + 1 \rangle. \tag{9.40}$$

When omitting bath fluctuations, i.e. the normal ordered terms, we find

$$\begin{aligned}
\frac{dH}{dB} &= \sum_k f_k \sum_{mnm'n'} \frac{\Delta_{mn}\Delta_{m'n'}\lambda_k}{2} [[\sigma_{mn}, \sigma_Z^{i_k}], \sigma_{m'n'}] (a_k + a_k^\dagger) \\
&+ \sum_k f_k \frac{\lambda_k \omega_k^2}{2} \sigma_Z^{i_k} (a_k + a_k^\dagger) \\
&+ \sum_k f_k \sum_{mn} \frac{\Delta_{mn}\lambda_k^2}{4} [[\sigma_{mn}, \sigma_Z^{i_k}], \sigma_Z^{i_k}] \langle 2a_k^\dagger a_k + 1 \rangle
\end{aligned} \tag{9.41}$$

We now revisit the generation of new coupling terms via  $[[\sigma_{mn}, \sigma_Z^{i_k}], \sigma_{m'n'}]$ , the arising of which marks an additional level of complexity in comparison with the single qubit case. Specifically, these additional terms are not addressed by the desired flow parameters: These are the  $\lambda_k$  and  $\Delta_{mn}$  which, for a straightforward implementation of flow equations, we need to be dependent on  $B$  and consequently  $\omega_0$ .

A possible approach would be to not omit terms of  $m, n \neq m', n'$  from leading order expression, such as the normal ordered terms of equation 9.40. This could be justified via treating  $\omega$  as big, yielding the second row dominant over the first. Note, however that the omitted terms are of the same order as for  $m, n = m', n'$ ; the distinction is made without justification, thus these terms need to be considered in the following. Furthermore, the approximation  $\omega_0 \gg \Delta_{mn}$  only appears at this step. Applying it nullifies a valuable advantage in comparison with poor man's scaling which is build upon this approximation. We summarize the omitted, i.e. non flowing terms as  $\Delta H_{\text{nf}}$ , yielding

$$\begin{aligned}
\frac{dH}{dB} &= \sum_k f_k \sum_{mn} \frac{\Delta_{mn}^2 \lambda_k}{2} [[\sigma_{mn}, \sigma_Z^{i_k}], \sigma_{mn}] (a_k + a_k^\dagger) \\
&+ \sum_k f_k \frac{\lambda_k \omega_k^2}{2} \sigma_Z^{i_k} (a_k + a_k^\dagger) \\
&+ \sum_k f_k \sum_{mn} \frac{\Delta_{mn}\lambda_k^2}{4} [[\sigma_{mn}, \sigma_Z^{i_k}], \sigma_Z^{i_k}] \langle 2a_k^\dagger a_k + 1 \rangle \\
&+ \Delta H_{\text{nf}}.
\end{aligned} \tag{9.42}$$

We introduce  $\kappa_{imn}$  to equal 2 if  $\sigma_{mn}$  does not commute with  $\sigma_Z^i$  and 0 otherwise. The derivative of equation 9.42 then simplifies to

$$\begin{aligned}
\frac{dH}{dB} &= - \sum_k \sum_{mn} f_k \frac{\Delta_{mn}^2 \lambda_k}{2} 2\kappa_{i_k mn} \sigma_Z^{i_k} (a_k + a_k^\dagger) \\
&+ \sum_k f_k \frac{\lambda_k \omega_k^2}{2} \sigma_Z^{i_k} (a_k + a_k^\dagger)
\end{aligned}$$

$$\begin{aligned}
& + \sum_k f_k \sum_{m,n} \frac{\Delta_{mn} \lambda_k^2}{2} \sigma_{mn} \kappa_{i_k mn} \langle 2a_k^\dagger a_k + 1 \rangle \\
& + \Delta H_{\text{nf}}.
\end{aligned} \tag{9.43}$$

Except  $\Delta H_{\text{nf}}$ , the terms in equation 9.43 only change parameters of the original Hamiltonian, they induce the flow equations

$$\frac{d\lambda_k}{dB} = f_k \lambda_k \left( \omega_k^2 - 2 \sum_{mn} \Delta_{mn}^2 \kappa_{i_k mn} \right) \tag{9.44}$$

$$\frac{d\Delta_{mn}}{dB} = \sum_k \sum_{mn} \frac{f_k \Delta_{mn} \lambda_k^2}{2} \kappa_{i_k mn} \langle 2a_k^\dagger a_k + 1 \rangle. \tag{9.45}$$

As for poor man's scaling or the single qubit case, we adapt those findings to a continuous spectral function. The transition  $\sum_k \lambda_k^2 \rightarrow \int J(\omega) d\omega$  is justified by defining  $J(\omega) \equiv \sum_k \lambda_k^2 \delta(\omega - \omega_k)$ ; the flow equations for the spectral function are then given by

$$\frac{dJ_i(\omega, B)}{dB} = J_i(\omega, B) f_i(\omega) \left( \omega^2 - 2 \sum_{mn} \Delta_{mn}^2 \kappa_{i_k mn} \right) \tag{9.46}$$

$$\frac{d\Delta}{dB} = \sum_i \int J_i \frac{f_i(\omega) \Delta}{2} \kappa_{i mn} \langle 2a_k^\dagger a_k + 1 \rangle. \tag{9.47}$$

To treat the non flowing parts  $\Delta H_{\text{nf}}$  we revert to discrete modes. Including those terms can be done in first order via simple integration. However, that does not account for their contribution to the derivative, as they have not been considered for the calculation of the flow equations. The previously neglected terms in the first line of equation 9.39 are of particular interest. We therefore look at the effect of the integrated  $H_{\text{nf}}$  while not taking normal ordered terms into account. One finds

$$\begin{aligned}
H_{\text{nf}}(B) &= \int_0^B dB' \sum_k \sum_{mn \neq m'n'} f_k \frac{\Delta_{mn}(B') \Delta_{m'n'}(B') \lambda_k(B')}{2} \\
&\quad \left[ [\sigma_{mn}, \sigma_Z^{i_k}], \sigma_{m'n'} \right] (a_k + a_k^\dagger) \\
[\eta, H_{\text{nf}}] &= \int_0^B dB' \sum_k \sum_{mn \neq m'n'} \sum_{\tilde{m}\tilde{n}} f_k(B) f_k(B') \\
&\quad \frac{\Delta_{\tilde{m}\tilde{n}}(B) \Delta_{mn}(B') \Delta_{m'n'}(B') \lambda_k(B') \lambda_k(B)}{4} \\
&\quad \left[ [\sigma_{\tilde{m}\tilde{n}}, \sigma_Z^{i_k}], [\sigma_{mn}, \sigma_Z^{i_k}], \sigma_{m'n'} \right] \langle 2a_k^\dagger a_k + 1 \rangle
\end{aligned} \tag{9.48}$$

$$\begin{aligned}
& - \int_0^B dB' \sum_k \sum_{mn \neq m'n'} f_k(B) f_k(B') \\
& \quad \frac{\Delta_{\tilde{m}\tilde{n}}(B) \Delta_{mn}(B') \lambda_k(B') \lambda_k(B) \omega_k}{4} \\
& \quad \left\{ \sigma_Z^{i_k}, [[\sigma_{mn}, \sigma_Z^{i_k}], \sigma_{m'n'}] \right\}. \tag{9.49}
\end{aligned}$$

Here, the form of  $\eta$  remains unchanged from equation 9.35; it can be chosen freely to only depend on the flowing parameters. Despite the non-Markovianity of the above contribution, it only introduces terms not coupled to bath modes, which can be treated within the native shape of the Hamiltonian. They contribute to specific  $\Delta_{mn}$ . Including the effects of  $H_{\text{nf}}$ , rather than  $H_{\text{nf}}$  itself, results in a substantially less compact but closed expression for the flow of the Hamiltonian,

$$\begin{aligned}
\frac{dH}{dB} = & - \sum_k \sum_{mn} f_k \frac{\Delta_{mn}^2 \lambda_k}{2} 2\kappa_{i_k mn} \sigma_Z^{i_k} (a_k + a_k^\dagger) \\
& + \sum_k f_k \frac{\lambda_k \omega_k^2}{2} \sigma_Z^{i_k} (a_k + a_k^\dagger) \\
& + \sum_k f_k \sum_{m,n} \frac{\Delta_{mn} \lambda_k^2}{2} \sigma_{mn} \kappa_{i_k mn} \langle 2a_k^\dagger a_k + 1 \rangle \\
& + \int_0^B dB' \sum_k \sum_{mn \neq m'n'} \sum_{\tilde{m}\tilde{n}} f_k(B) f_k(B') \\
& \quad \frac{\Delta_{\tilde{m}\tilde{n}}(B) \Delta_{mn}(B') \Delta_{m'n'}(B') \lambda_k(B') \lambda_k(B)}{4} \\
& \quad [[\sigma_{\tilde{m}\tilde{n}}, \sigma_Z^{i_k}], [[\sigma_{mn}, \sigma_Z^{i_k}], \sigma_{m'n'}]] \langle 2a_k^\dagger a_k + 1 \rangle \\
& - \int_0^B dB' \sum_k \sum_{mn \neq m'n'} f_k(B) f_k(B') \\
& \quad \frac{\Delta_{\tilde{m}\tilde{n}}(B) \Delta_{mn}(B') \lambda_k(B') \lambda_k(B) \omega_k}{4} \left\{ \sigma_Z^{i_k}, [[\sigma_{mn}, \sigma_Z^{i_k}], \sigma_{m'n'}] \right\}. \tag{9.50}
\end{aligned}$$

In theory the above expression, together with an appropriate choice for the  $f_k$ , solves the flow equation approach to the multi spin Boson model. However, its little accessible form of non-Markovian flow equations and additional interaction between Pauli strings, renders it unfeasible for numerical implementation as well as further calculation. We conclude that for second order poor man's scaling, as well as flow equations, the benefits of added precision and less dependence on large frequency approximation are outweighed by the additional complexity in comparison to the first order findings presented in section 9.1. We discuss these findings in the regime of scalable adiabatic quantum computers in the following chapter.



# Chapter 10

## Implications for Quantum Annealing

In quantum annealing, as opposed to circuit-based quantum computing, the solution to a computational problem is encoded in the ground state of a quantum system. This distinction results in a vastly different treatment of errors. A quantum circuit sets a well defined trajectory for every initial state, every deviation of which can be quantified via state overlap. Furthermore, the faultiness of a single gate is given by the average error, the entirety of these errors provides a good understanding of the reliability of the implementation as well as the output of the algorithm. While in theory the trajectory of a quantum annealer is given by the instantaneous ground state, deviations from that path are not considered harmful as long as the system relaxes back to the ground state before the end of the schedule. The effects of couplings to the environment are therefore harder to quantify but not less important than for gate-based algorithms.

In previous work, adiabatic quantum computing has been conceived to be less prone to or even benefiting from coupling to the environment [124–126]. However, theoretical derivations have been based on master equations and consequently limited to small effects. We go beyond weak coupling and apply the findings of section 9.1 to describe the effect of Ohmic baths in a regime more suitable to describe scalable adiabatic quantum computation. We show qualitative change to the effective Hamiltonian as well as the reduced qubit density matrix encoding entanglement between system and bath. An effective dephasing of the reduced density matrix limits the extractable information from many qubit entangled ground states. We find that the annealing process is no longer restricted to the qubits and discuss possible drawbacks or benefits of annealing in the combined system-bath states.

## 10.1 LCGD Regime

We revisit the multi spin Boson Hamiltonian of equation 9.1 with the qubit Hamiltonian given by a sum of Pauli strings, i.e.,  $H_q \equiv \sum_{\vec{s}} \Delta_{\vec{s}} \sigma_{s_1} \otimes \sigma_{s_2} \dots \sigma_{s_n}$  to describe an adiabatic quantum computer under the influence of environmental effects. We assume the bath modes to be Ohmically distributed and  $\omega_0 \gg \Delta_{\vec{s}}$  continuous. In the previous chapter we have derived

$$\Delta_{\vec{s}}(\omega_0) = \Delta_{\vec{s}} \left( \frac{\omega_0}{\omega_c} \right)^{c(\vec{s})} \quad (10.1)$$

in leading order in  $\Delta/\omega_0$ . The suppression of specific Pauli strings in the Hamiltonian via poor man's scaling depends on the combined bath coupling constant  $c(\vec{s}) = \sum_{i \in \mathcal{M}} \alpha_i$  with  $\mathcal{M} = \{i | [\sigma_{s_i}, \sigma_Z] \neq 0\}$ . Consequently,  $\Delta_{\vec{s}}$  is either constant or monotonically increasing function of  $\omega_0$ . That is decreasing the effective cutoff frequency  $\omega_0$  reduces the contribution of the Pauli strings not commuting with the  $\sigma_Z$  coupling to the bath. Note that the more general model of bath modes coupling to multiple qubits produces additional effects on the qubit Hamiltonian  $H_q$ . However, these are negligibly small compared to those of equation 10.1.

First focusing on individual Pauli strings with  $c(\vec{s}) = 1$ , one sees that  $\Delta_{\vec{s}}$  is linear in  $\omega_0$ , thus marking the transition between complete and incomplete suppression of  $\Delta_{\vec{s}}$ . For  $H_q \propto \sigma_X^i$  we reproduce the single qubit case with the known phase transition at  $\alpha = 1$ . It is however important to remember that the above discussion covers special cases where the qubit Hamiltonian consists of a set of Pauli strings that sponsor equal  $c(\vec{s})$ . In more general settings the assumption  $\omega_0 \gg \|H_q\|$  is evaluated for the ensemble of  $\Delta_{\vec{s}}$ , i.e., dynamics of individual Pauli strings are only independent as long as the entire qubit Hamiltonian is much smaller than  $\omega : 0$ . For examples complete suppression requires all relevant  $c(\vec{s}) \geq 1$ . However, despite a final  $\omega_0 \neq 0$ , Pauli strings with  $c(\vec{s}) \geq 1$  are suppressed significantly stronger than those with weaker bath coupling representing more gradual transitions.

It is important to note that while the eigenvalues of the effective Hamiltonian are the energies of the system, the corresponding eigenstates  $|\Psi_1\rangle$  do not describe full qubit states but rather their renormalized projection onto a Hilbert space with lower cutoff frequency. This encodes entanglement between the qubit system and the eliminated bath modes. To account for that, we derive effective qubit operators  $Q_{\text{eff}}$  that describe the system as seen by accessible measurement operators  $Q$ . Or rather we derive the reduced density matrix such that  $\langle Q_{\text{eff}} \rangle = \text{Tr} [\rho_r Q]$ . In section 9.1 we show that the transformation of the reduced density matrix under poor man's scaling coincides with that of the Hamiltonian described in equation 10.1.

Notably, one can rewrite the effect of the bath modes interacting with qubit  $i$  to

$$\rho \rightarrow \frac{1 + (\omega_0/\omega_c)^{\alpha_i}}{2} \rho + \frac{1 - (\omega_0/\omega_c)^{\alpha_i}}{2} \sigma_Z^i \rho \sigma_Z^i \quad (10.2)$$

which translates to a dephasing of that qubit with probability  $1 - (\omega_0/\omega_c)^{\alpha_i}$ . This notation is equivalent to the operator-sum representation [10]. As the effects on different qubits commute, we identify the effects of poor man's scaling with simultaneous local dephasing of all qubits. However, it is important to differentiate between the gradual dephasing associated with the coherence time  $T_2$  and the fixed dephasing occurring in our case, which poses a limit to the measurable phase correlation on any qubit of the system.

Entanglement is an essential feature of quantum technologies, necessary to allow for supremacy in comparison to its classical counterparts; so does a ground state that is a single qubit product state not provide an advantage for quantum annealing over classical computation. The classification of multipartite entanglement is less straightforward than for just two parties reflecting the complexity of increasingly large quantum systems. However, the Greenberger–Horne–Zeilinger (GHZ) state  $|\Psi\rangle_{\text{GHZ}} = 1/\sqrt{2}(|00\dots 0\rangle + |11\dots 1\rangle)$  is considered to be a maximally entangled state [144]. Assuming identical  $\alpha_i \equiv \alpha$  and the GHZ state being the entangled ground state of an effective Hamiltonian, we find that the dephasing of equation 10.2, which accompanies the poor man's scaling, reduces the off-diagonal elements of the density matrix – and therefore the phase relation between the two product states – by a factor of  $(\omega_0/\omega_c)^{n\alpha}$ . This depends to great extent on the ratio of initial and final cutoff frequency and therefore the specific system settings; for large enough  $n$  the reduced density matrix converges to a complete mixture of product states  $|00\dots 0\rangle$  and  $|11\dots 1\rangle$ , which is neither coherent nor entangled. As many qubit entanglement implies long Pauli strings, we suspect that this multipartite entanglement is typically suppressed in the reduced density matrix.

A Hamiltonian is  $k$ -local if all of its terms are acting nontrivially on at most  $k$  qubits. These Hamiltonians can be used to engineer systems with arbitrary ground states for  $k \geq 2$  [67]. The terms of such a Hamiltonian are only affected by at most  $k$  bath couplings, which can be well controlled in experimental settings even when scaling to large qubit numbers. In contrast, large  $n$  pose a threat to the integrity of entangled density matrices as  $\sum \alpha_i$  grows with the number of qubits. To further investigate that we are especially interested in the locally coherent but globally dephased (LCGD) regime, where  $k\alpha$  is small but  $n\alpha$  is not. This regime naturally arises with the scaling to larger quantum computers but limited shielding against the environment. We showcase the regime in figure 10.1. We focus on an antiferromagnetic Hamiltonian, which is a realistic setting for quantum annealing

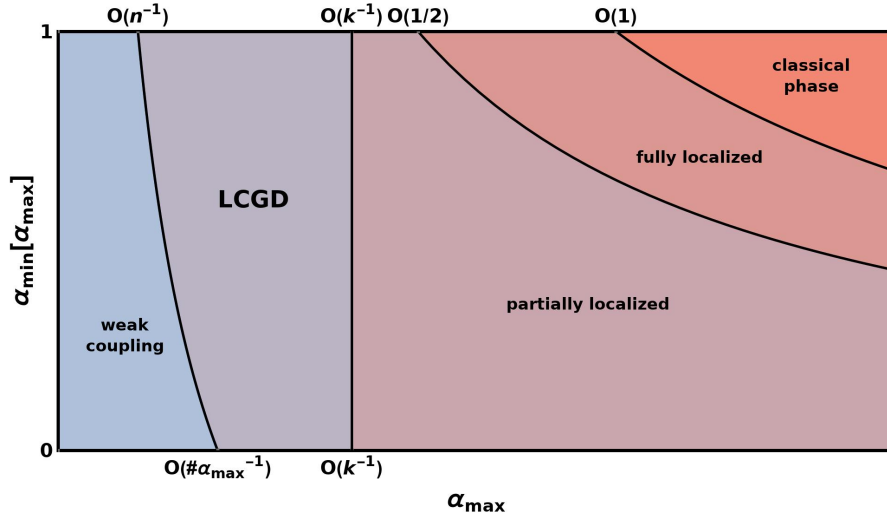


Figure 10.1: **The LCGD regime**

Diagram of different regimes of the  $\alpha_i \in [\alpha_{\min}, \alpha_{\max}]$  for  $n$  qubits. For simplicity we assume that all  $\alpha_i$  are either minimal or maximal. We find that in the weak coupling regime all  $c(\vec{s})$  are small, hence while the transformation changes the ratio between the different couplings it does not prohibit any Pauli strings. In contrast, many-qubit  $\sigma_{X/Y}$  strings are strongly suppressed in the LCGD regime while  $k$ -local interactions are only affected weakly. In the partially and fully localized regimes, increasingly many  $k$ -local terms are suppressed, thereby limiting the possible ground states of the system. The classical phase describes a system where all terms commute and hence the qubits' effective behaviour can be described classically.

application [145]. We use the specific example Hamiltonian<sup>1</sup>

$$H_{\text{afm}} = (1 - s) \sum_i \sigma_Z^i + s(1 - s) \sum_{ij} c_{ij} \sigma_Z^i \sigma_Z^j + s \sum_{ij} c_{ij} \sigma_X^i \sigma_X^j \quad (10.3)$$

with  $c_{ij} \in \{0, 1\}$  specifying which qubit pairs are coupled and  $s$  being the annealing parameter. With an appropriate set of  $c_{ij} \neq 0$  this two-local Hamiltonian can support multipartite entangled ground states. Showcasing a specific 12-qubit example in figure 10.2, we verify the expected behaviour in the LCGD regime. When  $2\alpha$  is significantly smaller than one, the effective Hamiltonian is affected weakly resulting in a combined system bath density matrix  $\rho_{\text{sb}}$  close to the ideal state. Contrarily, the qubit state as observed via external measurement is affected

<sup>1</sup>courtesy of Itay Hen

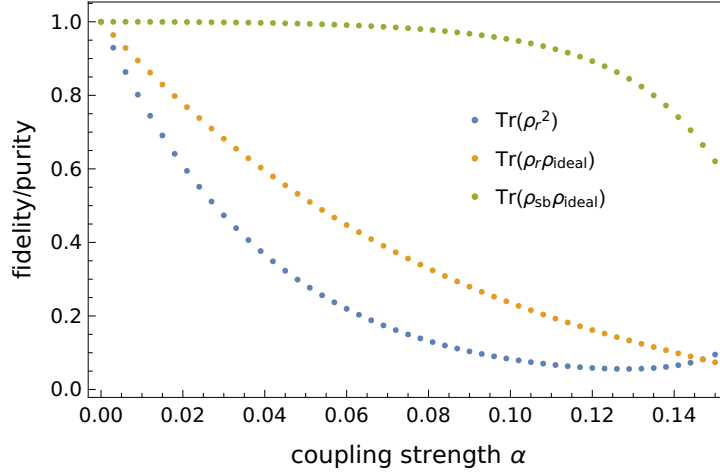


Figure 10.2: **Analysis of an antiferromagnetic Hamiltonian I**  
 Analysis of the ground state of the antiferromagnetic Hamiltonian  $H_{\text{afm}}$  for a specific 12-qubit example at  $s = 0.8$ . We calculated the ground state for both original and effective qubit Hamiltonian corresponding to minimal  $\omega_0$  within  $H_{\text{eff}}(\omega_0) \ll \omega_0$ . The reduced density matrix is found by applying the transformation of equation 10.1 to the latter. One finds that while the system-bath state is relatively close to the intended ground state for  $\alpha < 0.1$  or  $2\alpha < 0.2$ , the measurable state is not only considerably deformed but also incoherent at  $\alpha = 0.02$  which corresponds to  $12\alpha = 0.24$ .

stronger indicating long Pauli strings in the density matrix. To demonstrate the prohibition of entanglement, we compute the purity and entropy of  $\rho_r$  as entanglement is limited by coherence. We find that in the regime where effective Hamiltonian and its ground state are still intact –  $2\alpha$  is still small – the observable state is significantly or totally incoherent.

In figure 10.3 a) we depict the entropy for these settings. The simulation confirms a significant loss of coherence even at  $\alpha = 0.02$ . Notably, after a strong increase, the entropy declines again coinciding with a structural change of the effective Hamiltonian: We see in figure 10.3 b) that in the limit of large  $\alpha$ , i.e., strong effects on both Hamiltonian and reduced density matrix, the reduced density matrix represents a pure state. If all  $\sigma_X \sigma_X$  terms in the Hamiltonian are eliminated, it solely consists of  $\sigma_Z$  terms thus its eigenstates commute with those. As  $\sigma_Z$  eigenstates are invariant under dephasing, the reduced density matrix is pure. However, these states are product states and hence the revival of coherence does not coincide with a revival of entanglement. In figure 10.4 we observe these effects for smaller  $\alpha$  than in the first example, as the  $\sigma_Z$  terms of the Hamiltonian

are stronger for smaller annealing parameter  $s$ .

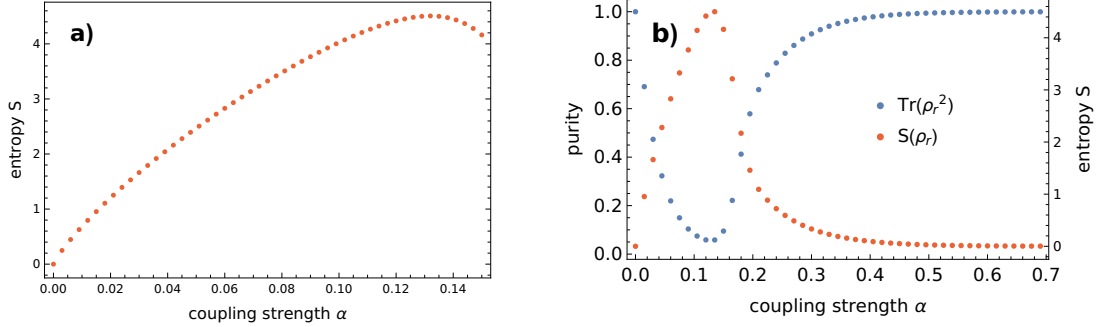


Figure 10.3: **Analysis of an antiferromagnetic Hamiltonian II**  
Further analysis of the system examined in figure 10.2. The increase in entropy at small  $\alpha$  indicates strong dephasing of a multipartite entangled ground state. For larger values of  $\alpha$ , purity and entropy show that the reduced density matrix converges back to a pure state.

We see that in the LCGD regime, the effective Hamiltonian can sponsor a multipartite entangled state which, however, does not exist in the qubit space alone but also represent entanglement between qubit and high-frequency bath modes. This needs to be taken into account when calculating system dynamics. Due to the effective dephasing of the reduced density matrix that ground state appears incoherent under qubit measurement.

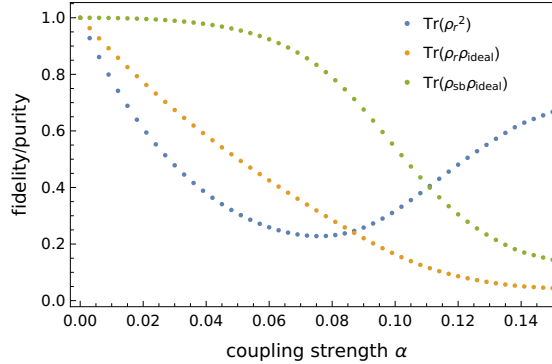


Figure 10.4: **Analysis of an antiferromagnetic Hamiltonian III**  
An instance of the 12-qubit antiferromagnetic Hamiltonian generated by a different set of  $c_{ij}$  at  $s = 0.7$ . The deformation of the system-bath ground state and revival of coherence take place for smaller  $\alpha$ .

## 10.2 Discussion

We have investigated the effects of an environment, that is represented by an Ohmic bath, on quantum annealing using renormalization group theory. We derived the suppression of terms in the qubit Hamiltonian that are not commuting with the bath coupling, which is increasingly strong for many-qubit terms. The same suppression can be seen for the reduced density matrix in leading order of effects, encoding an entanglement between system and bath. We focus on the LCGD regime, which inevitably arises when scaling to large systems: a robust  $k$ -local Hamiltonian can sponsor any multipartite entangled ground state which is not accessible by qubit measurement due to strong dephasing of the density matrix. We discuss the implications for quantum annealing due to inaccessibility of the ground state as well as the entanglement between system and bath.

The benefits of entanglement to annealing protocols often do not require a many qubit entangled desired state but rather it may only manifest during the annealing schedule. For example the adiabatic Grover or Deutsch-Josza algorithms do end up in product states [124], thus the readout of these is only perturbed weakly in the LCGD regime. However, many-qubit entangled ground states occur e.g. in many quantum simulations where the final Hamiltonian represents a physical system that is hard to solve classically, i.e., is not a product state [146, 147]. Those are limited in extractable information. More specifically, the LCGD-dephased density matrix allows for high-fidelity measurements only for  $k$ -local operators while many-qubit correlations are strongly suppressed and thus not represented in the measurement.

While the final Hamiltonian does not generally produce an entangled ground state, the system passes those on an efficient annealing path [148]. This means that while one starts and ends with a pure qubit state, the quantum annealing happens in both system and bath. Contrary to common intuition, this does not per se prohibit quantum computation and may even be beneficial to the annealing process. We believe, that the combined system-bath state no longer evolves adiabatically, but rather behaves more thermally, which has been shown to be beneficial [126]. While experiments with low qubit numbers seem to support this reasoning [149], it remains to be investigated further: First with regard specifics of system architecture and protocols and second on a device in the LCGD-regime with  $n \gg k$ .

The multispin Bose model has been extensively studied [150, 151], however, mostly not focused on spin dynamics which is required to investigate qubit based applications. Previous work on environmental effects on quantum annealing, however, relies on perturbative master equations, thus restricts itself to weak coupling and therefore weak effects [124, 132]. With the renormalization group approach we go beyond this limit, hence are able to treat the LCGD regime between the

weak and strong coupling limit investigated by Albash and Lidar [124]. We could conclude that quantum annealing partially happens in both qubits and environment and only provides limited access to a multipartite entangled ground state which, however, is sufficient for a lot of algorithms.

# Conclusion

The research involved in apprehending and engineering quantum information technologies is a quickly evolving field. Only a few decades after their proposal quantum computers approach the 50-100 qubit mark – the limit of what is possible to simulate on a classical machine. Attempts on adiabatic quantum computation even reach several thousand qubits, however, the computational power of these machines is severely limited by connectivity. While the growth in qubit numbers is fundamental to outperform a classical computer, scaling to larger systems introduces a number of additional challenges to the complex task of engineering and controlling individual qubits. For instance it becomes increasingly difficult to individually address qubits, while simultaneously allowing for sufficient connectivity. In case of nuclear magnetic resonance the lack of scalability turned a promising candidate for physical implementation into a dead end. It is not only important for any approach in building a quantum computer to involve a scaling strategy but also for that strategy to be efficient in required resources to not lose the potential advantage over classical computation.

A specific task in gate-based quantum computing that requires scalability is the assessment of implementations of quantum gates – two main hindrances make it significantly more complex than for classical gates: First, a quantum channel is described by exponentially many parameters and second, it is only accessible via projective measurement. Direct measurement of the full quantum channel parameters is denoted as quantum process tomography. Its efficiency can be improved upon by protocols such as Monte Carlo sampling, however, not avoiding an exponential effort. Randomized Benchmarking is an efficient protocol to experimentally assess the average gate error of specific sets of gates, such as the prominent Clifford group, via random gate sequences. It does so with effort polynomial in the number of qubits and is robust against state preparation and measurement errors due to error amplification as well as leakage outside the computational subspace and varying error channels for different gates. It allows to benchmark individual gates via interleaved Randomized Benchmarking but is at this restricted to just Clifford gates, which are insufficient for universal quantum computation.

In chapter 6 we built upon previous research of the author to combine the indi-

vidually restricted methods of interleaved Randomized Benchmarking and Monte Carlo sampling. We have extended the former to arbitrary quantum operations, outside of the Clifford group, while reducing the enormous overheads and avoiding the dependence on state preparation and measurement associated with the latter. The extension to non-Clifford gates is made possible by treating the sequence fidelity of Randomized Benchmarking as a state fidelity that is estimated via Monte Carlo sampling. This avoids the actual physical implementation of the inverting gate in the RB sequence which, for a non-Clifford gate, would require availability of a universal quantum computer. The protocol presented in chapter 6 inherits robustness with respect to SPAM errors from IRB. For current experimental settings these errors can completely mask the actual error channel. The resulting hybrid algorithm reduces the total number of necessary experimental measurements compared to direct Monte Carlo sampling of the gate fidelity due to error amplification and yields exponential savings in the classical preprocessing resources.

Despite the improvement given by the hybrid benchmarking protocol, both quantum simulation and quantum algorithms can involve complex processes that cannot be efficiently predicted classically, especially when scaling to regimes where these applications outperform classical computers. In chapter 7 we showed that this restriction does not prohibit validation, provided the implementation being benchmarked can be found or engineered to conserve symmetries in the system. Such is the case for many quantum simulation tasks as well as for fault-tolerant quantum computation, where stabilizers of error correcting codes are preserved by logical operations. We presented a symmetry benchmarking protocol relying on randomization via unitary one-designs on conserved subspaces, that allows estimation of average channel error while maintaining robustness to state preparation and measurement imperfections. We demonstrated the protocol for gate sets that either preserve the number of excitations or the parity thereof, representing Cooper pairs. We used a specifically engineered unitary one-design to assess the average violation of the given symmetries in polynomial time allowing for an estimate of the gate error.

Current implementations of adiabatic quantum computers typically consist of more qubits than the gate-base ones. The reason being that quantum annealing is conceived to be less vulnerable to the influence of environmental effects or even benefit from external coupling. However, in the adiabatic case, these environmental effects are much less defined and not yet fully understood. An adiabatic quantum computer can be modeled by the multi spin Boson model, with the Boson part given by Ohmically distributed bath modes: A model which we investigated in chapter 9, relying on renormalization group techniques. In particular, we applied poor man's scaling to derive the effective suppression of certain terms in the qubit Hamiltonian, specifically those Pauli strings, which are not commuting

with the spin bath coupling terms. We specified the strength of the suppression correlated to how many bath couplings a term does not commute with. In that, we generalized the known phenomenon of adiabatic renormalization of a single spin Boson Hamiltonian while going beyond the master equation approach used in previous research. We also showed that the reduced density matrix undergoes a similar transformation when reducing the cutoff frequency resulting in an effective dephasing – this can be interpreted physically as entanglement between system and bath. We expanded on the renormalization approach by investigating higher order terms of poor man’s scaling as well as flow equations.

In chapter 10 we focused on the locally coherent but globally dephased regime which inevitably arises when scaling to larger systems. It describes a range of coupling strength where  $k$ -local Hamiltonian are only affected mildly by environmental effects and hence can sponsor many qubit entangled ground states which are suppressed in the reduced density matrix. First, this implies that in a scaled up quantum annealer the access to the ground state is limited to few body correlation, i.e. measurement of  $k$ -local operators and, second, that quantum annealing partially happens in both qubits and environment. These findings, however, are not per se prohibitive to adiabatic quantum computations but rather change the theoretical description of the annealing process which we conclude to behave more thermally rather than purely adiabatic.

The field of quantum computing is at the verge of outgrowing the stage of proof of concept and approaches actual implementations of noisy intermediate size quantum computer, which can no longer be simulated classically. This transition to scaled up machines brings up additional challenges – not only quantum mechanical ones but including different fields of physics and beyond. Some of these challenges have been addressed in this thesis, specifically with regards to dealing with imperfect implementations and external effects for both gate-based and adiabatic quantum computation. How these approaches will develop, which new challenges will arise with this development as well as what new applications for quantum devices will emerge – these questions will be of interest for not only scientists in the near future.



# List of Publications

## Published

- [Tobias Chasseur](#), Daniel M. Reich, Christiane P. Koch, and Frank K. Wilhelm  
*Hybrid benchmarking of arbitrary quantum gates*  
[Phys. Rev. A](#) **95**, 062335 (2017)

## Submitted

- [Tobias Chasseur](#), Felix Motzoi, Michael Kaicher, Pierre-Luc Dallaire-Demers, and Frank K. Wilhelm  
*Benchmarking non-simulable quantum processes via symmetry conservation*  
[arXiv:1710.04563](#) (2017)
- [Tobias Chasseur](#), Stefan Kehrein, and Frank K. Wilhelm  
*Environmental effects in quantum annealing*  
[arXiv:1809.08897](#) (2018)

## Previous

- [Tobias Chasseur](#) and Frank K. Wilhelm  
*Complete randomized benchmarking protocol accounting for leakage errors*  
[Phys. Rev. A](#) **92**, 042333 (2015)
- [Tobias Chasseur](#), Lukas S. Theis, Yuval R. Sanders, Daniel J. Egger, and Frank K. Wilhelm  
*Engineering adiabaticity at an avoided crossing with optimal control*  
[Phys. Rev. A](#) **91**, 043421 (2015)



# Bibliography

- [1] Benioff, P. The computer as a physical system: A microscopic quantum mechanical hamiltonian model of computers as represented by turing machines. *Journal of Statistical Physics* **22**, 563–591 (1980).
- [2] Feynman, R. P. Simulating physics with computers. *International Journal of Theoretical Physics* **21**, 467–488 (1982).
- [3] Deutsch, D. Quantum theory, the Church-Turing principle and the universal quantum computer. *Proceedings of the Royal Society A: Mathematical, Physical and Engineering Sciences* **400**, 97–117 (1985).
- [4] Shor, P. W. Polynomial-time algorithms for prime factorization and discrete logarithms on a quantum computer. *SIAM Journal on Computing* **26**, 1484–1509 (1997).
- [5] Grover, L. K. From Schrödinger’s equation to the quantum search algorithm. *American Journal of Physics* **69**, 769–777 (2001).
- [6] DiVincenzo, D. P. The physical implementation of quantum computation. *Fortschritte der Physik* **48**, 771–783 (2000).
- [7] Preskill, J. Quantum computing in the NISQ era and beyond. *Quantum* **2**, 79 (2018).
- [8] McClean, J. R., Romero, J., Babbush, R. & Aspuru-Guzik, A. The theory of variational hybrid quantum-classical algorithms. *New Journal of Physics* **18**, 023023 (2016).
- [9] Albash, T. & Lidar, D. A. Adiabatic quantum computation. *Reviews of Modern Physics* **90** (2018).
- [10] Nielsen, M. A. & Chuang, I. L. *Quantum Computation and Quantum Information* (Cambridge University Press, 2000).

- [11] Kaye, P., Laflamme, R. & Mosca, M. *An Introduction to Quantum Computing* (Oxford University Press, 2006).
- [12] Einstein, A., Podolsky, B. & Rosen, N. Can quantum-mechanical description of physical reality be considered complete? *Physical Review* **47**, 777–780 (1935).
- [13] Bell, J. On the Einstein Podolsky Rosen paradox. *Physics* **1(3)**, 195–200 (1964).
- [14] Deutsch, D. Quantum computational networks. *Proceedings of the Royal Society A: Mathematical, Physical and Engineering Sciences* **425**, 73–90 (1989).
- [15] Gottesman, D. The Heisenberg representation of quantum computers. In Corney, S., Delbourgo, R. & Jarvis, P. (eds.) *Group22: Proceedings of the XXII International Colloquium on Group Theoretical Methods in Physics*, 32–43 (Cambridge, MA, International Press, 1999). ArXiv:quant-ph/9807006.
- [16] Aaronson, S. & Gottesman, D. Improved simulation of stabilizer circuits. *Physical Review A* **70** (2004).
- [17] Dankert, C., Cleve, R., Emerson, J. & Livine, E. Exact and approximate unitary 2-designs and their application to fidelity estimation. *Phys. Rev. A* **80**, 012304 (2009).
- [18] Haar, A. Der Massbegriff in der Theorie der kontinuierlichen Gruppen. *Ann. Math.* **34**, 147–169 (1933).
- [19] Dawson, C. & Nielsen, M. The Solovay-Kitaev algorithm. *Quantum Inf Comput* **6**, 081–095 (2006).
- [20] Grassl, M., Langenberg, B., Roetteler, M. & Steinwandt, R. Applying Grover’s algorithm to AES: quantum resource estimates. In *Proceedings of the 7th International Conference on Post-Quantum Cryptography (PQCrypto’16), Fukuoka, Japan*, vol. 9606, 29–43 (Springer, 2016).
- [21] Makhlin, Y., Schön, G. & Shnirman, A. Quantum-state engineering with josephson-junction devices. *Reviews of Modern Physics* **73**, 357–400 (2001).
- [22] Devoret, M. H. & Martinis, J. M. Implementing qubits with superconducting integrated circuits. *Quantum Information Processing* **3**, 163–203 (2004).
- [23] Schoelkopf, R. J. & Girvin, S. M. Wiring up quantum systems. *Nature* **451**, 664–669 (2008).

- [24] Clarke, J. & Wilhelm, F. K. Superconducting quantum bits. *Nature* **453**, 1031–1042 (2008).
- [25] Devoret, M. H. & Schoelkopf, R. J. Superconducting circuits for quantum information: An outlook. *Science* **339**, 1169–1174 (2013).
- [26] Monroe, C. & Kim, J. Scaling the ion trap quantum processor. *Science* **339**, 1164–1169 (2013).
- [27] Wineland, D. J. Quantum information processing and quantum control with trapped atomic ions. *Physica Scripta* **T137**, 014007 (2009).
- [28] Rohde, F. & Eschner, J. Quantum computation with trapped ions and atoms. In *Ultracold Gases and Quantum Information*, 218–252 (Oxford University Press, 2011).
- [29] Saffman, M. Quantum computing with atomic qubits and rydberg interactions: progress and challenges. *Journal of Physics B: Atomic, Molecular and Optical Physics* **49**, 202001 (2016).
- [30] Loss, D. & DiVincenzo, D. P. Quantum computation with quantum dots. *Physical Review A* **57**, 120–126 (1998).
- [31] Stehlik, J. *et al.* Landau-zener-stückelberg interferometry of a single electron charge qubit. *Physical Review B* **86** (2012).
- [32] Dobrovitski, V., Fuchs, G., Falk, A., Santori, C. & Awschalom, D. Quantum control over single spins in diamond. *Annual Review of Condensed Matter Physics* **4**, 23–50 (2013).
- [33] Kalra, R., Laucht, A., Hill, C. D. & Morello, A. Robust two-qubit gates for donors in silicon controlled by hyperfine interactions. *Physical Review X* **4** (2014).
- [34] Wilhelm, F. K. *et al.* Studie: Entwicklungsstand Quantencomputer. *Bundesamt für Sicherheit und Informationstechnik* (2018).
- [35] Beckman, D., Chari, A. N., Devabhaktuni, S. & Preskill, J. Efficient networks for quantum factoring. *Physical Review A* **54**, 1034–1063 (1996).
- [36] Lenstra, A. K., Lenstra, H. W., Manasse, M. S. & Pollard, J. M. The number field sieve. In *Proceedings of the twenty-second annual ACM symposium on Theory of computing - STOC '90* (ACM Press, 1990).

- [37] Deutsch, D. & Jozsa, R. Rapid solution of problems by quantum computation. *Proceedings of the Royal Society A: Mathematical, Physical and Engineering Sciences* **439**, 553–558 (1992).
- [38] Cleve, R., Ekert, A., Macchiavello, C. & Mosca, M. Quantum algorithms revisited. *Proceedings of the Royal Society A: Mathematical, Physical and Engineering Sciences* **454**, 339–354 (1998).
- [39] Georgescu, I. M., Ashhab, S. & Nori, F. Quantum simulation. *Reviews of Modern Physics* **86**, 153–185 (2014).
- [40] Montanaro, A. Quantum algorithms: an overview. *npj Quantum Information* **2** (2016).
- [41] Pednault, E. *et al.* Breaking the 49-qubit barrier in the simulation of quantum circuits (2017). ArXiv:1710.05867.
- [42] Harrow, A. W. & Montanaro, A. Quantum computational supremacy. *Nature* **549**, 203–209 (2017).
- [43] Boixo, S. *et al.* Characterizing quantum supremacy in near-term devices. *Nature Physics* **14**, 595–600 (2018).
- [44] Theis, L. S., Motzoi, F. & Wilhelm, F. K. Simultaneous gates in frequency-crowded multilevel systems using fast, robust, analytic control shapes. *Physical Review A* **93** (2016).
- [45] Barends, R. *et al.* Superconducting quantum circuits at the surface code threshold for fault tolerance. *Nature* **508**, 500–503 (2014).
- [46] Ballance, C., Harty, T., Linke, N., Sepiol, M. & Lucas, D. High-fidelity quantum logic gates using trapped-ion hyperfine qubits. *Physical Review Letters* **117** (2016).
- [47] Hamming, R. W. Error detecting and error correcting codes. *Bell System Technical Journal* **29**, 147–160 (1950).
- [48] Park, J. L. The concept of transition in quantum mechanics. *Foundations of Physics* **1**, 23–33 (1970).
- [49] Wootters, W. K. & Zurek, W. H. A single quantum cannot be cloned. *Nature* **299**, 802–803 (1982).
- [50] Dieks, D. Communication by EPR devices. *Physics Letters A* **92**, 271–272 (1982).

- [51] Shor, P. W. Scheme for reducing decoherence in quantum computer memory. *Physical Review A* **52**, R2493–R2496 (1995).
- [52] Steane, A. Multiple-particle interference and quantum error correction. *Proceedings of the Royal Society of London. Series A: Mathematical, Physical and Engineering Sciences* **452**, 2551–2577 (1996).
- [53] Laflamme, R., Miquel, C., Paz, J. P. & Zurek, W. H. Perfect quantum error correcting code. *Physical Review Letters* **77**, 198–201 (1996).
- [54] Bravyi, S. B. & Kitaev, A. Y. Quantum codes on a lattice with boundary (1998). ArXiv:quant-ph/9811052.
- [55] Dennis, E., Kitaev, A., Landahl, A. & Preskill, J. Topological quantum memory. *Journal of Mathematical Physics* **43**, 4452–4505 (2002).
- [56] Freedman, M. H. Quantum computation and the localization of modular functors. *Foundations of Computational Mathematics* **1**, 183–204 (2001).
- [57] Fowler, A. G., Mariantoni, M., Martinis, J. M. & Cleland, A. N. Surface codes: Towards practical large-scale quantum computation. *Physical Review A* **86** (2012).
- [58] Born, M. & Fock, V. Beweis des Adiabatenatzes. *Zeitschrift für Physik* **51**, 165–180 (1928).
- [59] Apolloni, B., Carvalho, C. & de Falco, D. Quantum stochastic optimization. *Stochastic Processes and their Applications* **33**, 233–244 (1989).
- [60] Apolloni, B., Cesa-Bianchi, N. & de Falco, D. A numerical implementation of “quantum annealing”. In *Stochastic Processes, Physics and Geometry: Proceedings of the Ascona-Locarno Conference*, 97–111 (River Edge, NJ: World Scientific, 1988).
- [61] Finnila, A. B., Gomez, M. A., Sebenik, C., Stenson, C. & Doll, J. D. Quantum annealing: A new method for minimizing multidimensional functions. *Chemical Physics Letters* **219**, 343–348 (1994).
- [62] Kadowaki, T. & Nishimori, H. Quantum annealing in the transverse Ising model. *Physical Review E* **58**, 5355–5363 (1998).
- [63] van Dam, W., Mosca, M. & Vazirani, U. How powerful is adiabatic quantum computation? In *Proceedings 2001 IEEE International Conference on Cluster Computing* (IEEE Comput. Soc, 2001).

- [64] Aharonov, D. *et al.* Adiabatic quantum computation is equivalent to standard quantum computation. *SIAM Journal on Computing* **37**, 166–194 (2007).
- [65] Jansen, S., Ruskai, M.-B. & Seiler, R. Bounds for the adiabatic approximation with applications to quantum computation. *Journal of Mathematical Physics* **48**, 102111 (2007).
- [66] Elgart, A. & Hagedorn, G. A. A note on the switching adiabatic theorem. *Journal of Mathematical Physics* **53**, 102202 (2012).
- [67] Kempe, J., Kitaev, A. & Regev, O. The complexity of the local Hamiltonian problem. *SIAM Journal on Computing* **35**, 1070–1097 (2006).
- [68] Farhi, E., Goldstone, J., Gutmann, S. & Sipser, M. Quantum computation by adiabatic evolution (2000). ArXiv:quant-ph/0001106.
- [69] Kitaev, A., Shen, A. & Vyalıy, M. *Classical and Quantum Computation* (American Mathematical Society, 2002).
- [70] Wei, Z. & Ying, M. A modified quantum adiabatic evolution for the Deutsch-Jozsa problem. *Physics Letters A* **354**, 271–273 (2006).
- [71] Aharonov, D. & Ta-Shma, A. Adiabatic quantum state generation and statistical zero knowledge. In *Proceedings of the thirty-fifth ACM symposium on Theory of computing - STOC '03* (ACM Press, 2003).
- [72] Wick, G. C. The evaluation of the collision matrix. *Physical Review* **80**, 268–272 (1950).
- [73] Perron, O. Zur Theorie der Matrices. *Math. Ann.* **64**, 248–263 (1907).
- [74] Frobenius, G. über Matrizen aus nicht negativen Elementen. *Sitzungsber. Königl. Preuss. Akad. Wiss. -*, 456–477 (1912).
- [75] Meyer, C. *Matrix analysis and applied linear algebra* (SIAM, 2000).
- [76] Henze, N. *Stochastik für Einsteiger* (Springer Fachmedien Wiesbaden, 2013).
- [77] Hoeffding, W. Probability inequalities for sums of bounded random variables. *Journal of the American Statistical Association* **58**, 13–30 (1963).
- [78] Blume-Kohout, R. Optimal, reliable estimation of quantum states. *New Journal of Physics* **12**, 043034 (2010).

- [79] Knill, E. *et al.* Randomized benchmarking of quantum gates. *Phys. Rev. A* **77**, 012307 (2008).
- [80] Magesan, E., Gambetta, J. & Emerson, J. Scalable and robust randomized benchmarking of quantum processes. *Phys. Rev. Lett.* **106**, 180504 (2011).
- [81] Magesan, E. *et al.* Efficient measurement of quantum gate error by interleaved randomized benchmarking. *Phys. Rev. Lett.* **109**, 080505 (2012).
- [82] Gross, D., Liu, Y.-K., Flammia, S. T., Becker, S. & Eisert, J. Quantum state tomography via compressed sensing. *Physical Review Letters* **105** (2010).
- [83] Flammia, S. & Liu, Y. Direct fidelity estimation from few Pauli measurements. *Phys. Rev. Lett.* **106**, 230501 (2011).
- [84] da Silva, M., Landon-Cardinal, O. & Poulin, D. Practical characterization of quantum devices with tomography. *Phys. Rev. Lett.* **107**, 210404 (2011).
- [85] Reich, D., Gualdi, G. & Koch, C. Optimal strategies for estimating the average fidelity of quantum gates. *Phys. Rev. Lett.* **111**, 200401 (2013).
- [86] Chasseur, T. & Wilhelm, F. Complete randomized benchmarking protocol accounting for leakage errors. *Phys. Rev. A* **92**, 042333 (2015).
- [87] Gambetta, J. *et al.* Characterization of addressability by simultaneous randomized benchmarking. *Phys. Rev. Lett.* **109**, 240504 (2012).
- [88] Wallman, J. & Flammia, S. Randomized benchmarking with confidence. *New. J. Phys.* **16**, 103032 (2014).
- [89] Egger, D. & F.K.Wilhelm. Adaptive hybrid optimal quantum control for imprecisely characterized systems. *Phys. Rev. Lett.* **112**, 240503 (2014).
- [90] Kelly, J. *et al.* Optimal quantum control using randomized benchmarking. *Phys. Rev. Lett.* **112**, 240504 (2014).
- [91] Dolde, F. *et al.* High fidelity spin entanglement using optimal control. *Nat. Commun.* **5**, 3371 (2014).
- [92] Xia, T. *et al.* Randomized benchmarking of single-qubit gates in a 2d array of neutral-atom qubits. *Phys. Rev. Lett.* **114**, 100503 (2015).
- [93] Epstein, J., Cross, A., Magesan, E. & Gambetta, J. Investigating the limits of randomized benchmarking protocols. *Phys. Rev. A* **89**, 062321 (2014).

- [94] Córcoles, A. *et al.* Process verification of two-qubit quantum gates by randomized benchmarking. *Phys. Rev. A* **87**, 030301 (2013).
- [95] Barenco, A. *et al.* Elementary gates for quantum computation. *Phys. Rev. A* **52**, 3457 (1995).
- [96] Knill, E. Approximation by quantum circuits (1995). ArXiv:9508006.
- [97] Magesan, E., Gambetta, J. & Emerson, J. characterizing quantum gates via randomized benchmarking. *Phys. Rev. A* **85**, 042311 (2012).
- [98] Harty, T. *et al.* High-fidelity preparation, gates, memory, and readout of a trapped-ion quantum bit. *Phys. Rev. Lett.* **113**, 220501 (2014).
- [99] Aspect, A., Dalibard, J. & Roger, G. Experimental test of bell's inequalities using time-varying analyzers. *Physical Review Letters* **49**, 1804–1807 (1982).
- [100] Goldreich, O. *P, NP, and NP-Completeness: The Basics of Computational Complexity* (Cambridge University Press, 2010).
- [101] Cramer, M. *et al.* Efficient quantum state tomography. *Nature Communications* **1**, 149 (2010).
- [102] Gross, D. Recovering low-rank matrices from few coefficients in any basis. *IEEE Transactions on Information Theory* **57**, 1548–1566 (2011).
- [103] Shabani, A. *et al.* Efficient measurement of quantum dynamics via compressive sensing. *Physical Review Letters* **106** (2011).
- [104] Lloyd, S. Universal quantum simulators. *Science* **273**, 1073–1078 (1996).
- [105] Aspuru-Guzik, A. Simulated quantum computation of molecular energies. *Science* **309**, 1704–1707 (2005).
- [106] Kassal, I., Whitfield, J. D., Perdomo-Ortiz, A., Yung, M.-H. & Aspuru-Guzik, A. Simulating chemistry using quantum computers. *Annual Review of Physical Chemistry* **62**, 185–207 (2011).
- [107] Barends, R. *et al.* Digital quantum simulation of fermionic models with a superconducting circuit. *Nature Communications* **6** (2015).
- [108] Wecker, D., Hastings, M. B. & Troyer, M. Progress towards practical quantum variational algorithms. *Physical Review A* **92** (2015).

- [109] Bauer, B., Wecker, D., Millis, A. J., Hastings, M. B. & Troyer, M. Hybrid quantum-classical approach to correlated materials. *Physical Review X* **6** (2016).
- [110] Dallaire-Demers, P.-L. & Wilhelm, F. K. Quantum gates and architecture for the quantum simulation of the fermi-hubbard model. *Physical Review A* **94** (2016).
- [111] Salathé, Y. *et al.* Digital quantum simulation of spin models with circuit quantum electrodynamics. *Physical Review X* **5** (2015).
- [112] Martinez, E. A. *et al.* Real-time dynamics of lattice gauge theories with a few-qubit quantum computer. *Nature* **534**, 516–519 (2016).
- [113] Zohar, E., Farace, A., Reznik, B. & Cirac, J. I. Digital lattice gauge theories. *Physical Review A* **95** (2017).
- [114] Carignan-Dugas, A., Wallman, J. & Emerson, J. Characterizing universal gate sets via dihedral benchmarking. *Phys. Rev. A* **92**, 060302(R) (2015).
- [115] Cross, A., Magesan, E., Bishop, L., Smolin, J. & Gambetta, J. Scalable randomised benchmarking of non-clifford gates. *npjqi* **2**, 16012 (2016).
- [116] Chasseur, T., Reich, D. M., Koch, C. P. & Wilhelm, F. K. Hybrid benchmarking of arbitrary quantum gates. *Physical Review A* **95** (2017).
- [117] Wightman, A. S. (ed.) *The Collected Works of Eugene Paul Wigner* (Springer Berlin Heidelberg, 1993).
- [118] Whitfield, J. D., Biamonte, J. & Aspuru-Guzik, A. Simulation of electronic structure hamiltonians using quantum computers. *Molecular Physics* **109**, 735–750 (2011).
- [119] Bravyi, S. B. & Kitaev, A. Y. Fermionic quantum computation. *Annals of Physics* **298**, 210–226 (2002).
- [120] Tranter, A. *et al.* The bravyi–kitaev transformation: Properties and applications. *Int. J. Quant. Chem.* **115**, 1431–1441 (2015).
- [121] Lafarge, P., Joyez, P., Esteve, D., Urbina, C. & Devoret, M. H. Two-electron quantization of the charge on a superconductor. *Nature* **365**, 422–424 (1993).
- [122] Dallaire-Demers, P.-L. & Wilhelm, F. A method to efficiently simulate the thermodynamical properties of the Fermi-Hubbard model on a quantum computer. *Phys. Rev. A* **93**, 032303 (2016).

- [123] Combes, J., Granade, C., Ferrie, C. & Flammia, S. T. Logical randomized benchmarking (2017). ArXiv:1702.03688.
- [124] Albash, T. & Lidar, D. A. Decoherence in adiabatic quantum computation. *Physical Review A* **91** (2015).
- [125] Passarelli, G., Filippis, G. D., Cataudella, V. & Lucignano, P. Dissipative environment may improve the quantum annealing performances of the ferromagnetic p -spin model. *Physical Review A* **97** (2018).
- [126] Kechedzhi, K. & Smelyanskiy, V. N. Open-system quantum annealing in mean-field models with exponential degeneracy. *Physical Review X* **6** (2016).
- [127] Gibney, E. D-Wave upgrade: How scientists are using the world's most controversial quantum computer. *Nature* **541**, 447–448 (2017).
- [128] Leggett, A. J. *et al.* Dynamics of the dissipative two-state system. *Reviews of Modern Physics* **59**, 1–85 (1987).
- [129] Zel'dovich, Y. B. & Starobinskii, A. A. Particle production and vacuum polarization in an anisotropic gravitational field. *JETP* **6**, 1159 (1972).
- [130] Lupaşcu, A., Bertet, P., Driessen, E. F. C., Harmans, C. J. P. M. & Mooij, J. E. One- and two-photon spectroscopy of a flux qubit coupled to a microscopic defect. *Physical Review B* **80** (2009).
- [131] Kehrein, S. *The Flow Equation Approach to Many-Particle Systems* (Springer Berlin Heidelberg, 2007).
- [132] Deng, Q., Averin, D. V., Amin, M. H. & Smith, P. Decoherence induced deformation of the ground state in adiabatic quantum computation. *Scientific Reports* **3** (2013).
- [133] Bethe, H. A. The electromagnetic shift of energy levels. *Physical Review* **72**, 339–341 (1947).
- [134] Gell-Mann, M. & Low, F. E. Quantum electrodynamics at small distances. *Physical Review* **95**, 1300–1312 (1954).
- [135] Wilson, K. G. The renormalization group: Critical phenomena and the Kondo problem. *Reviews of Modern Physics* **47**, 773–840 (1975).
- [136] Pavarini, E., Koch, E. & Coleman, P. *Many-Body Physics: From Kondo to Hubbard* (Verlag des Forschungszentrum Jülich, 2015).

- [137] Bylander, J. *et al.* Noise spectroscopy through dynamical decoupling with a superconducting flux qubit. *Nature Physics* **7**, 565–570 (2011).
- [138] Morel, P. & Anderson, P. W. Calculation of the superconducting state parameters with retarded electron-phonon interaction. *Physical Review* **125**, 1263–1271 (1962).
- [139] Anderson, P. W. A poor man’s derivation of scaling laws for the Kondo problem. *J. Phys. C: Solid State Phys* **3**, 2436 (1970).
- [140] Wegner, F. Flow-equations for Hamiltonians. *Annalen der Physik* **506**, 77–91 (1994).
- [141] Glazek, S. D. & Wilson, K. G. Renormalization of Hamiltonians. *Physical Review D* **48**, 5863–5872 (1993).
- [142] Glazek, S. D. & Wilson, K. G. Perturbative renormalization group for Hamiltonians. *Physical Review D* **49**, 4214–4218 (1994).
- [143] Mohseni, M. *et al.* Commercialize quantum technologies in five years. *Nature* **543**, 171–174 (2017).
- [144] Greenberger, D. M., Horne, M. A. & Zeillinger, A. Going beyond Bell’s theorem. ArXiv:0712.0921.
- [145] Hen, I. Realizable quantum adiabatic search. *EPL (Europhysics Letters)* **118**, 30003 (2017).
- [146] Babbush, R., Love, P. J. & Aspuru-Guzik, A. Adiabatic quantum simulation of quantum chemistry. *Scientific Reports* **4** (2014).
- [147] Harris, R. *et al.* Phase transitions in a programmable quantum spin glass simulator. *Science* **361**, 162–165 (2018).
- [148] Lanting, T. *et al.* Entanglement in a quantum annealing processor. *Physical Review X* **4** (2014).
- [149] Dickson, N. G. *et al.* Thermally assisted quantum annealing of a 16-qubit problem. *Nature Communications* **4** (2013).
- [150] Schehr, G. & Rieger, H. Strong-disorder fixed point in the dissipative random transverse-field Ising model. *Physical Review Letters* **96** (2006).
- [151] Winter, A. & Rieger, H. Quantum phase transition and correlations in the multi-spin-Boson model. *Physical Review B* **90** (2014).